STUDIES ON RADULA TOOTH MINERALIZATION IN THE POLYPLACOPHORA

Thesis by

Michael Harvey Nesson

In Partial Fulfillment of the Requirements
For the Degree of
Doctor of Philosophy

California Institute of Technology
Pasadena, California
1969
(Submitted July 1, 1968)

. . . to Arthur, Mark-Mark,
and S. C. Poobie

ACKNOWLEDGMENTS

I am grateful to Dr. Heinz A. Lowenstam for his advice and support throughout the course of this work. His broad scientific interests and his imaginative approach toward research have been a source of great intellectual stimulation for me. I shall always remember the joy and thrill of discovery, and the nautical discomforts, that we shared at the seashore and on shipboard.

I would like to thank Dr. Wheeler J. North for introducing me to the California coastline and for overseeing me for two summers at the Marine Laboratory. I would also like to acknowledge my appreciation to Dr. Robert S. Edgar for advising me during the early years of my tenure as a graduate student.

I am deeply indebted to Dr. Charles David for his valuable aid in many experiments and for his thoughtful and fruitful discussions on the material in this thesis.

I owe a debt of gratitude to Dr. Edward Berger for showing me the right way to cut thin sections.

Of the many other people who have given me aid and advice during my years at Caltech, special thanks are owed to Margarete Dekkers (especially for her sense of humor), Dr. Sudarshan Malhotra, Don Robberson, "Ben" Swart, Norman Shields, and Pat Koen.

I greatly appreciate the help of Joan Dubin, especially for coming to my aid in the final dark hours of thesis preparation.

For many years, LaVerne Wenzel has been my substitute mother. She

has fed me, lectured me, and lifted my sinking spirits on countless occasions till the wee hours of the morning. Our deep friendship is, perhaps, the best reward of my lengthy stay at Caltech.

Clyde A. Hutchinson, III, has provided me with friendship, torture, and much amusement.

My graduate student days gained much color from my association with Michael Fried, Stanley Krane, John Sedat, and Alexander Lyon.

For financial support during graduate training, I thank the National Science Foundation and the U.S. Public Health Service.

To my wife, Joyce, I am unable to express by words my appreciation of her love and understanding. Our first months of marriage have been overshadowed by this thesis which she has so skillfully typed. Now, she will have a full-time husband.

STUDIES ON RADULA TOOTH MINERALIZATION IN THE POLYPLACOPHORA

by Michael Harvey Nesson

Abstract

This report is concerned with several aspects of the process of iron mineralization of the radula teeth of chitons (Polyplacophora).

In Part I, the cusp cells of the radula sac, which are responsible for the deposition of iron into the major lateral teeth, are studied with the electron microscope. In *Mopalia muscosa* and *Lepidochitona* (*Cyanoplax*) *hartwegi*, it is found that these cells extend from a dorsal blood sinus to the surface of the teeth. The basal ends of the cusp cells, near the dorsal sinus, contain numerous rhopheocytotic vesicles filled with ferritin. Near the apical ends of the cells, there is high concentration of iron-containing membrane-bound granules. Some granules contain ferritin, others are filled with ferruginous particles of electron-dense material, and others contain ferritin cores with an outer layer of ferruginous particles. In each cusp cell, the granule region is separated from the tooth surface by a bundle of microvilli that arises from a layer of mitochondria-rich cytoplasm and terminates on the tooth surface. No electron-dense material is found in the microvilli. Double-membrane structures are observed in regions where iron-containing granules occur near the microvilli. A model of the pathway of iron through the cusp cells is deduced from the observations on their ultrastructure.

In Part II, it is shown that at least 90% of the iron contained in the blood of *Mopalia muscosa* (40 to 110 μg Fe per ml) occurs in the form of the protein-iron complex, ferritin. The blood ferritin is purified and compared with ferritin isolated from the superior epithelial cells and with vertebrate ferritins.

In Part III, it is determined, by Fe^{59}-labeling experiments, that the radula replacement rate of *Mopalia muscosa* is approximately 0.6 rows per day. The amount of iron contained in the major lateral teeth of *Mopalia muscosa* radulas is measured.

TABLE OF CONTENTS

Title . . . . . Page

General Introduction. 1

Part I: An Electron Microscope Study of the Superior Epithelial Cells of the Chiton Radula Sac. 21

Introduction. 22

Materials and Methods. 24

Observations. 30

Discussion. 170

Part II: Studies on Chiton Blood 180

Introduction. 181

Materials and Methods 182

Results. 188

Discussion 214

Part III: Studies on the Replacement Rate and Iron Content of the Radula of *Mopalia muscosa* 216

Introduction. 217

Materials and Methods 218

Results. 221

Discussion 237

General Discussion. 240

Bibliography. 244

GENERAL INTRODUCTION

The Polyplacophora, commonly known as chitons, are familiar members of the fauna of rocky coastlines throughout the world. Although the majority of these primitive molluscs live in the intertidal and shallow littoral zones, some species are found to depths of 4000 meters (1). The shallow water species are usually limited to hard substrates, to which they firmly adhere by means of their broad muscular foot. Under suitable conditions, they creep slowly over the substrate in search of food.

With respect to feeding behavior, most chitons can best be described as grazers (2,3,4,5). The major source of food for nearly all shallow water species consists of various types of algae which encrust and permeate the rock surfaces (2,4,5). However, sessile or sedentary animals may also be encountered and ingested during grazing. Large amounts of animal material (remains of sponges, hydroids, polyzoans) have been observed in the gut contents of several species of Mopalia (6).

The Anatomy and Function of the Radula Apparatus.

The characteristic feeding organ of the Polyplacophora, and of all Mollusca (excepting the Pelecypoda), is the radula complex (Figure 1). In chitons, the anatomical studies of Plate (7) show the radula complex to consist of a) the radula, a long membranous ribbon bearing numerous teeth arranged in transverse and longitudinal rows; b) a pair of elongate oval bodies, called bolsters or "cartilages,"

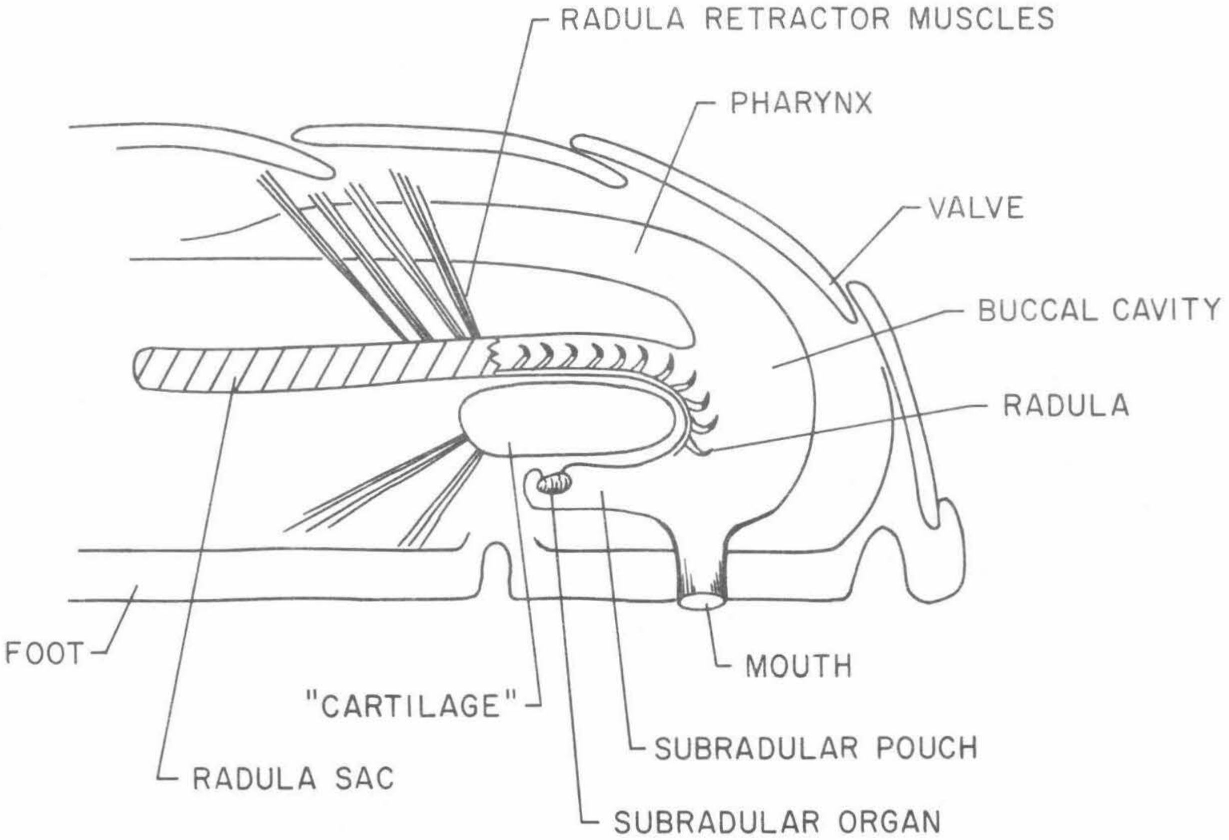
RADULA RETRACTOR MUSCLES
PHARYNX
VALVE
BUCCAL CAVITY
RADULA
FOOT
MOUTH
"CARTILAGE"
SUBRADULAR POUCH
RADULA SAC
SUBRADULAR ORGAN

FIGURE I. DIAGRAMMATIC TRANSVERSE SECTION THROUGH THE RADULA APPARATUS

which serve as supporting elements; and c) a complex array of myoglobin-containing (8,9) muscles, which function to protract, retract, and stabilize the radula and the bolsters. The paired bolsters together with several associated muscles form a discrete tongue-like tissue mass, called the odontophore, which comprises much of the posterior wall of the buccal cavity.

(a) The Radula.

The radula lies in a long, cylindrical radula sac which is a posteriorly directed outpocketing of the wall of the buccal cavity just below the pharynx. Within the radula sac, the edges of the radula membrane are curled dorsally to form a tube-like structure (with the teeth directed inward). The anterior end of the radula extends into the buccal cavity. Here, the radula membrane is stretched out flat over the odontophore and around its anterior border. The anterior radula membrane is firmly attached to a subradular membrane which covers the antero-dorsal surface of the odontophore.

Throughout the Polyplacophora, the radula is of quite uniform construction. The radula membrane bears up to 70 transverse rows of teeth: a central tooth and eight teeth symmetrically arranged on each side (10). The central tooth and the first lateral teeth are small and weakly scoop-shaped in profile. The second laterals, usually referred to as the major lateral teeth, are the largest and most distinctive teeth. They appear to be made up of two parts (11): a long tooth base (or stylus) which is attached at one end to the radula membrane, and a clearly demarcated, posteriorly recurved tooth cap (or cusp). The tooth caps are made of an opaque black material which presents a sharp contrast to the styli and to the other teeth, all of which are nearly transparent and only slightly pigmented. The shape of the tooth caps differs from family to family (10,12), ranging from a broad chisel-like form (in the Chitonidae) to a structure with one to three sharp cusps (in most other families). Five of the six marginal tooth pairs are small, polygonal, and of low flat profile. The third marginals have a narrow elongate curved form.

Several workers have noted that the major lateral tooth cusps show marked changes in appearance from the posterior to the anterior end of each individual radula (5,13). Posteriorly, the first several rows of tooth cusps are colorless, transparent, and soft. Over the next few rows, the cusps appear to be impregnated with increasing amounts of an opaque, reddish-brown material. These are followed in turn by cusps which are impregnated with an extremely hard, shiny black mineral. The black cusps appear uniform to the anterior end of the radula. The last few anterior rows of cusps usually show signs of apparent mechanical wear.

The bases of the major lateral teeth also show changes in appearance along the length of the radula (5,13). Posteriorly, the styli are soft, transparent, and colorless. They are gradually transformed, anteriorly, into tough transparent structures of red-brown color. The minor teeth show a transformation identical to that of the styli (14).

The sequence of changes in the radula of a European species of chiton, Acanthochitona communis, has been studied histochemically by Runham (11). Posteriorly, the radula is composed of protein and chitin (poly-N-acetyl-glucosamine), possibly in the form of a glycoprotein. The radula membrane exhibits a slight decrease of the various chitin and protein reactions in the region of row 25 to 30$^{(1)}$, which Runham interprets as being due to the formation of cross-links between the chitin end-groups and aspartic and glutamic residues of the protein.

The major lateral tooth bases lose the chitin and protein-carboxyl reactions completely in the first three to five rows, presumably by the same cross-linking reactions. These posterior styli are also impregnated with a protein that is rich in amino groups. This protein combines with the initial structural protein by linkages which involve phenolic derivatives. This "tanning" reaction takes place over row 10 to 25. From row 18 onward, the styli give a positive test for ferric (Fe^{3+}) iron. The occurrence of iron in the styli has been further documented by chemical analysis in Cryptochiton stelleri (15).

The histochemical reactions of the major lateral tooth cusps are qualitatively similar to those of their bases. However, all of the cross-links appear to be formed prior to the first reddish-brown tooth (approximately row 10). Ferric iron first appears in the cusps at about row 10, and a positive iron test continues to the end of the radula.

---

(1) In all subsequent discussion, the numbering of the tooth rows proceeds anteriorly; thus, the most posterior row is row 1.

(b) The Feeding Process.

When chitons feed, the first step is the protrusion of the subradular organ through the dilated oral opening (2). This organ is presumed to test the substrate for food, but no direct evidence for its chemosensory role has been published.

If suitable food is present, the subradular organ is retracted, and the odontophore moves forward and downward to the mouth (4). This movement causes the anterior rows of radula teeth to contact the substrate through the oral opening. Then, the radula retractor muscles contract, pulling the radula forward with respect to the substrate. The radula teeth scrape over the substrate, removing food, and then rake the abraded material into the mouth. The odontophore is then retracted and the chiton is ready to begin another cycle of feeding.

Many details of the feeding process can be observed in chitons feeding on the transparent walls of aquaria (4,14). The major lateral teeth appear to be the most important rasping agents. When the radula membrane is stretched flat over the odontophore, the major lateral teeth stand erect, nearly perpendicular to the membrane. The recurved tooth cusps firmly scrape the substrate as the radula is retracted. As they are drawn over the anterior tip of the odontophore, the major lateral teeth are pulled inward toward the midline by the curling of the radula membrane. As they collapse, these teeth carry the abraded material to the midline of the radula, where the more central teeth scoop it into the mouth.

In the course of rasping the rock surfaces for food, chitons also remove and ingest rock particles, as shown by analysis of gut contents (3,4) or fecal pellets (5). The most striking evidence of the erosional power of chitons is observed on limestone rocks. The characteristic chevron-shaped chiton feeding trails penetrate the rock surface, forming sharply defined scrape marks (16). Lowenstam (5) has observed that chitons living on limestone show only slight wear of the anterior four or five pairs of major lateral teeth, while individuals living on siliceous or granitic rocks commonly show severe mechanical wear of the anterior teeth.

The Composition of the Major Lateral Tooth Cusps.

Although Sollas, in 1907, stated that the major constituent of chiton teeth is ferric oxide (17), and although the presence of iron was later confirmed by several workers (11,18,19), not until recently have there been any investigations of the precise chemical and mineralogic composition of the black iron-containing mineral contained in the major lateral tooth cusps of the Polyplacophora.

In 1959, Tomlinson reported the remarkable finding that radulas of the ten species of chitons examined could all be picked up with a magnet (20). The black tooth cusps, which were shown to be responsible for the magnetic properties, give a positive chemical test only for iron among the common magnetic substances.

Lowenstam (5) undertook a detailed study of the physical and chemical properties of the major lateral tooth caps of several chiton species. Laboratory tests indicated that the caps have a hardness close to six on the Mohs hardness scale; i.e., they can scratch glass but not quartz. This is in agreement with the findings of the dependence of tooth wear on substrate hardness.

X-ray diffraction studies showed that the black tooth cusp mineral is the cubic iron oxide, magnetite ($FeO \cdot Fe_2O_3$). Although magnetite is a common mineral in igneous and metamorphic rock (in which it is formed by inorganic processes at elevated temperature and pressure), the only known occurrence in a biological system of this crystalline ferrous-ferric oxide is in Polyplacophoran radula teeth.

Chemical analysis indicated that the mature tooth cusps contain a minimum of 65% magnetite by weight. This has been confirmed by Carefoot (15), who found 47-57% dry weight of iron in mature cusps; these values correspond to magnetite concentrations of 64-78%.

Lowenstam also found that the X-ray diffraction patterns of teeth from several species (three species of the family Chitonidae, and Mopalia muscosa) showed a number of faint lines in addition to the magnetite pattern. Further study enabled him to report (32) that, in the Chitonidae, the major lateral tooth caps contain lepidocrocite (γ-FeOOH) and an apatite mineral (probably francolite, a carbonate fluorapatite) in addition to magnetite. Each of the three minerals forms a discrete unit in each tooth cap.

The presence of the extremely hard mineral, magnetite, as a tooth capping material in the Polyplacophora is presumably an important adaptation for feeding. It allows them to ingest the types of algae which enmesh and penetrate rocky surfaces (21,22), in addition to the algal felts growing on the rocks. It also readily explains the ability of chitons to cause mechanical erosion of certain kinds of rock. The occurrence of magnetite results directly in lengthening the effective rasping-life of the major lateral tooth caps of the Polyplacophora.

The Radula Replacement Mechanism.

For nearly a century, zoologists have believed that, in all radula-bearing molluscs, the radula is continually replaced throughout the life of the organism. The currently accepted view (23,24,25) is that new radula material is continually secreted at the posterior end of the radula sac, the whole radula continually moves anteriorly toward the buccal cavity, and the anterior region of the radula is broken down and eliminated. This view had been based, until quite recently, on a large body of indirect evidence: e.g., studies of the histology and histochemistry of the radula sac (26,27,28,29) measurements of radula size changes during normal growth (30), recovery of worn teeth from fecal pellets (31).

It should be emphasized here that the radula systems of nearly all the radula-bearing molluscs exhibit a striking uniformity of pattern. There are strong similarities in the anatomy, histology, and histochemistry of the radula apparatus throughout the phylum, from the Monoplacophora to the Cephalopoda. Thus, it is highly probable that information obtained about the processes involved in radula replacement for any individual species may have broader application to the phylum. In the following discussion of the mechanism of radula replacement, major emphasis will be placed on information obtained from studies on chitons, but mention will be made of important findings from other molluscan groups, in which the processes have been more fully investigated.

(a) Evidence for Radula Replacement.

Runham has presented the first direct evidence for continual replacement of the radula, in experiments with the pulmonate gastropod Lymnaea stagnalis (33). He surgically cauterized a portion of the tip of the radula sac, thereby destroying some of the presumed tooth-producing cells. By sacrificing animals at various times after the operation, he was able to show that the radula of this species is formed uninterruptedly and moves forward at a constant rate of 2.9 transverse rows per day.

The mechanism by which the radula moves forward is not yet clearly understood for any mollusc. Although many theories to explain the forward growth have been proposed (see Fretter and Graham (24) and Raven (23)), the definitive studies on the relative growth and movement of the membranes and epithelial cell layers have not been carried out.

Very few facts are known about the mechanism of breakdown of the anterior end of the radula. Runham (11,34) has reported that the staining properties of the extreme anterior end of the radula revert to those of the posterior newly-formed radula, which may imply a reversal of the "tanning" processes. It has been suggested that nearby epithelial cells may secrete enzymes which soften the radula membrane (26,34). Abrasion during the feeding process would then result in the elimination of the anterior rows of radula teeth.

(b) The Tooth Formation Process.

Much more is known about the production of new radula material within the posterior radula sac than about any other phases of the radula replacement mechanism. The cells which are responsible for the initiation of radula production are the odontoblasts. In the Polyplacophora, the odontoblasts are small, narrow epithelial cells, which form a roughly hemispherical cushion of tissue at the blind end of the radula sac (23). The cushion is divided into as many parts as there are teeth in a transverse row. The cells at the ventral and lateral edge of the cushion are presumed to secrete the radula membrane, while the rest of the mass of cells are responsible for the formation of the new radula teeth.

The first appearance of a tooth is a thin membrane secreted onto the surface of the cushion by the odontoblasts. As further material is secreted by the underlying cells, the membrane thickens and assumes the shape of a tooth (27,28). Gabe and Prenant (29) have observed in a number of molluscs that the cytoplasm of the odontoblasts contains inclusions which have the same staining properties as the substance of the newly-formed teeth. Most authors agree that the new radula arises by a true secretion process (see Raven (23), p.231-232).

Each portion of the odontoblast cushion consecutively produces all of the teeth of the respective longitudinal row (35,36). There are no cytological indications of degeneration of the odontoblasts. In pulmonate gastropods, autoradiographic studies provide evidence that the odontoblasts are permanent (34).

(c) Early Tooth Maturation.

While the odontoblasts continuously form consecutive rows of teeth, the newly-formed radula progresses anteriorly within the radula sac. As the new teeth move forward, they undergo changes in their chemical composition and physical properties (11,37,38). In the Polyplacophora, as we have previously discussed, histochemical findings indicate that the initial maturation steps consist of impregnation of the teeth with protein and formation of cross-links. The result of these processes is the transformation of the soft new teeth into structures of a much tougher and harder consistency (11). For the cusps of the major lateral teeth, further maturation takes the form of mineralization, resulting in extremely hard magnetite-impregnated tooth caps.

The cells of the dorsal wall of the radula sac are responsible for the maturation of the radula teeth. These long, columnar cells, called the superior (or internal) epithelium, extend to the surfaces of all of the teeth and almost entirely fill the intervening spaces (23,29). The small prismatic cells of the lateral and ventral walls of the radula sac, the so-called inferior (or external) epithelium, surround the U-shaped radula membrane and are responsible for its maturation (29,34). The whole radula sac is covered by a connective tissue sheath to which the radula retractor muscles are attached (23).

Autoradiographic studies have firmly established the origin and movement of the epithelial cells in the gastropod Lymnaea stagnalis (34). The superior epithelium is formed by the division of cells adjacent to the dorsal edge of the odontoblast cushion. The cells of this epithelium move forward at exactly the same rate as the radula itself (2.9 rows per day). Thus, the exceedingly complex interdigitation of the cells and teeth is not disturbed as the radula moves anteriorly. The inferior epithelium also arises by cell division in front of the odontoblast cushion. However, its initial rate of movement is only one-quarter that of the radula. Further anteriorly, the cells become very flat and probably move forward at the same rate as the radula. These flat cells secrete the subradula membrane. The forward growth of this thin cell pavement may play an important role in the mechanism of radula movement.

The cells of the superior epithelium appear to secrete the substances necessary for the maturation of the teeth. In the gastropods Bulla and Haminea, a zone of the epithelium has been observed to be rich in polysaccharides; these substances first appear in the teeth in the same zone (36). Similarly, in molluscs whose mature teeth are impregnated with either calcium- or iron-containing minerals, the superior epithelial cells in the region of mineralization are rich in calcium or iron respectively (29,36,39).

Late Tooth Maturation: The Mineralization Process.

(a) Cellular Aspects of Mineralization.

Histochemical studies of several species of Polyplacophora have revealed the presence of iron-containing granules (Fe^{3+}) in the cytoplasm of certain cells of the superior epithelium of the radula sac (18,39). The granules are observed mainly in those cells which terminate at the surface of the major lateral tooth cusps. The iron-bearing granules first appear in the cells one or two rows posterior to the first row in which the tooth cusps contain iron (i.e., the first brown tooth cusps). The number of granules per cell increases greatly over the next few rows, and then gradually decreases again. Altogether, granule-containing superior epithelial cells are present in a segment of the radula sac about ten tooth rows long.

The iron-containing granules are mainly localized at the two ends of the superior epithelial cells. At the apical end (near the surface of the tooth), they are so thickly concentrated that it is difficult to distinguish the size or shape of an individual granule. At the basal end of the cell, there are fewer granules but many of them are quite large. Often, the basal granules appear to be arranged in a row within the cell. Usually, a few small granules are scattered through the rest of the cell, especially in the vicinity of the oval nucleus, which is situated toward the apical end.

From these cytologic findings, Gabe and Prenant have concluded that the superior epithelial cells receive iron at their basal pole, presumably from the blood or the connective tissue, that the iron is transported across the length of the cells, and that the iron accumulated in the apical region is secreted into the teeth.

(b) Chiton Ferritin.

Towe, Lowenstam, and Nesson examined the iron-containing granules of the superior epithelium of Cryptochiton stelleri in the electron microscope (40). The granules of the apical pole are situated 6 to 8µ away from the surface of the tooth cusps. The granules appear to consist of crystalline or paracrystalline arrays of electron-dense micelles, 50 to 60Å across, which are morphologically identical to the iron-containing protein, ferritin. By applying Granick's method for the isolation of ferritin from horse spleen (41), these workers were able to prepare the yellowish-brown octahedral crystals which are characteristic of ferritin from extracts of the epithelial tissue of the chiton radula sac.

Ferritin has been the subject of intensive study in the twenty years since its discovery, because of its role as the major iron-storage protein of mammals and because of its interesting structure. Ferritin or ferritin-like proteins have been reported in a variety of mammalian tissues (42), in elasmobranchs (43), in the polychaete worm Arenicola (44), in plants (45,46), and in the fungus Phycomyces (47).

Ferritin consists of a well-defined protein moiety, known as apoferritin, and micelles of an iron-rich complex for which the approximate chemical composition $(FeOOH)_8 \cdot (FeO \cdot OPO_3H_2)$ has been suggested (48,49). The apoferritin molecule is a hollow shell, probably composed of twenty protein subunits arranged at the vertices of a pentagonal dodecahedron (50). The iron micelles are situated within the protein shell and the size of the micelle is limited by the space inside the protein (51). In the electron microscope, the micelles are found to be 55 to 60Å across, and reported values for the external diameter of the protein shell range from 94 to 110Å (51,52,53).

Generally, preparations of ferritin contain molecules which vary greatly in iron content, ranging from the empty protein shells (molecular weight 480,000) to molecules completely filled with micellar iron (molecular weight 900,000) (50,54,55). A fully-filled ferritin molecule contains close to 5,000 iron atoms (50,54).

Two studies of the mineralogical composition of the ferritin micelle have recently appeared. Towe and Bradley (56) and Harrison *et al.* (57) both conclude, from diffraction data, that the micellar mineral has a hexagonal crystal lattice. However, they have presented slightly different interpretations of the precise structure of the unit cell: Harrison *et al.* suggest that the micelle is a ferric oxyhydroxide (FeOOH), while Towe and Bradley propose that it is a ferric oxide hydrate ($4Fe_2O_3 \cdot 6H_2O$). Towe and Bradley have utilized additional techniques (e.g., infra-red absorption spectroscopy, differential thermal analysis) to provide data which support their proposed interpretation. Both studies further indicate that the phosphorus which is contained in the ferritin micelle has no effect on the crystal structure; phosphorus-free reconstituted ferritin (57) and the heat-hydrolysis product of $Fe(NO_3)_3$ (56) both give diffraction patterns identical to native ferritin.

The release of iron from ferritin can be achieved *in vitro* by reducing agents (e.g., cysteine, glutathione, ascorbic acid) (58,59), or by strong chelating agents (60). The mechanism of *in vivo* iron release is not yet known. There is some evidence to suggest that, in mammalian liver, reduction of ferritin iron, involving xanthine oxidase, occurs (61).

(c) Mineral Formation in the Tooth Cusp.

Carefoot has reported that the iron content of the major lateral tooth cusps is greater in the mature black caps than in the more posterior brown cusps (15). However, the process of mineralization cannot be viewed as a simple deposition and accumulation of magnetite within the chitin-protein matrix of the teeth. Towe and Lowenstam (13) have clearly demonstrated that the reddish-brown iron mineral, which is initially deposited in the cusps, is quite different from magnetite, the mineral found in the mature teeth.

Chemical tests indicate that the reddish-brown mineral contains no ferrous (Fe^{2+}) iron. It does contain a small percentage of phosphorus. The diffraction pattern of this material agrees closely, in both the spacing and the intensity of diffraction lines, with that of the ferritin micelle. This similarity has been noted by Towe (62) and by Harrison *et al.* (57). These findings strongly indicate that the iron-containing mineral of the brown tooth cusps is a partially phosphorylated ferric oxide hydrate, similar to, or identical to, the micellar mineral of ferritin.

The direct transformation of the brown mineral into magnetite requires some rather drastic changes. One-third of the iron atoms must be reduced from the ferric to the ferrous state. Further, the crystal lattice must be altered from a hexagonal one to the cubic inverse spinel structure of magnetite.

Towe and Lowenstam (13) have also carried out an electron microscope examination of the tooth cusps of Cryptochiton stelleri. In the unmineralized cap, the presumed protein-chitin complex forms a three-dimensional meshwork of 50 Å diameter fibrils which are twisted and gathered into bundles about 200 Å thick. The bundles interlock and enmesh to form a regular array of elongated polygonal cavities which are 0.1 to 0.5 μ in width.

Thin sections of the brown tooth cusps reveal the incipient deposition of the ferric mineral as small (∿ o.1 μ), roughly spherical bodies which frequently appear to be in contact with the fibrous cavity walls. At high magnification, the spherules are seen to be aggregates of smaller crystallites, which range down to 20 Å in size. These spherules are extremely similar in appearance to the ferric oxide hydrate particles formed by heat-hydrolysis of ferric nitrate (56).

Examination of surface replicas of mature magnetite-containing cusps indicates that crystallites of magnetite completely fill the interspaces of the polygonal meshwork of organic material. The tooth surface resembles a cobblestone pavement in which magnetite crystallites are the rocks and chitin-protein fibrils are the mortar.

The Present Study.

In the report which follows, we present the results of an investigation of some of the cellular and biochemical aspects of the process of mineralization of the major lateral tooth caps in two California species of chitons, *Mopalia muscosa* and *Lepidochitona* (*Cyanoplax*) *hartwegi*.

The deposition of an iron mineral similar to the micelle of ferritin as the first step of tooth mineralization, and the occurrence of ferritin in the superior epithelium of the radula sac, determined by Lowenstam and his co-workers, has led us to further study the role of ferritin in the mineralization process.

Part I of this study is a report of an electron microscope examination of the superior epithelial cells of the radula sac. Of major concern are the location and nature of the ferritin molecules within these cells and the occurrence and structure of organelles which may be involved in the mineralization process.

In Part II, we present our findings on the identification of the iron-containing substance present in the blood of *Mopalia muscosa*. This information is relevant to the determination of the mode of iron-transport to the cells of the radula sac.

The results of experiments to determine the rate of formation of the radula of *Mopalia muscosa* are reported in Part III.

Finally, in the General Discussion, we consider some of the more general aspects and implications of our findings and we suggest several avenues of approach for further investigation of the details of the mineralization process in the Polyplacophora.

PART I

AN ELECTRON MICROSCOPE STUDY OF THE SUPERIOR EPITHELIAL CELLS OF THE CHITON RADULA SAC

INTRODUCTION

In the Polyplacophora, the cusps of the mature major lateral radular teeth have been discovered to be composed of crystalline magnetite within a framework of chitin-protein fibrils (5,13). The process of mineralization occurs in two phases. The early mineralization phase consists of the deposition of brown mineral, hydrated ferric oxide (56,62) on the organic matrix of the cusps (13). In the late phase, the brown mineral is presumably transformed into magnetite, a ferrous-ferric oxide, and the cusps are further impregnated with additional magnetite (13).

As we have described in the General Introduction, a developmental sequence of mineralization can be observed along the length of each individual radula. Starting at its posterior end, the radula bears approximately ten tooth rows of unmineralized transparent cusps, a few rows of cusps which are impregnated with increasing amounts of the brown mineral, and then many rows with black, magnetite-containing cusps (5,13).

The mineralization process occurs within the radula sac, where the cusps and other teeth are surrounded by the cells of the superior epithelium of the radula sac (18,39). From histochemical and cytological studies of the radular tissues, many workers have concluded that the superior epithelium is responsible for the secretion of iron into the major lateral tooth cusps (15,18,39). The zone of mineralization covers a segment of the radula sac approximately ten tooth rows long.

The zone includes one or two rows of transparent cusps, the rows of brown cusps and several rows of black cusps. Within the mineralization zone, the cells of the superior epithelium which are associated with the tooth cusps contain large accumulations of iron-containing granules. Prenant (18) has suggested that these cells pick up iron at their basal ends and then secrete it into the tooth cusps from their apical ends.

The central topic of the following study is an electron microscope investigation of these cusp-associated superior epithelial cells within the zone of mineralization. However, we first present several findings on the gross histoanatomy of the radula sac of *Mopalia muscosa* and *Lepidochitona hartwegi*. These light microscope observations provide information that aids in the interpretation of the ultrastructure of the superior epithelial cells.

MATERIALS AND METHODS

Animals.

Lepidochitona (*Cyanoplax*) *hartwegi* and *Mopalia* *muscosa* are collected from the intertidal zone at Little Corona Beach, Newport, California. The animals are maintained in the laboratory in aquaria equipped with a gravel-filtered recirculating sea-water system (at 15° C.). Usually, algae-encrusted rocks are gathered from the site of collection and are placed in the aquaria to provide an attachment substrate for the animals and to serve as a source of food similar to that of the natural habitat.

Fixation.

Various fixation and post-fixation procedures were attempted. Fixation was unsatisfactory with formaldehyde or glutaraldehyde buffered with phosphate or cacodylate or with buffered osmic acid (66). However, fixation in 2.5% glutaraldehyde (purchased from Aldrich Chemical Company) in unbuffered filtered sea-water (as suggested by S.K. Malhotra) proved valuable and was routinely used.

The buccal region of the animals is exposed by removal of the first three valves. Cold 2.5% glutaraldehyde in sea water (0° to 4° C.) is immediately poured into the body cavity. The posterior one-third to one-half of the radula sac is carefully dissected free from the surrounding digestive gland, the attached muscle fibres are severed, and the sac and posterior radula are removed from the animal. The tissue is placed in fresh cold fixative for thirty minutes and transferred to another change of fixative. The material remains in the fixative for 12 to 20 hours (at 0° to 4° C.).

Although the radula sac of L. hartwegi is only 0.4 to 0.5 millimeters in diameter, the fixation of the deeper-lying regions of the tissue is only fair, at best. The radula membrane, which underlies most of the circumference of the radula sac, appears to act as a diffusion barrier, so that the fixative can penetrate into the sac only through the short dorsal arc that is free of radula membrane. Fixation is somewhat improved by cutting the radula sac into segments of approximately eight to ten tooth rows in length, thereby increasing the effective surface area for diffusion of fixative through exposure of the cut ends. However, the process of cutting through the tough radula within the sac often disturbs the intimate relationships between the cells and the radula structures.

The radula sac of M. muscosa is 1.0 to 1.2 mm in diameter. Even when the sac is cut into short segments three to four teeth rows long, fixation of the more internal tissue is very poor. Consequently, the electron microscope investigation of the radula tissue has been performed primarily on L. hartwegi. The few minor differences that we have observed between the radula tissue of the two species will be noted.

Most of the material examined is post-fixed with osmic acid. After fixation, the tissue is washed in filtered sea-water (2 x 15 minutes) and placed in cold 2% OsO_4 in filtered sea-water for two hours. After post-fixation, the tissue samples are washed in filtered sea-water to remove excess osmic acid (3 x 5 min.).

Dehydration.

Dehydration is accomplished in an increasing concentration series of ethyl alcohol, as follows: 30% - 10 min.; 50% - 10 min.; 70% - 10 min.; 95% - 10 min.; anhydrous absolute ethanol - 2 x 5 min. Samples are then placed in propylene oxide (2 x 15 min.).

Embedding.

The embedding medium used for all samples is the epoxy resin, Epon 812 (obtained from the Shell Chemical Company). We closely follow the embedding procedure described by Luft (63). Initially, we used a mixture of 3A:7B (Cf. (63)), to produce a very hard final embedment which was expected to prevent any displacement of the hard radula teeth during sectioning. Later, it was discovered that more reliable and better quality sectioning was obtained with much softer final mixtures. A mixture of 7A:3B was then routinely employed.

Infiltration of the tissue proceeds in propylene oxide-Epon mixtures: 1 part propylene oxide to 1 part Epon - 30 min.; 1 part propylene oxide to 2 parts Epon - 2 hours; complete Epon - 10 hours (at 21° C.).

The specimens are oriented and embedded in fresh Epon, either in BEEM capsules (obtained from Better Equipment for Electron Microscopy, Inc.) or in disposable plastic embedding dishes. The Epon is then polymerized at 60° C. for about 30 hours.

Sectioning.

Specimens are trimmed into pyramids by hand. Thick sections

(0.5 to 1.0μ) for light microscopy and thin sections (300 to 800Å) for electron microscopy are cut on an LKB Ultratome with glass knives.

Grids.

Copper-mesh grids (75- or 100-mesh) and keyhole grids are used for examination of thin sections. The grids are covered with a Formvar supporting film prepared from 0.20% Formvar in ethylene dichloride. Grids are lightly carbon-coated in a vacuum evaporator to improve their thermal stability.

Staining of Thin Sections.

Three staining procedures are used throughout the study.

a) Lead staining. Grids are floated face down on a drop of 0.3% lead citrate, prepared by the method of Venable and Coggeshall (64). The grids are stained for 2 to 8 minutes, dependent upon the thickness of the sections. The grids are washed in distilled water and air-dried.

b) Uranyl staining. The technique of Brody (65) is used. Grids are floated on filtered, supersaturated uranyl acetate in distilled water in small closed weighing bottles. The grids are stained for 1 to 2 hours at 60° C. The bottles are then dipped below the surface of a large water-filled vessel. The grids float onto the water surface, which affords a great dilution of the staining solution and prevents the formation of crystals on the sections.

c) Double staining. Grids are first uranyl acetate stained, as described in b), and then lead stained as described in a).

Electron Microscopy.

A Phillips EM-200 electron microscope, operated at 60 or 80kV, is used for all phases of this study. The instrument is normally operated with a 45μ thin-metal aperture, but a 25μ aperture is used with some ultrathin (∿ 300Å) sections.

Selected-area electron diffraction studies on some unstained sections is performed by the technique described in the Operating Manual of the Phillips EM-200.

Staining of Thick Sections.

For topographic studies, 0.5 to 1.0μ Epon-embedded sections are stained by a method similar to the procedure described by Richardson *et al*. (67). The only difference in our method is the replacement of methylene blue by 1% toluidine blue, which is mixed with Azure II to prepare the staining reagent.

We have also used a modification of Bunting's Prussian blue method (68) to demonstrate the presence of ferric iron in Epon-embedded material. Sections are placed in a solution of 1% potassium ferrocyanide in 1% HCl for 1 to 2 hours at 60° C. The reagent is not very stable at 60° C. and must be replaced every 15 minutes in order to prevent non-specific deposition of Prussian blue. We counterstain with 5% aqueous neutral red at 60° C. for 15 minutes.

Histochemical Methods.

We have examined several *M. muscosa* radula sacs prepared by standard histological procedures. Excised radular tissue is fixed in phosphate-buffered (pH 7) 10% formalin (68), embedded in paraffin or celloidin-paraffin (69), and 5 to 15 μ sections are cut with a rotary microtome.

We perform a variety of histological and histochemical staining reactions on this material: Delafield's haematoxylin and eosin (70) for general study; Masson's trichrome (71) and Greenstein's five-dye (72) for connective tissue; the Prussian blue method (68) for ferric iron; and the Turnbull's blue method (73) and bathophenanthroline (74) for ferrous iron.

OBSERVATIONS

Anatomy of the Radula Sac.

The general anatomical relationships between the tissues of the radula sac and the structures which comprise the radula have been investigated by studying serial sections with the light microscope. In our experience, Epon-embedded thick sections of material prepared for electron microscopy are much more informative than paraffin-embedded sections for these topographical studies.

Figures 2 and 4 are, respectively, transverse and longitudinal sections through the radula sac of *L. hartwegi*, in the zone of early mineralization (i.e., at the level of the brown major lateral tooth cusps). In cross-section, the radula membrane is a U-shaped structure which opens dorsally. The exterior (or inferior) epithelium consists of a thin sheet of small prismatic cells which covers the outer surface of the radula membrane. This epithelium is, in turn, surrounded by a layer of connective tissue which continues over the dorsal region of the sac. The outer connective tissue sheath serves as the insertion site for several muscles, including the radula retractors.

All of the radula teeth of each transverse row are embedded in the radula membrane. The teeth can be easily distinguished in Figure 3, a transverse section through the posterior radula sac of *M. muscosa*. The bases of the major lateral teeth project towards the center of the sac (Figures 2 and 3) and extend anteriorly (Figure

Figure 2a. Light micrograph of a transverse section through the radula sac of *L. hartwegi*, at the level of the first brown tooth cusp (∿ row 13). Note the cell-filled stylus canals, the tricuspid tooth caps, and the dorsal sinus. (1μ Epon section, gluteraldehyde -OsO_4, toluidine blue-Azure II) X 300.

Figure 2b. Diagram of Figure 2a.

C.E.	superior epithelial cusp cells
D.S.	dorsal sinus
I.E.	inferior epithelium
M.E.	superior epithelial minor cells
R.M.	radula membrane
T.C.	major lateral tooth cusp
T.S.	major lateral tooth stylus

C.	central tooth
L_I	first lateral tooth
L_{II}	second lateral tooth
M_{II} - M_{IV}	second to sixth marginal teeth

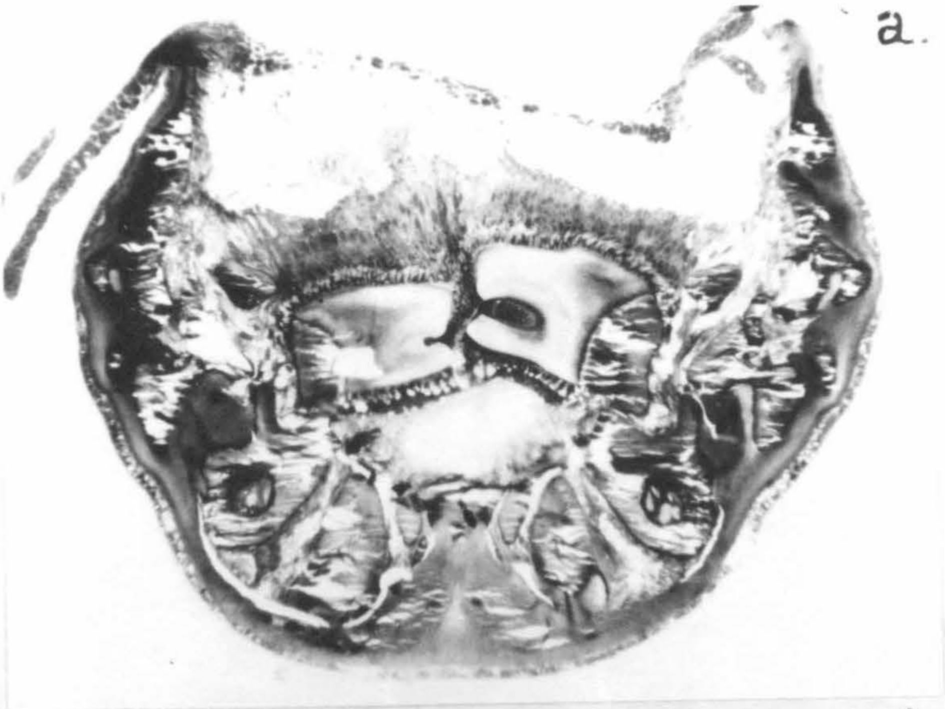

a.

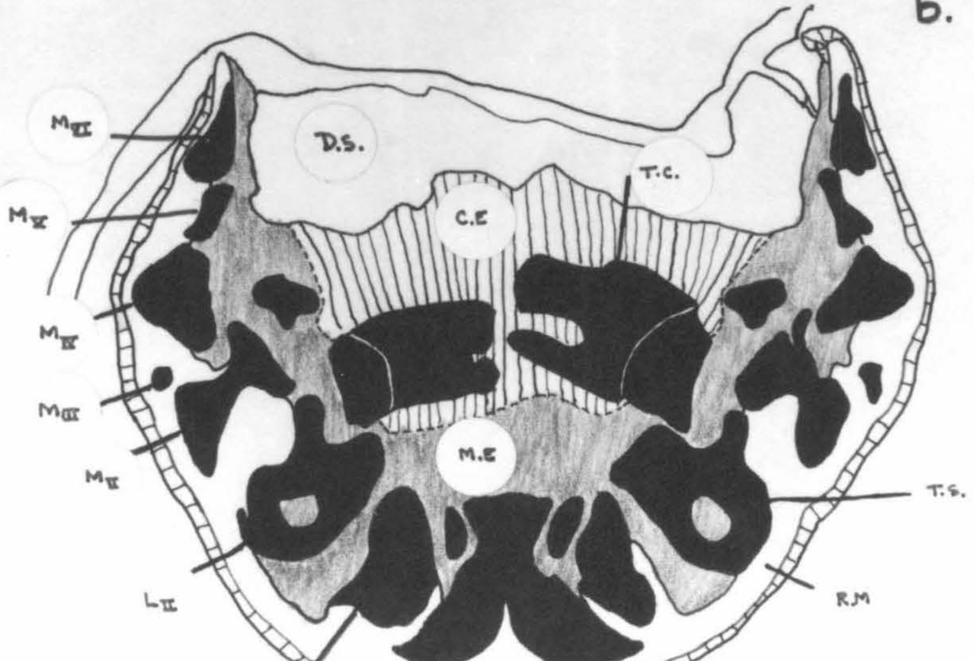

b.

MVII
MV
MIV
MIII
MII
LII
LI
C.
D.S.
T.C.
C.E
M.E
T.S.
R.M
I.E.

Figure 3. Light micrograph of a transverse section through the radula sac of _M_. _muscosa_ at row 7. Note the darkly stained teeth embedded in the radula membrane and the strands of cells entering the stylus canal. Also note the absence of a dorsal sinus. (12 μ paraffin section, neutral formalin, Masson trichrome)

X 110.

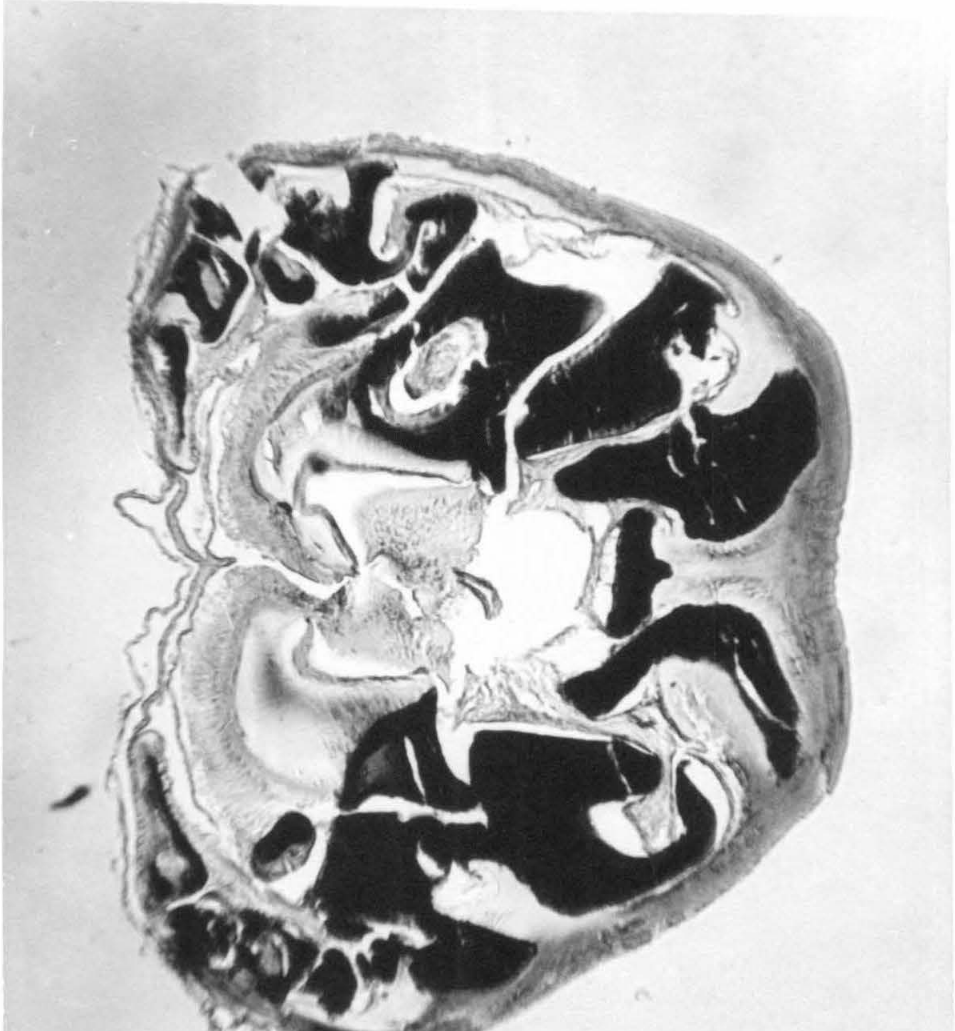

4), so that the cusps of the major lateral teeth of one row lie directly dorsal to the basal ends of the styli of the succeeding anterior row. The major lateral styli, in contrast to the minor teeth, are not solid structures; serial sections reveal that a long hollow canal extends through each stylus and terminates in the vicinity of the stylus-cusp junction. The canal opens to the exterior through a pore that is located on the inner face of the stylus near the basal end (Figure 3). The styli and the minor teeth appear to be poorly impregnated with embedding material. They generally fracture or shatter as they are being sectioned.

The major lateral tooth cusps are of markedly different consistency from the styli, as evidenced by their behavior during sectioning. The unmineralized cusps, the brown cusps, and even the first rows of black cusps all section easily and smoothly, indicating that they are well-impregnated with Epon. The longitudinal section in Figure 4 shows several rows of cusps which together comprise the zone of early mineralization. Upon visual examination of this material in the light microscope, one can see one colorless cusp, three brown cusps, and two rows of black magnetite-containing cusps. This region of the radula sac is the major focus of the electron microscope studies which follow below.

The dorsal region of the radula sac is occupied by a hitherto undescribed cavity that we refer to as the dorsal sinus. In the paraffin-embedded material that we have examined (Cf. Figure 3), the dorsal sinus is not readily discernable because of the shrinkage and

Figure 4. Longitudinal section through the zone of early mineralization of the radula sac of L. hartwegi (rows 11-16). Note the dorsal sinus, the colorless (row 11), brown (rows 12-14), and black (rows 15,16) major lateral tooth cusps, surrounded by the cusp cells. Also note the dorsal sinus and the anteriorly directed major lateral styli. (Same preparative techniques as Figure 2). X 480.

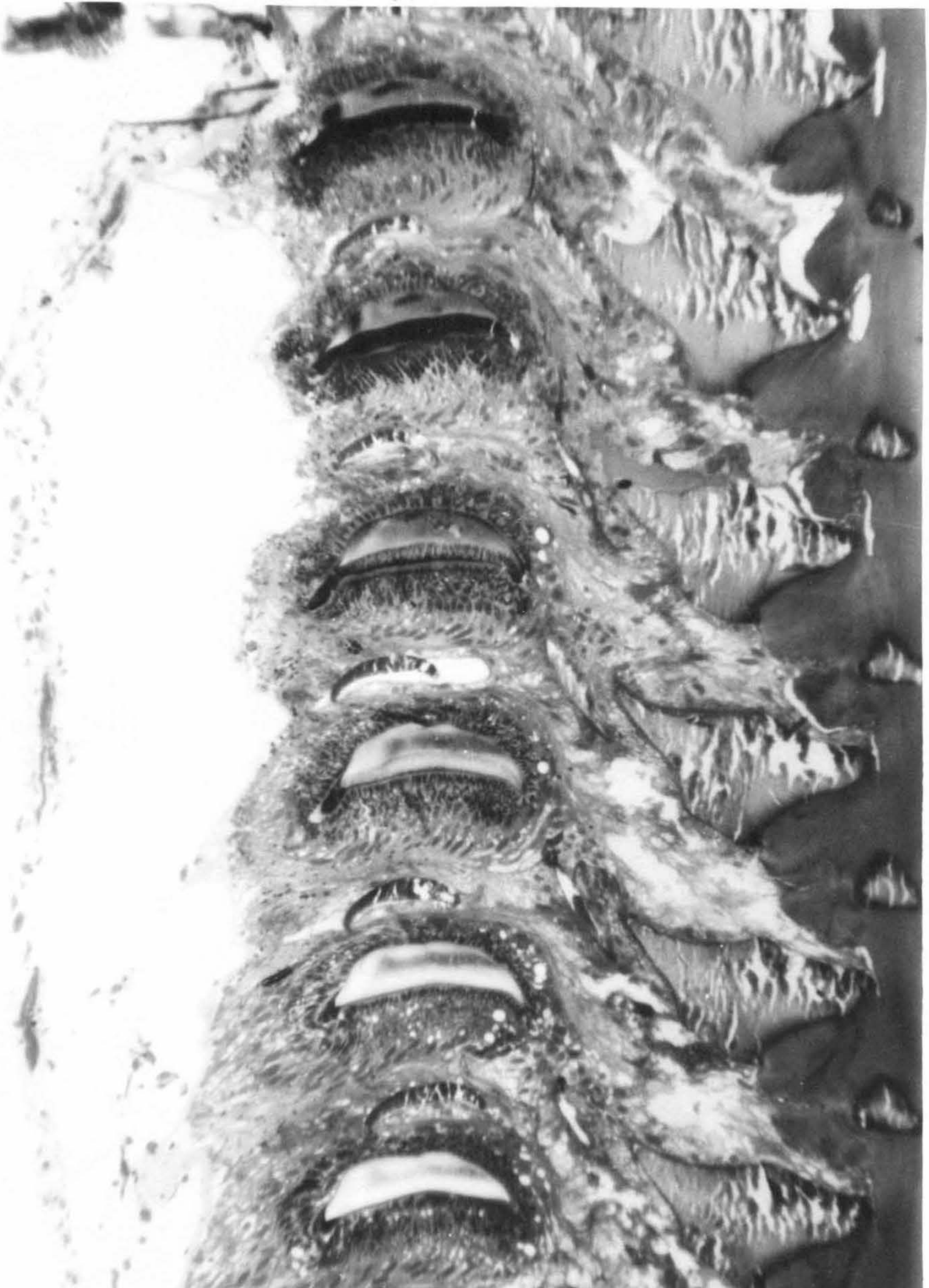

distortion of the surrounding tissues. We strongly suspect that the use of classical histological preparative techniques precluded the observation of this important structure in earlier studies on the anatomy of the radula sac (7,18).

In sections of an Epon-embedded radula sac, the dorsal sinus is seen to lie between the outer connective tissue sheath and the basal ends of the cells which comprise the superior epithelium (Figures 2,4, 5). In most sections, a very thin layer of dark-staining material appears to mark the outer circumference of the lumen of the sinus; usually, this layer cannot be resolved in photomicrographs. Examination of serial cross-sections reveals that the sinus extends nearly to the posterior end of the radula sac. We have been unable to trace the sinus very far in the anterior direction because we have encountered great difficulty in attempting to section the anterior region of the radula sac, where the tooth cusps are completely impregnated with magnetite.

Within the zone of mineralization, the superior epithelium is composed of two distinct types of cells. The first class of cells is associated with the cusps of the major lateral teeth. They will be referred to as the cusp cells or the cusp epithelium. The second type, which we call the minor cells, appear to terminate on the surfaces of the styli and the minor teeth. The cusp cells can be readily distinguished from the minor cells by their intense staining reaction with toluidine blue-Azure II, and by the presence of large numbers of iron-containing granules in their cytoplasm.

Figure 5. Higher power light micrograph of the major lateral cusp region from a longitudinal section similar to Figure 4. Note the basement material separating the cusp cells from the dorsal sinus, above. Observe the paths of the cusp cells from the sinus to the teeth. Also note the darkly stained iron granules in the basal and apical poles of the cells, and the lightly stained zone that contacts the cusp surface. (Glutaraldehyde -OsO_4, toluidine blue-Azure II)

X 1650.

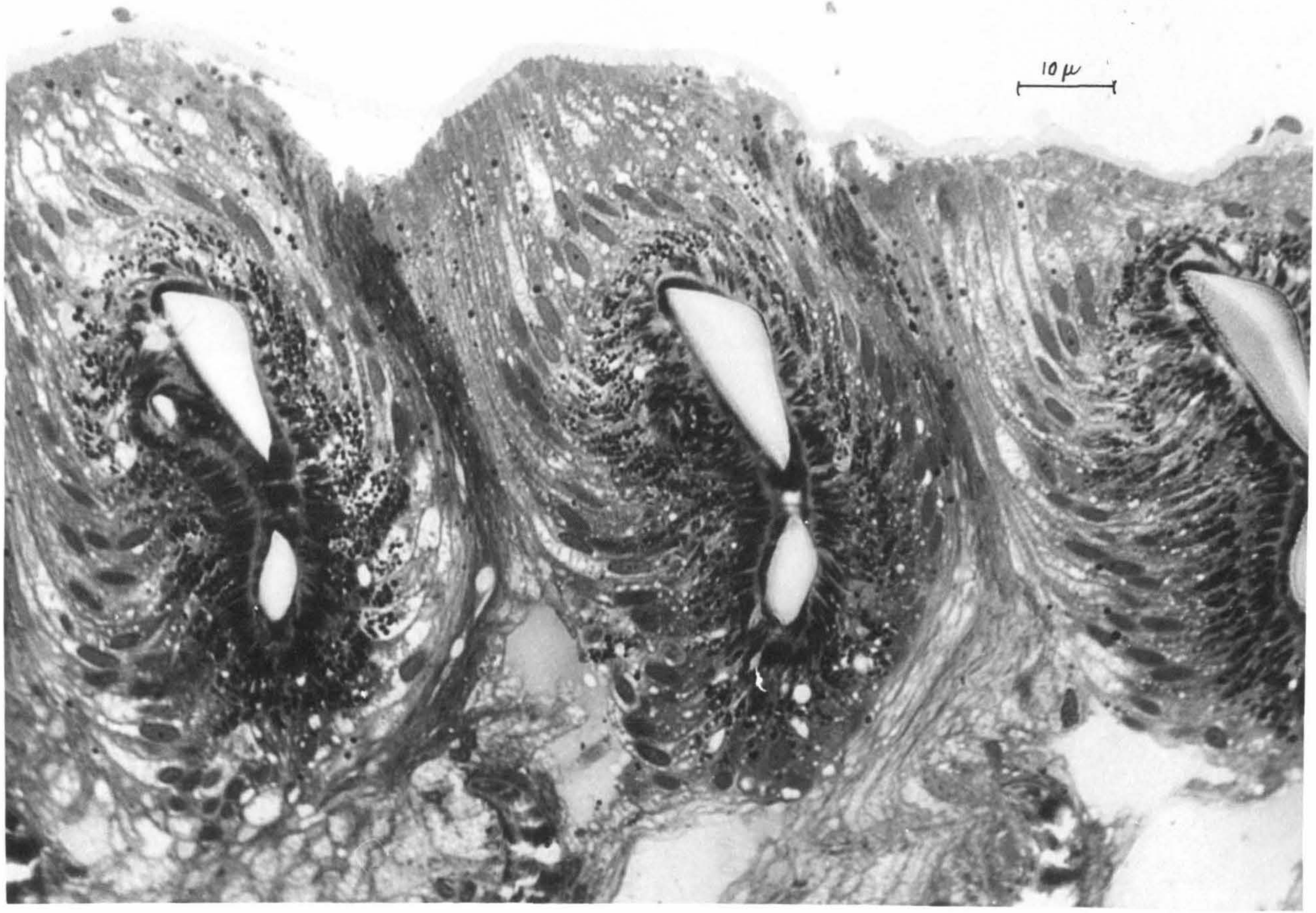
10μ

The cusp cells are grouped into compact masses of tissue (Figures 2 and 5). Each individual tissue mass surrounds the two major lateral tooth cusps which occur in an individual transverse row of radula teeth (Figures 2 and 4). Each tissue mass is distinct and is separated from the ones which surround the cusps of the preceding and succeeding transverse tooth rows (Figures 4 and 5). The spaces between the adjoining cusp cell masses are filled with strands of minor cells.

The so-called minor cells appear to extend from the dorsal sinus to the surfaces of the major lateral tooth styli and the minor teeth. Strands of the minor cells also enter the basal pore of each stylus (Figure 3) and totally fill the hollow stylus canal (Figure 2). In a transverse view of the radula sac (Figure 2), the minor cells can be seen to originate from the lateral margins of the floor of the dorsal sinus. In longitudinal view (Figures 4 and 5), the cells appear to arise at the dorsal sinus and to pass between the cusp cell tissue masses to the minor teeth. Thus, the minor cells surround and isolate each cusp cell mass. The minor cells contain only a small number of iron-containing granules, most of which are in the cytoplasm of those cells which terminate on either the inner or outer surfaces of the hollow major lateral tooth styli.

Light Microscopy of the Cusp Cells.

Light microscope studies reveal that the cusp cells of M. muscosa and L. hartwegi are cytologically identical to the cusp-associated cells described by Prenant (18) and Gabe and Prenant (39) for several

European species of chiton.

For purposes of discussion, the long columnar cusp cells which lie within the mineralization zone can be divided into three major regions: the basal pole, the central region, and the apical pole. All of the cusp cells associated with an individual tooth cusp appear to arise near the medial part of the floor of the dorsal sinus, to extend towards the cusp, and to terminate directly on the cusp surface (Figures 5,6). Typically, the apical ends of the cells abut almost perpendicular to the surface of the tooth.

The basal region of each cell is situated close to the dorsal sinus and appears highly vacuolar. Generally, a thin layer ($\sim$ 1.5 μ) of lightly-stained material separates the basal pole from the lumen of the sinus. A small accumulation of Fe^{3+}-containing granules is frequently observed in the basal cytoplasm. No ferrous iron is detectable either within the basal region or anywhere else within the cusp cell.

A large ovoid nucleus lies in the apical half of the central region. Scattered iron-containing granules, sometimes arranged in rows within a cell, are found throughout the central cytoplasm. Gabe and Prenant (39) have reported that the central cytoplasm contains ferric iron that is not within the granules. This cytoplasmic iron is undetectable by the Prussian blue method but is visible as a red ash in spodograms.

The apical pole of the cusp cells consists of two distinct regions: a granule zone ($\sim$ 15 μ thick), which contains a dense accumulation of iron-containing granules, and a 5-10 μ wide zone which lies between the

Figure 6. A high power light micrograph of the cusp cells from a cross-section through the L. hartwegi radula sac. X 2900.

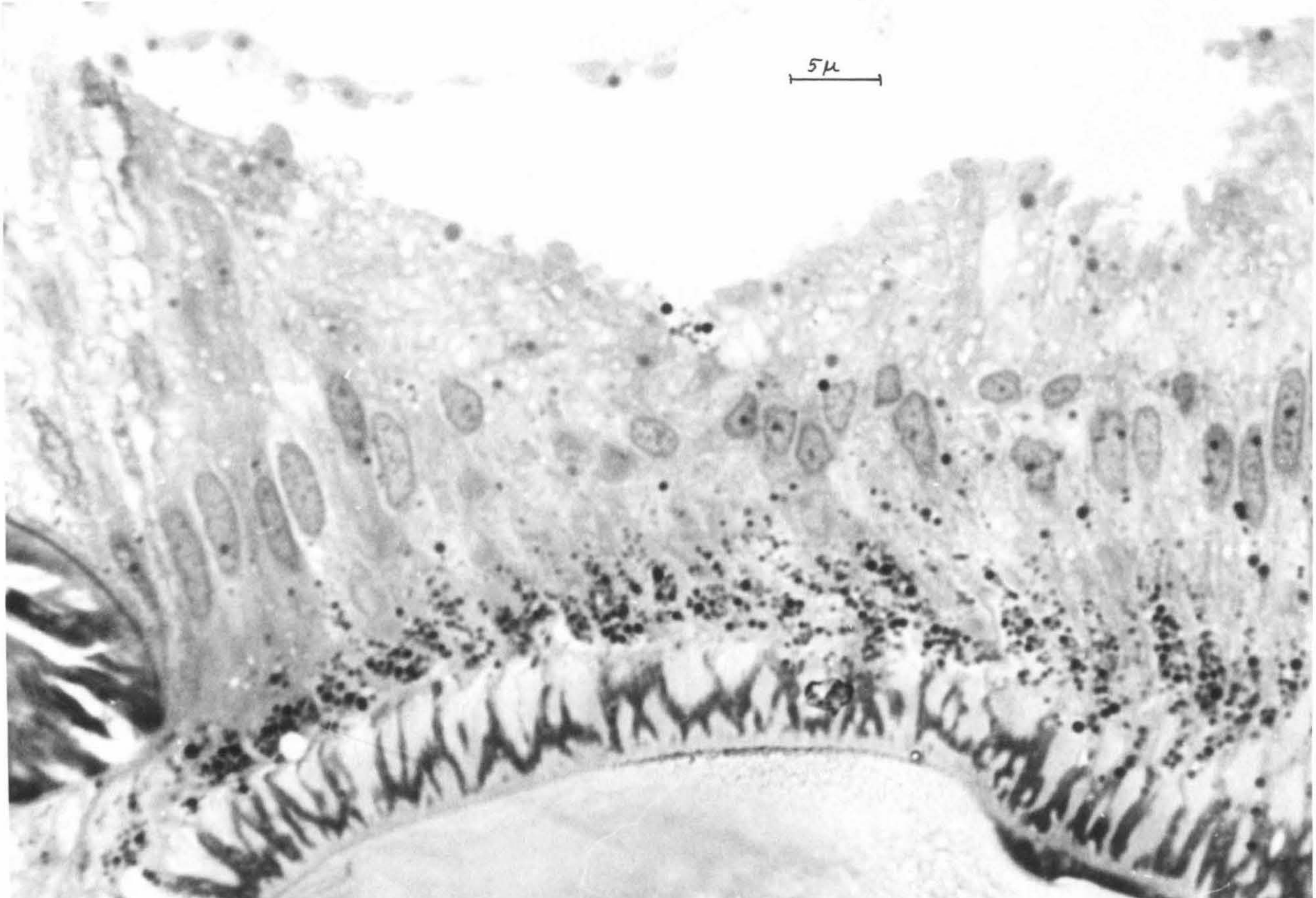
5μ

granules and the tooth cusp (13,40). This terminal zone contains no iron detectable by the Prussian blue method. Toluidine blue-Azure II staining shows this region to be formed of a densely-stained portion, present as a band contiguous to the granule zone and as thin projections towards the cusp, and a very weakly-stained layer that terminates on the cusp surface.

The Ultrastructure of the Basal Region.

It has been suggested by several workers (15,18,39) that the basal ends of the cusp cells are the site of uptake of the iron needed for the process of cusp mineralization. These workers suggest that the source of iron is either the blood or amoebocytes in the connective tissue. This view is based on general anatomical considerations and on the presence of large iron-containing granules at the basal pole of the cusp cells. Examination of this region in the electron microscope reveals several distinctive features which tend to support and strengthen this hypothesis.

(a) The Dorsal Sinus.

On the basis of the appearance of the boundaries of the dorsal sinus, in the light microscope and in the electron microscope, we have inferred that the lumen of the dorsal sinus is lined with an extremely thin wall, composed of a single layer of flattened endothelial cells (Figures 7-12,18,19,22,23). Dorsally, the endothelial lining appears to be directly apposed to the connective tissue sheath; ventrally, the endothelial cells are separated from the basal ends of the superior

Figure 7. Low power electron micrograph of the basal region of the cusp cells of L. *hartwegi*. Note the endothelial cells lining the dorsal sinus. The endothelial nucleus has pulled away from the underlying basement material during fixation. Observe the banding pattern in parts of the basement material. Note the iron-containing dense granules in the cytoplasm of the cusp cells. Note also the ramifying intercellular spaces.

X 8100.

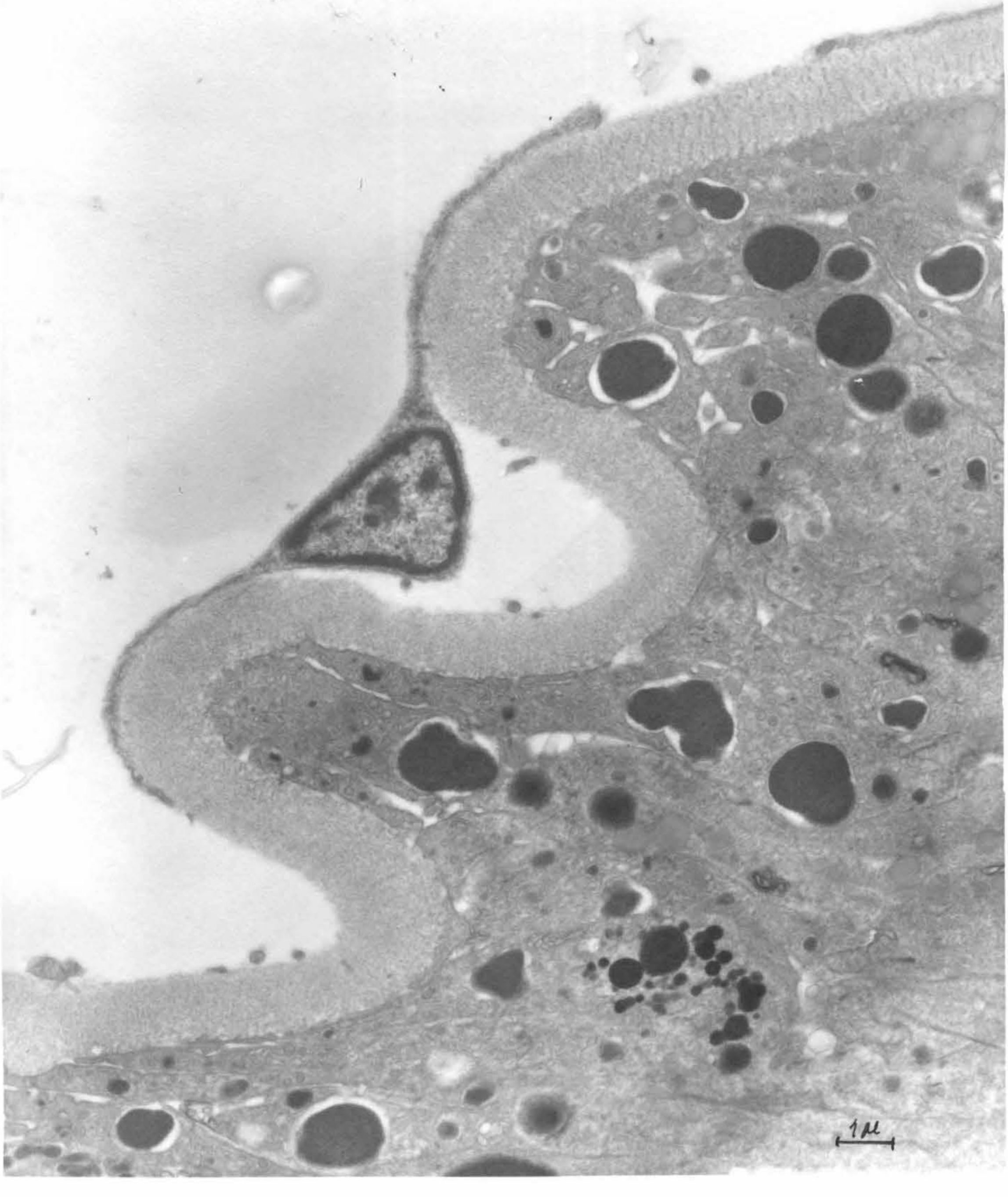
1µ

epithelial cells by a layer of extracellular material, which we call the basement material.

We have not been able to unequivocally demonstrate the continuity of the endothelial lining. Often, gaps occur between the endothelial cells, the cells are frequently pulled away from the basement material, and in many areas the cells cannot be detected at all (Figures 7,11).

The endothelial layer appears to be highly delicate, and hence, is probably quite prone to the creation of artifacts in the course of specimen preparation. Non-ideal fixatives, the process of dehydration, and the necessary handling of the tissue all cause distortion, shrinkage, and even loss of the endothelial cell layer.

The cells of the endothelium contain a flattened nucleus which usually bulges into the lumen of the sinus (Figure 22). The cytoplasm contains scattered cisternae of rough endoplasmic reticulum and a few mitochondria (Figures 8,9,12,19). Often, membrane-bound vacuolar structures are observed in the cytoplasm. These vesicles contain an amorphous-looking substance of low electron-density in which electron-dense 60 Å micelles, identical to ferritin, are frequently embedded (Figure 8).

In some specimens, the lumen of the dorsal sinus also contains clumps of similar amorphous material which include several electron-dense ferritin-like structures (Figures 10,11,12). Further posteriorly in the dorsal sinus (close to its blind end), the lumen often appears to contain a much higher concentration of these clumps, as well as a number of cells (Figure 13). These cells have properties similar to

→ p59

Figure 8. Higher power view of the endothelial cell and the basement material. Note the endoplasmic reticulum, the dense body, and the mitochondria in the endothelial cell. Also note the vesicle that contains ferritin-like micelles.

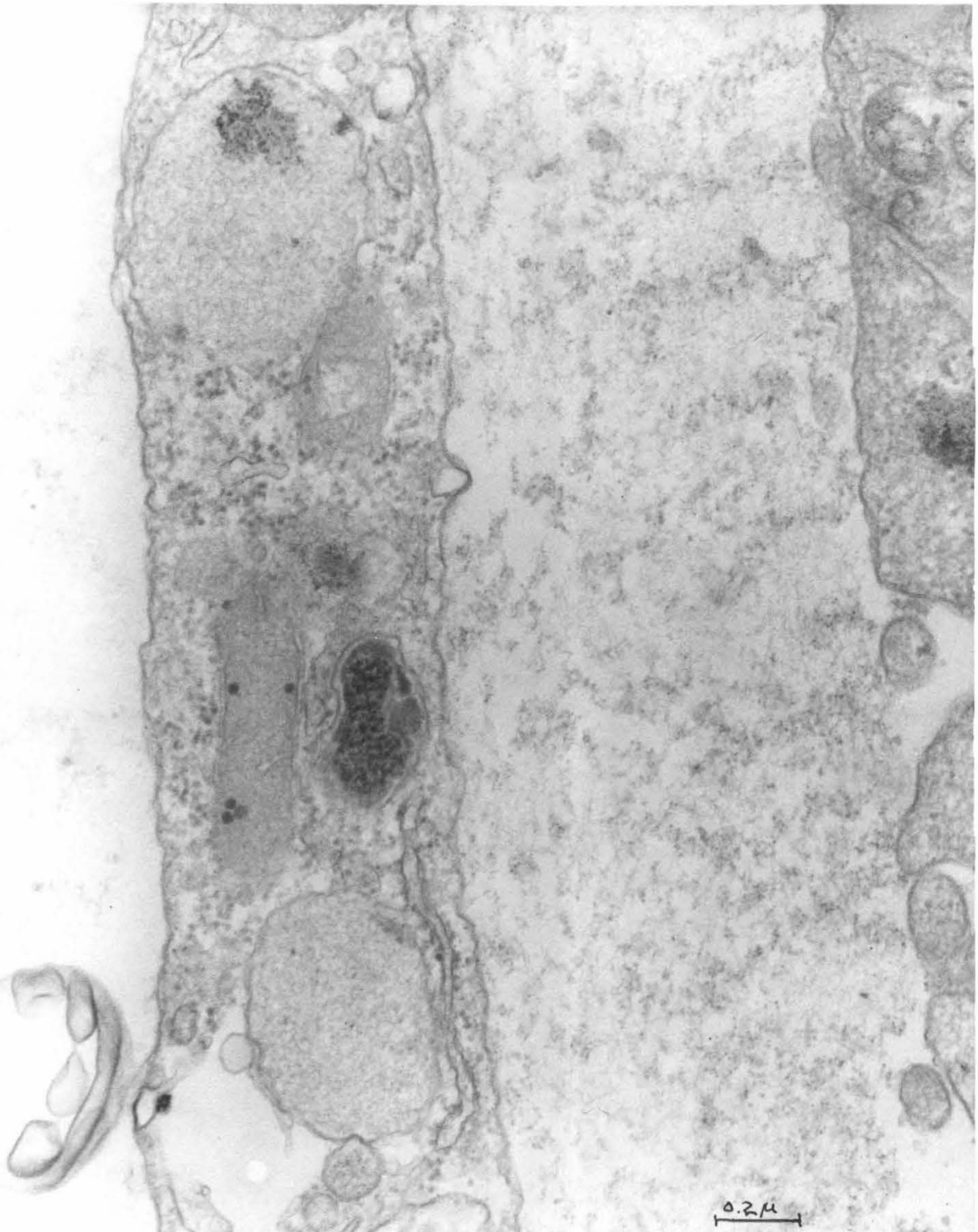
0.2μ

Figure 9. Higher power view of the region of the basal pole of the cusp cells. Note the ferritin within the intercellular spaces. Observe that no ferritin is associated with the cell membranes of the mitochondria-containing minor cells at the bottom.

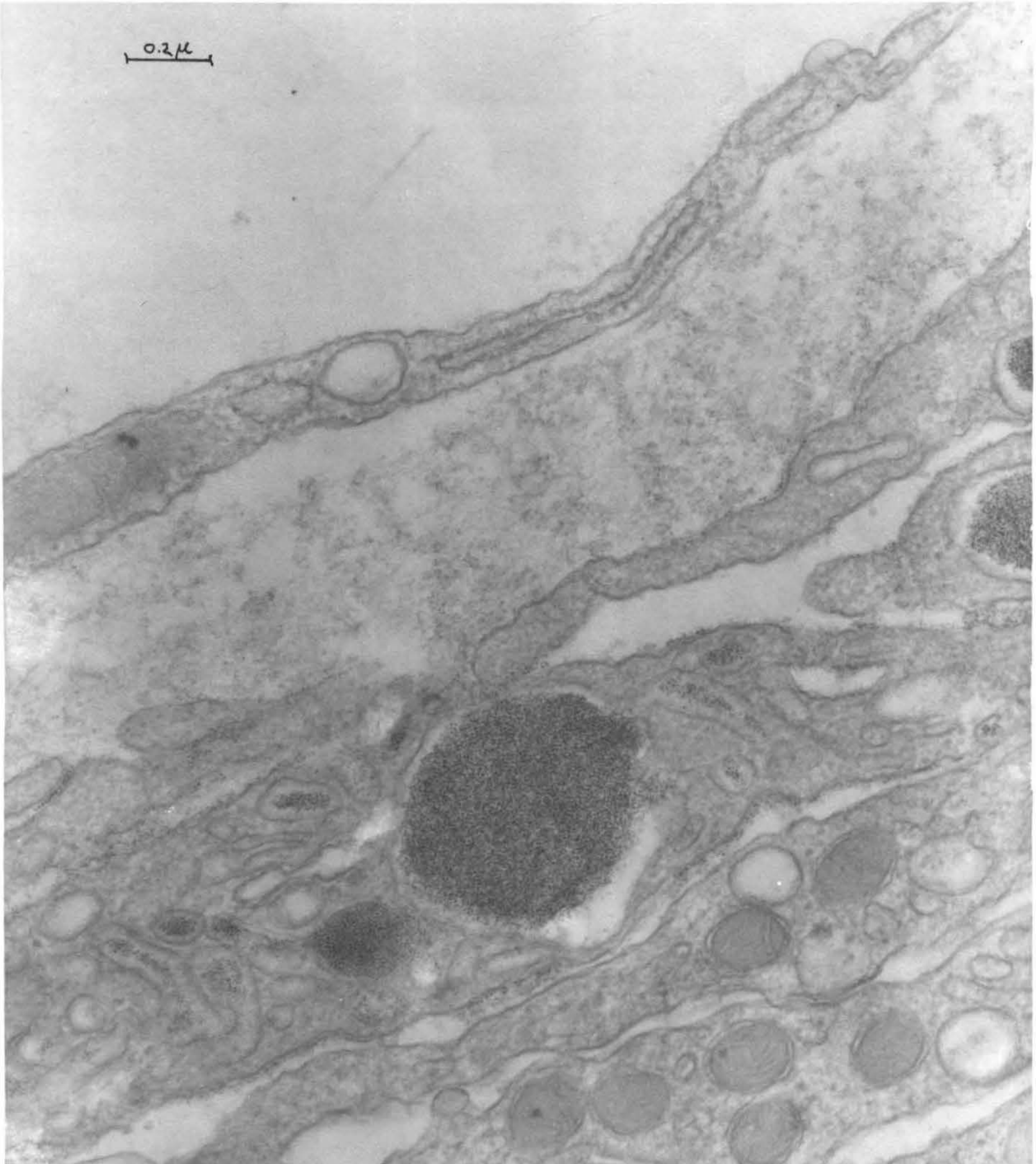
0.2μ

Figures 10 and 11. The same region as in Figures 8 and 9. Note especially, the presence of ferritin-like 60 Å micelles within the lumen of the dorsal sinus.

Figure 10: X 35,600.

Figure 11: X 65,000.

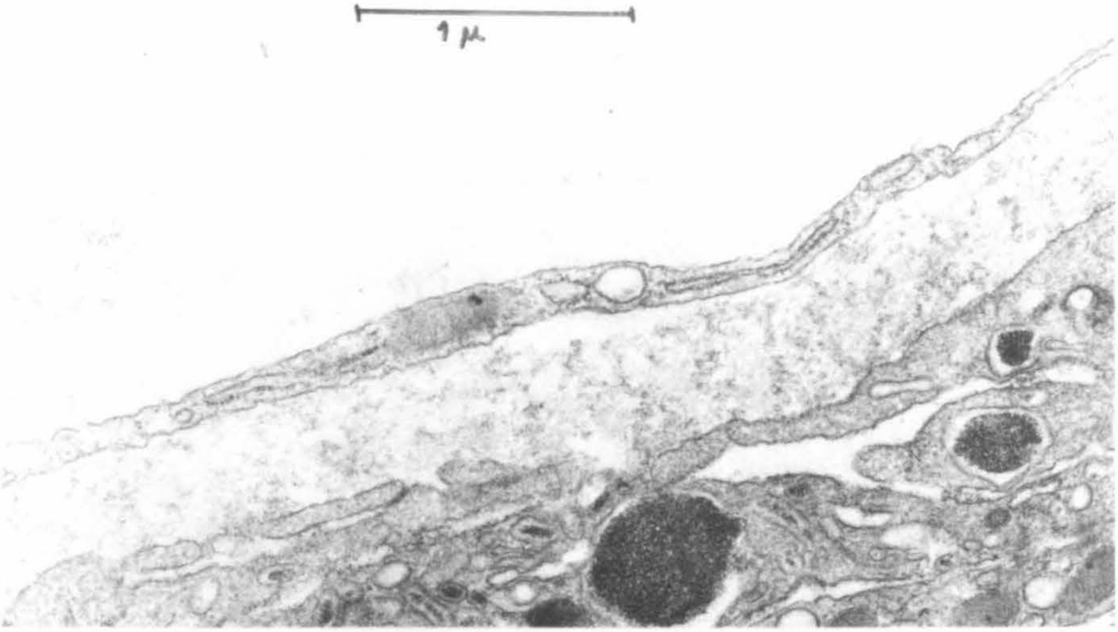
1 µ

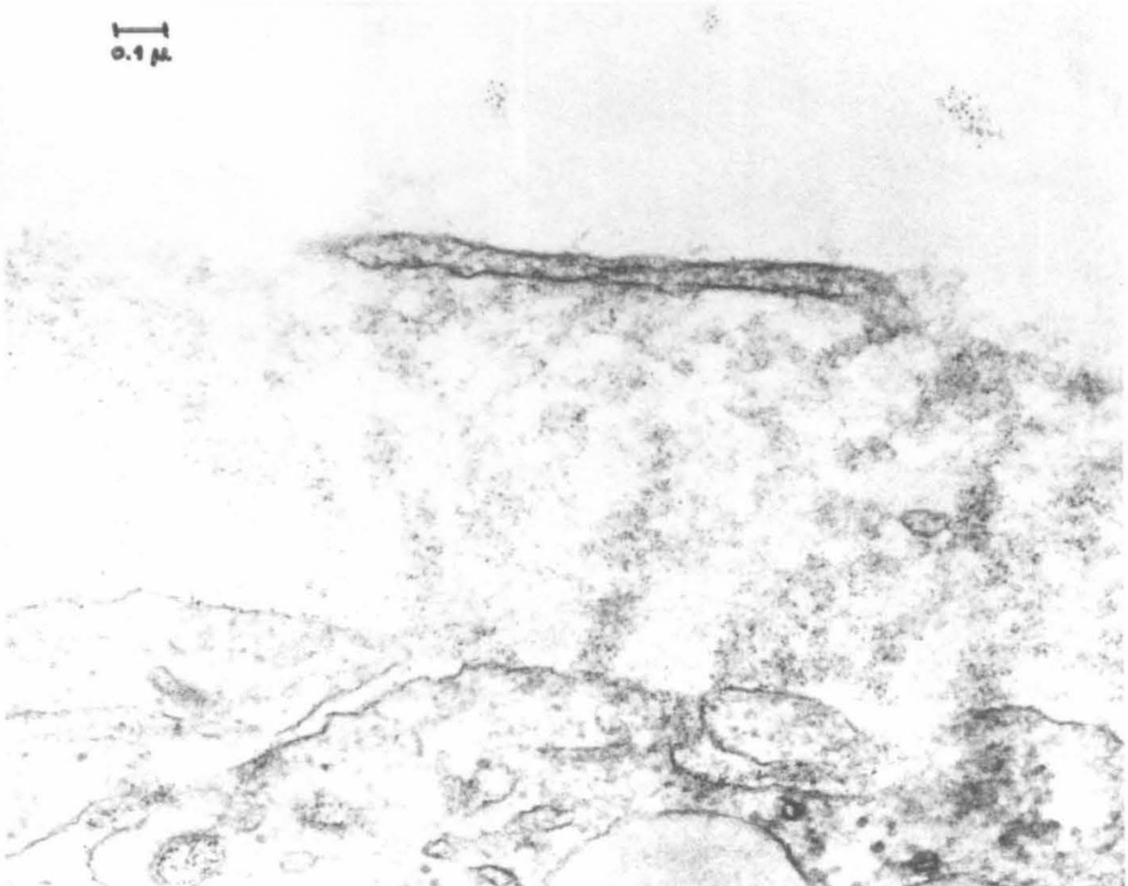
0.1 µ

Figure 12. The same region as Figures 10 and 11. Note the ferritin-like material in the lumen of the sinus. Also note the occurrence of dense micelles apparently free in the cusp cell cytoplasm.

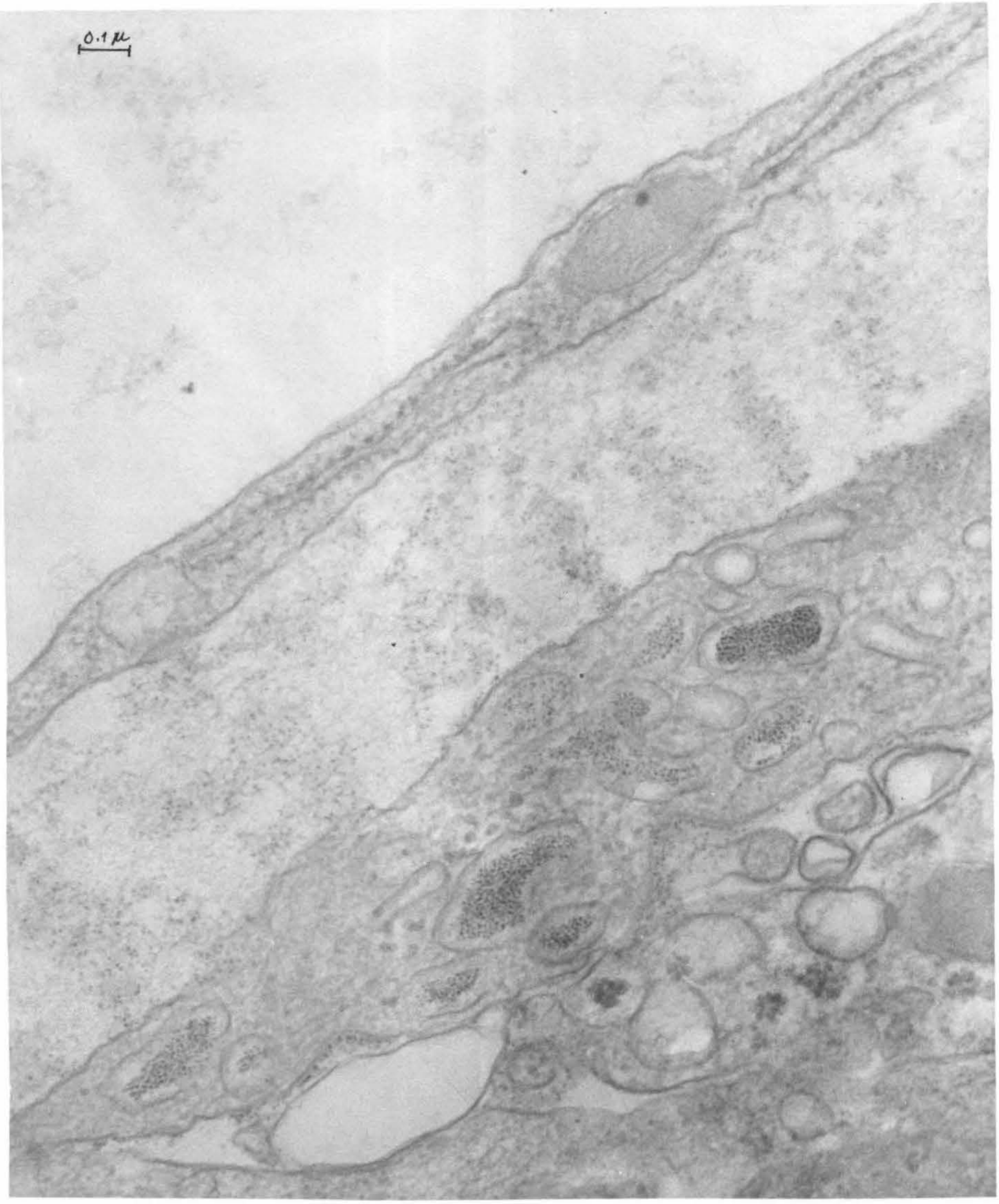
0.1 μ

Figure 13. The lumen of the dorsal sinus at the posterior of the radula sac. Note the numerous micelle-containing aggregates. Note also the cell consisting of a large nucleus and some ribosome-rich cytoplasm.

X 58,000.

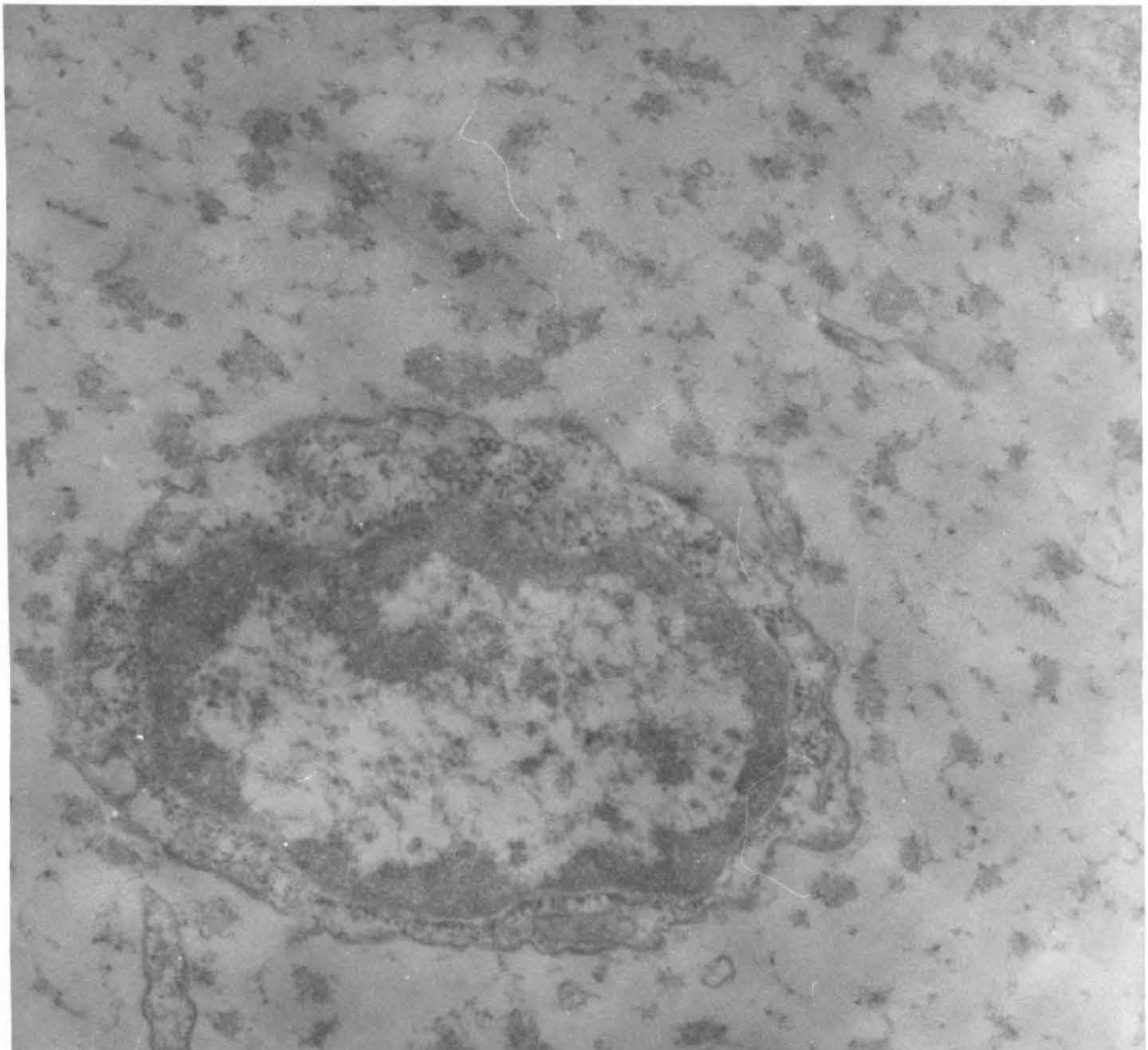

the blood amoebocytes described by Arvey and Gabe (75). They consist of a large nucleus and a small amount of ribosome-rich, basophilic cytoplasm.

We suggest that the material observed in the lumen of the dorsal sinus is representative of blood, and that the dorsal sinus is part of the haemal system of the chiton. Direct proof of these assertions must await an anatomical investigation of the origin of the sinus, which is presumably located toward the anterior of the radula sac.

(b) The Basement Material.

The basement material forms a continuous layer between the endothelium and the superior epithelial cells. Its thickness varies greatly, ranging from less than 0.1 μ, where it is contiguous to the basal ends of the minor cells (Figures 22,23), to over 1.5 μ, where it contacts the cusp cells (Figures 7-12). Probably, the basement material is strongly bound to the superior epithelial cells, since it remains intact even in regions where the endothelial cells are no longer present (Figures 7,11).

In the medial region, near the cusp cells, the basement material is of rather uniform thickness (∿ 1.5 μ), but it is quite inhomogeneous in appearance. Where it is transversely sectioned, one can see electron-dense bands 40-50 mμ thick, alternating with wider, less-dense zones, with a repeat period of about 200 mμ (Figure 7). In tangential view, the electron-dense regions form a regular array of polygonal units which are about 200 mμ on a side (Figure 15). Most of the patterns of the dense material which we have observed in numerous sections can be derived from a model in which the dense material is arranged in long, parallel, straight-sided honey-comb-like partitions.

At higher magnification, the electron-dense regions are seen to be produced by bands of concentrated 60 Å micelles of ferritin-like material (Figures 8,9,14,16-21). The less-dense zones are composed of very fine, possibly fibrillar, material less than 30 Å in diameter. We have not observed any apparent correlation of the position of the dense bands with any visible structures of either the endothelial or the cusp cells.

Near the minor cells, the basement material consists of a thin layer of material which is similar to that of the less-dense zones near the cusp cells (Figures 22,23).

(c) The Basal Pole of the Cusp Cells.

The basal region of the superior epithelial cusp cells contains numerous large iron-containing granules. In this area, the tissue has a "spongy" appearance, due to the extensive development of a system of intercellular and extracellular spaces (Figures 7,9,12,18,19,20). These ramifying channels produce a large increase in the surface area of the basal termini of the cells. Most of the spaces contain many electron-dense micelles, typical of ferritin molecules. Many sites along the proliferated plasma membranes have an appearance which is highly characteristic of the process of rhopheocytosis, a phenomenon, related to pinocytosis, by which cells incorporate macromolecules (76). The cell membranes, whether in contact with the basement material or the intercellular spaces, show numerous vesicles in all stages of form-

Figure 14. A transverse section through the basement material. Note the repeating bands of concentrated ferritin. Also note the rhopheocytotic invaginations of the cusp cell membrane. X 75,600.

Figure 15. An oblique section through the basement membrane. Note the regular pattern of electron-dense material. X 39,200.

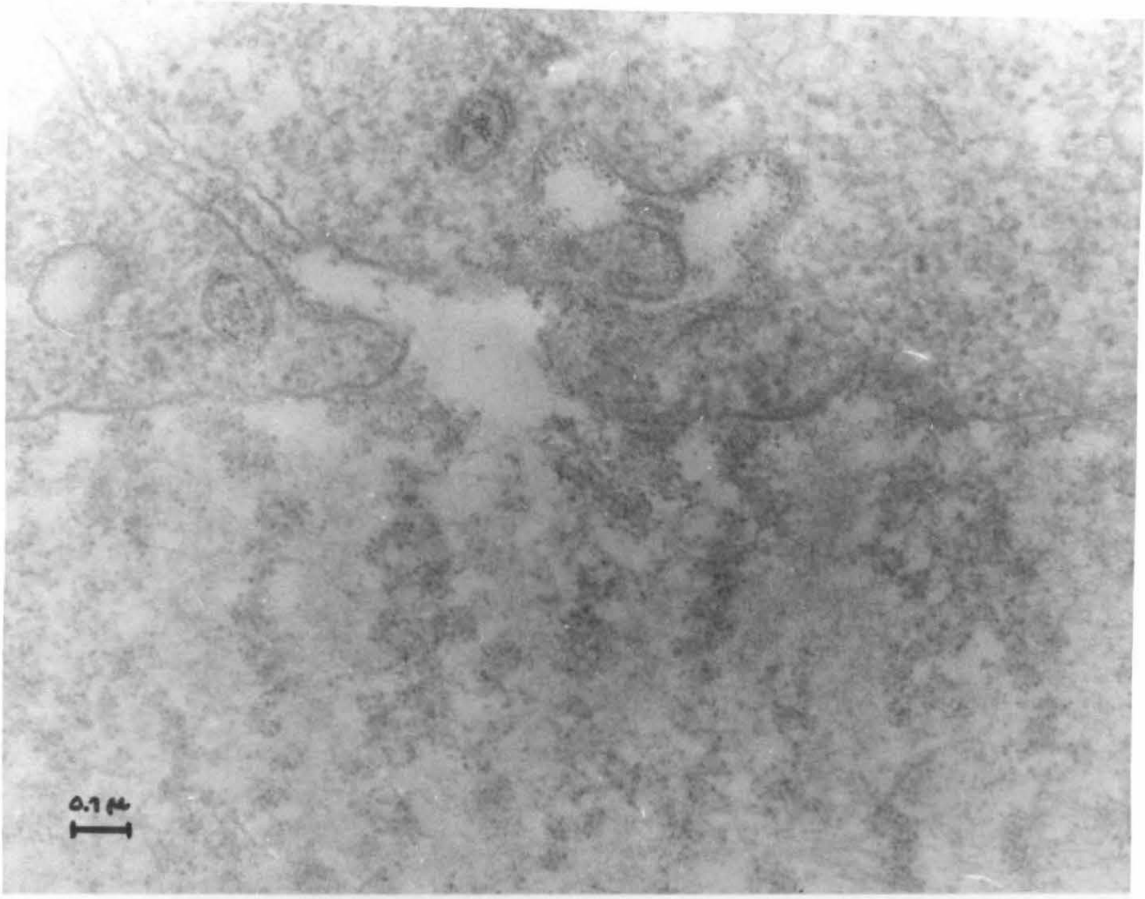
0.1 μ

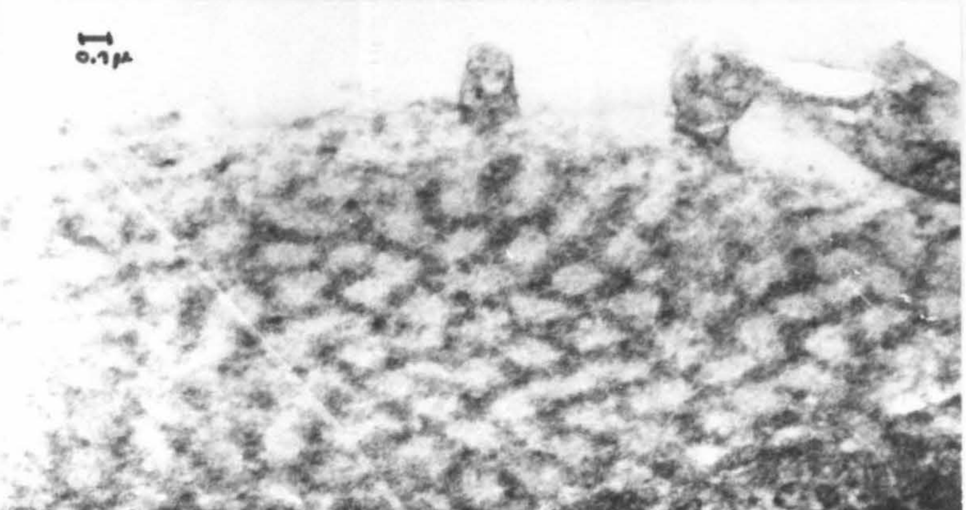
0.1 μ

Figures 16 and 17. The basal end of the cusp cell. Note the rhopheocytotic vesicles on the basal membrane of the cell.
Figure 16: X 53,300.
Figure 17: X 82,500.

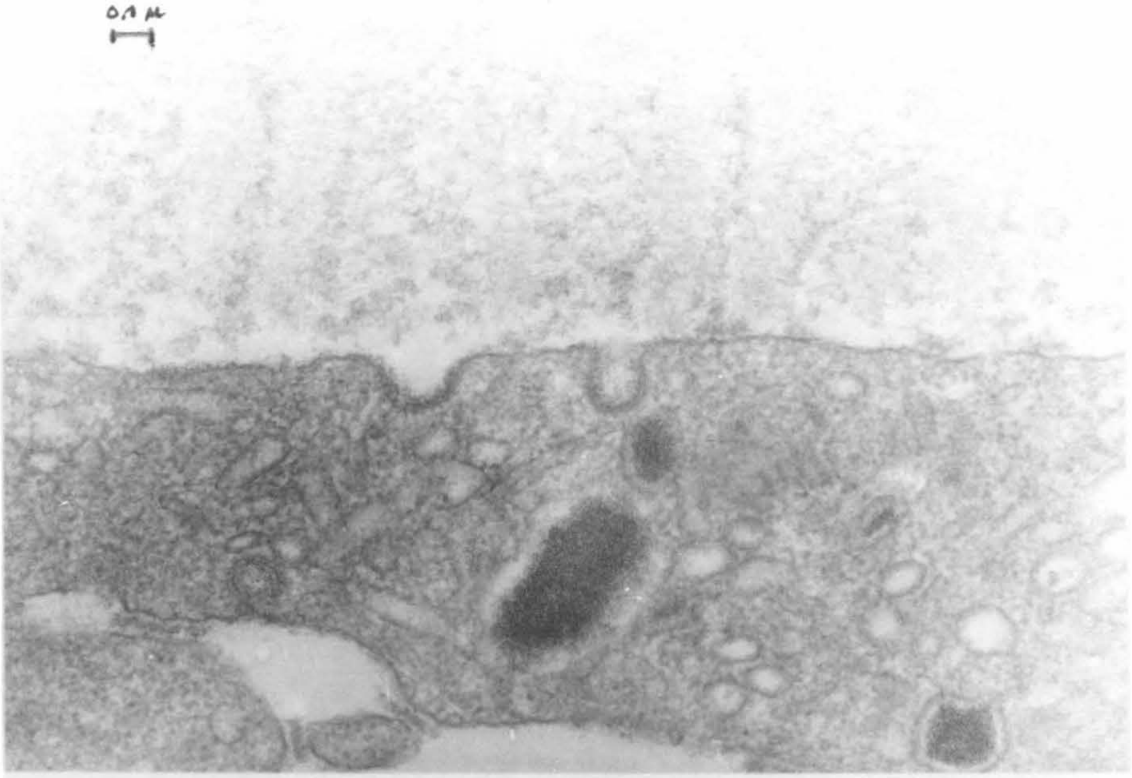
0,1 µ

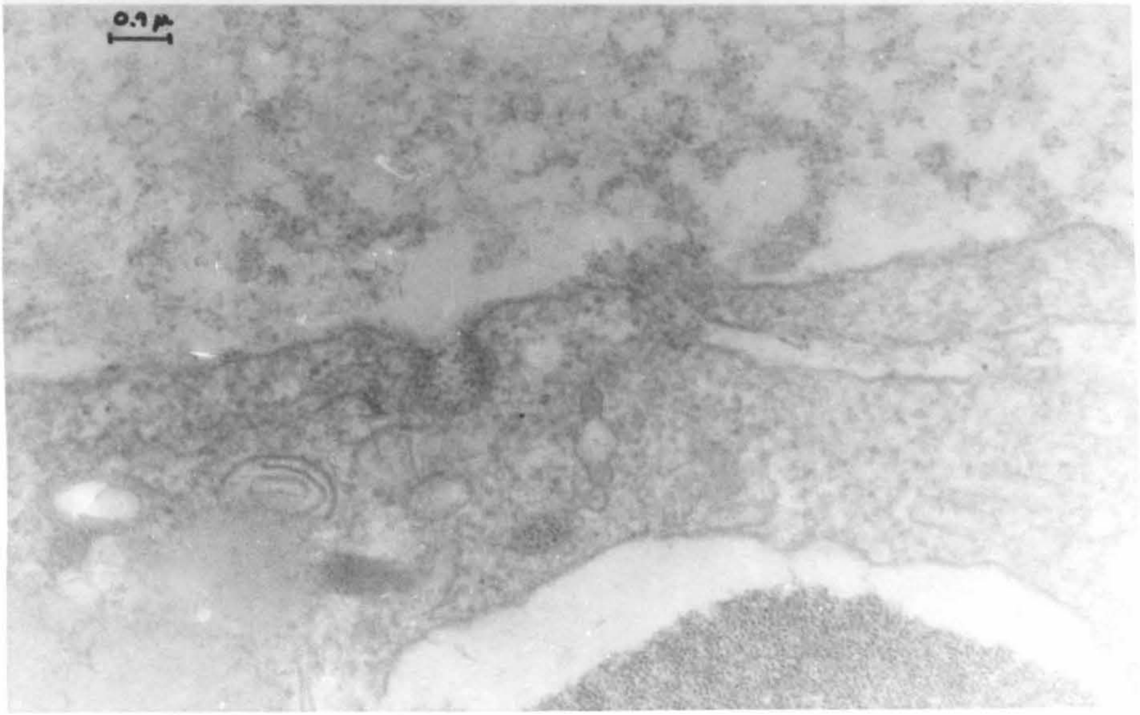
0.1 µ

ation (Figures 9,14,16-21). In the presumed order of their development, there are slightly depressed regions of ferritin-coated cell membrane (Figures 9,14,20), shallow, rounded ferritin-containing invaginations (Figures 16,17,20,21), and deeper invaginations with a constricted neck (Figures 16,17,20,21). Throughout the basal cytoplasm, there are small membrane-bound vesicles, filled with varying numbers of ferritin molecules. Some of these undoubtedly represent cross-sections through extracellular channels, but many are intracellular vesicles which have been pinched off from the plasma membrane. Presumably, the vesicles migrate into the cells and combine with others to form the larger ferritin-containing granules that are present in this region (Figures 7,9,20). All of the ferritin-containing granules of the basal region that we have observed can be classed as paracrystalline (13,40).

Nearly all of the intracellular ferritin is present within membrane-bound vesicles. In certain areas, however, some ferritin molecules appear to occur free in the cytoplasm (Figures 12,18,19). We believe that these sites mark the location of tangentially grazed membrane-bound granules, and are not caused by the diffusion of ferritin molecules across the cell membranes.

We have not seen any mitochondria in the basal region of the cusp cells (cf. Figure 7). Many sections contain large membrane-bound vesicles (0.5 to 1.5 μ in diameter), which are filled with an amorphous, lightly staining substance (Figures 7,11,17,19). The composition and function of these structures is unknown at the present time.

Figure 18. The basal end of the cusp cell. Note the numerous ferritin-containing vesicles within the cytoplasm. Note also the invaginated ferritin-coated membranes lining the intercellular spaces.
X 46,500.

Figure 19. Note the granules, filled with amorphous material, in the cusp cell cytoplasm.
X 46,500.

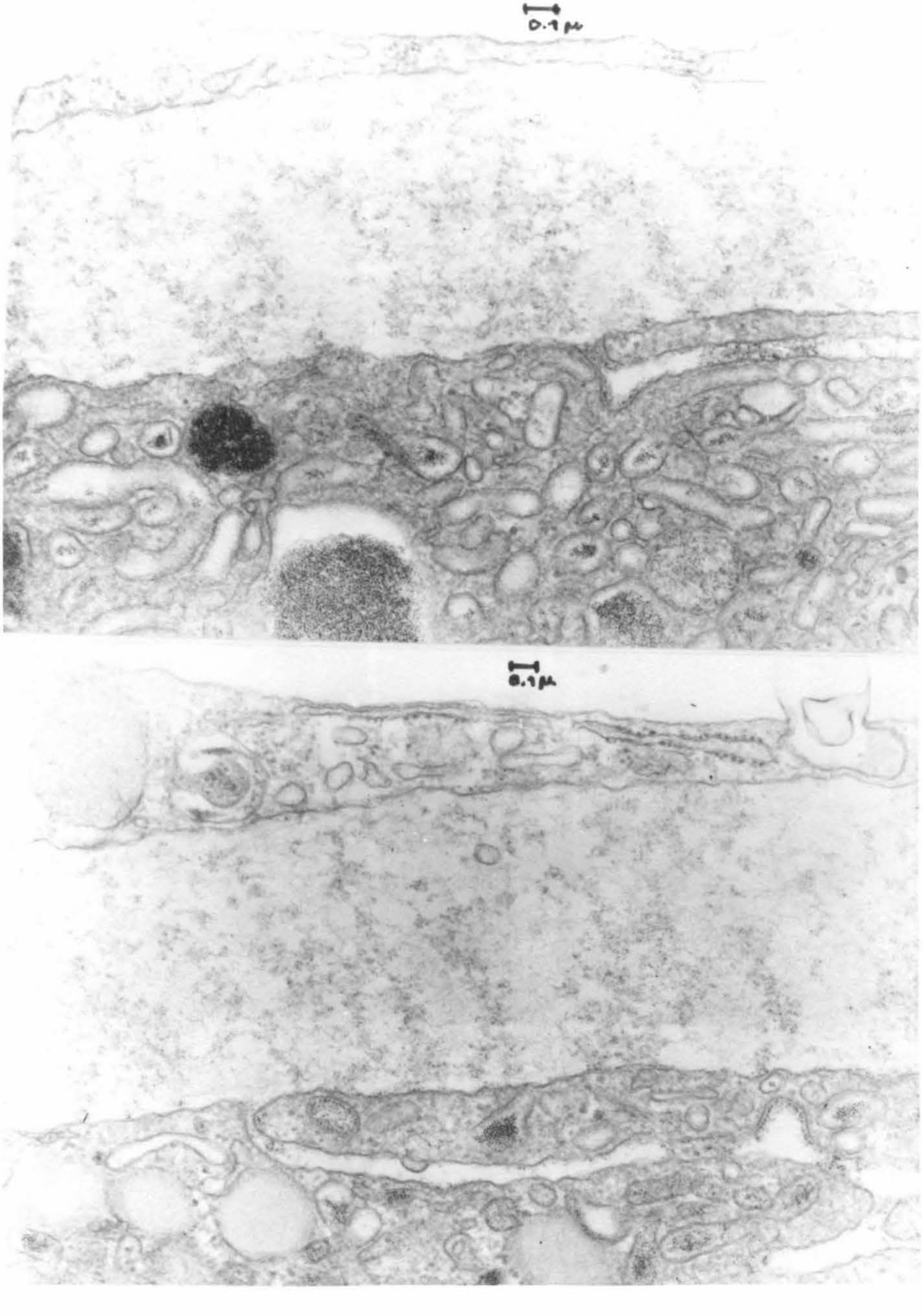
0.1 μ
0.1 μ

Figures 20 and 21. Higher resolution view of the rhopheocytotic vesicles.

Figure 20: X 107,000.

Figure 21: X 122,000.

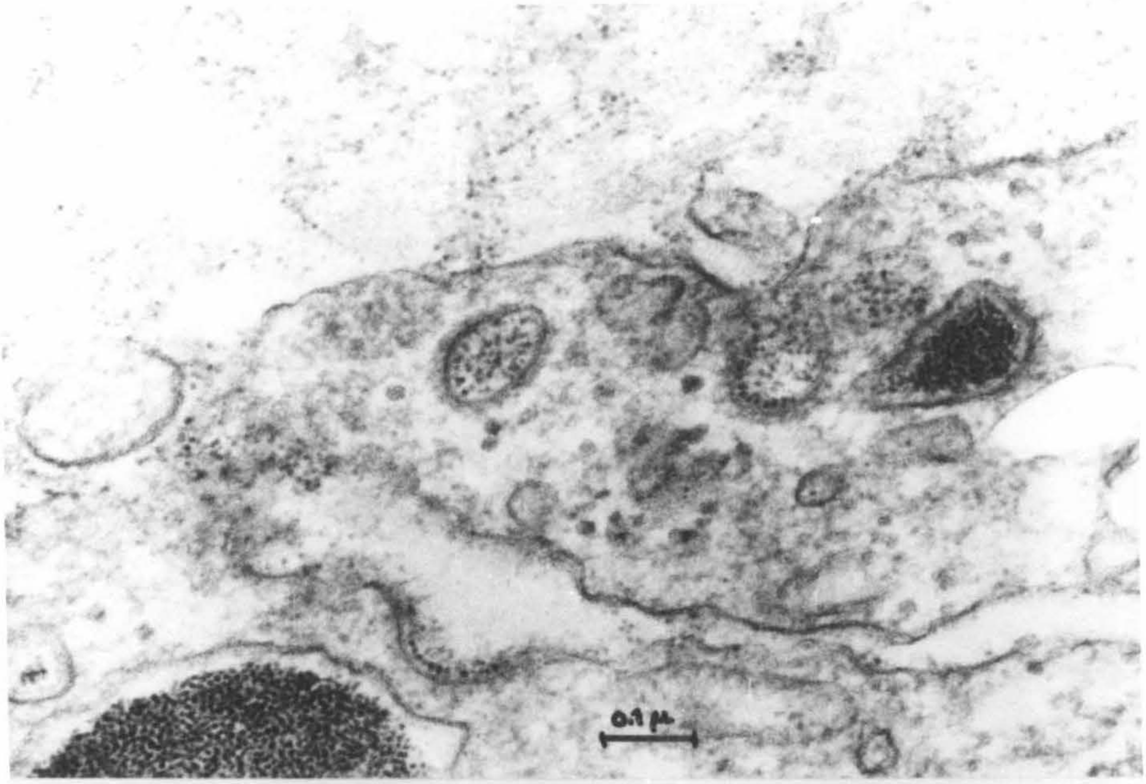

0.1 μ

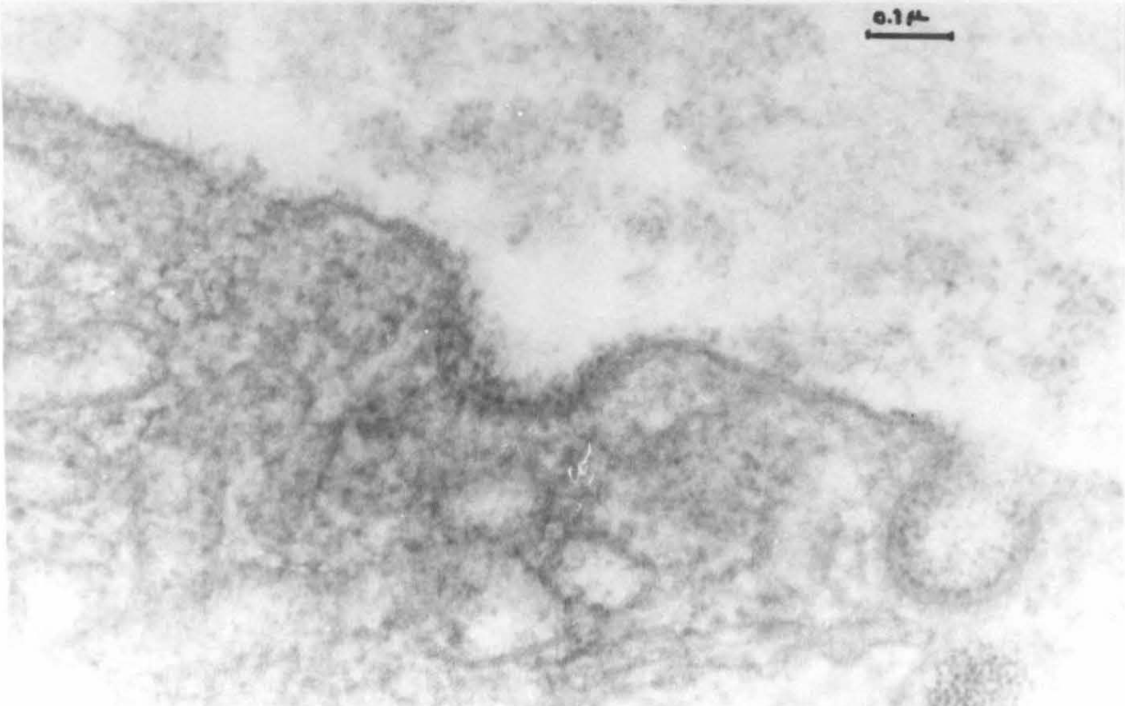

0.1 μ

(d) The Basal Pole of the Minor Cells.

The minor cells can be readily distinguished from the cusp cells by a number of criteria. The minor cells are generally of small diameter, and they always contain a large number of densely-staining mitochondria, which are uniformly about 0.2 μ in diameter and 1.0 μ long (Figures 23-25). There are well-developed intercellular spaces, but, although ferritin molecules are sometimes visible within them (Figures 9,25), we have not observed any rhopheocytotic activity by the minor cells. In Figure 9, a mitochondria-containing minor cell can be seen lying next to a cusp cell. Although the cusp cell plasma membrane is almost completely coated with ferritin, not a single molecule of ferritin is near the cell membrane of the adjacent minor cell. We have seen no ferritin-containing granules within the basal region of the minor cells. Large numbers of vesicles that contain amorphous material, similar to those described within the cusp cells, can be seen within the cytoplasm of these cells (Figures 23,24).

The Central Region of the Cusp Cells.

From the basal region to the level of the nuclei, the cusp cells possess few distinctive features, except for the ferritin-containing granules. Often, chains of ferritin granules can be observed within an individual cell (Figures 26). Typically, with increasing distance away from the basal pole, there is a reduction of the free space within the granule membrane. The deeper-lying granules are round or oval membrane-bound vesicles completely filled with ferritin molecules (Figures 26,27).

Figures 22 and 23. The basal ends of the minor cells.

Figure 22. Note the very thin layer of basement material and the endothelial cell nucleus.

X 9,180.

Figure 23. Note the intercellular spaces, the densely staining mitochondria and the granules containing amorphous material.

X 19,700.

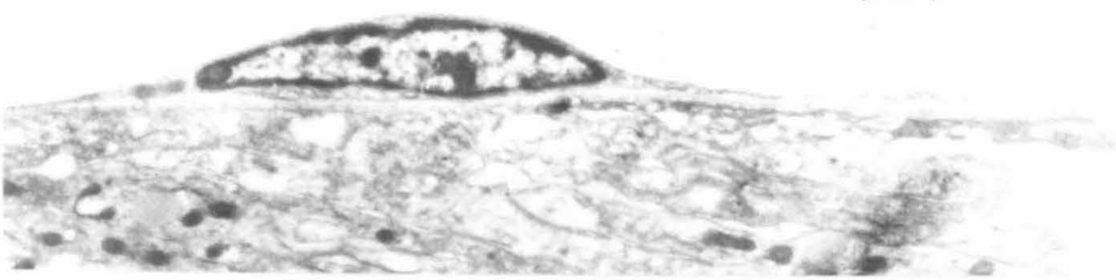
1 μ

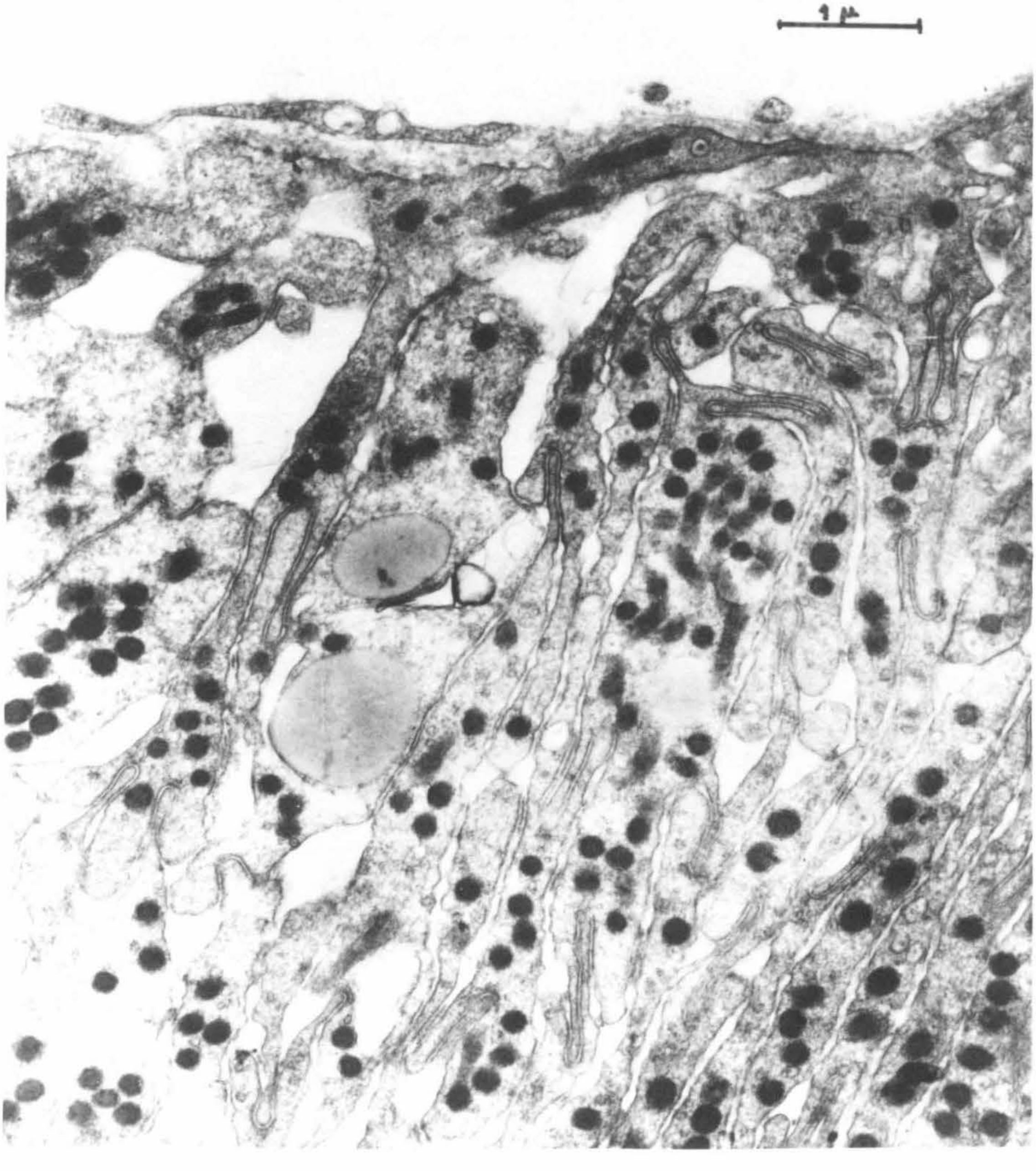
1 μ

Figure 24. Oblique section through the basal portions of the minor cells. Note the intercellular spaces and the numerous uniform mitochondria.
X 27,600.

Figure 25. Higher power view of a region similar to Figure 24. Note the ferritin micelles in the intercellular space.
X 108,800.

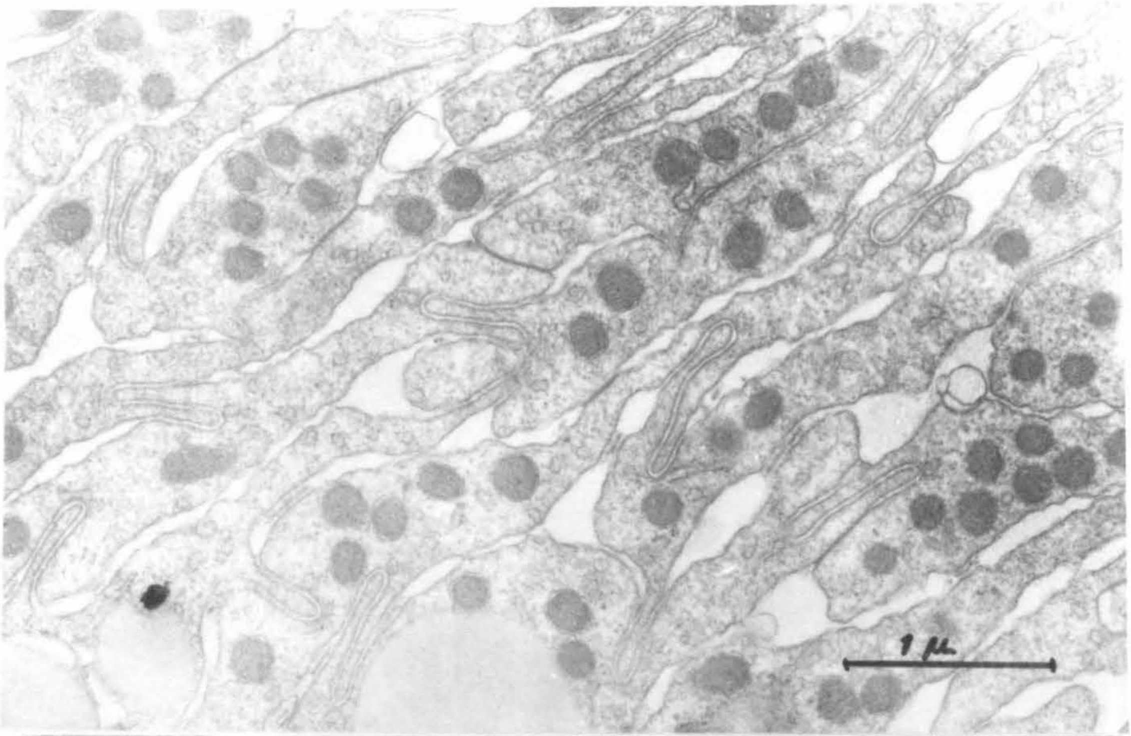
1 μ

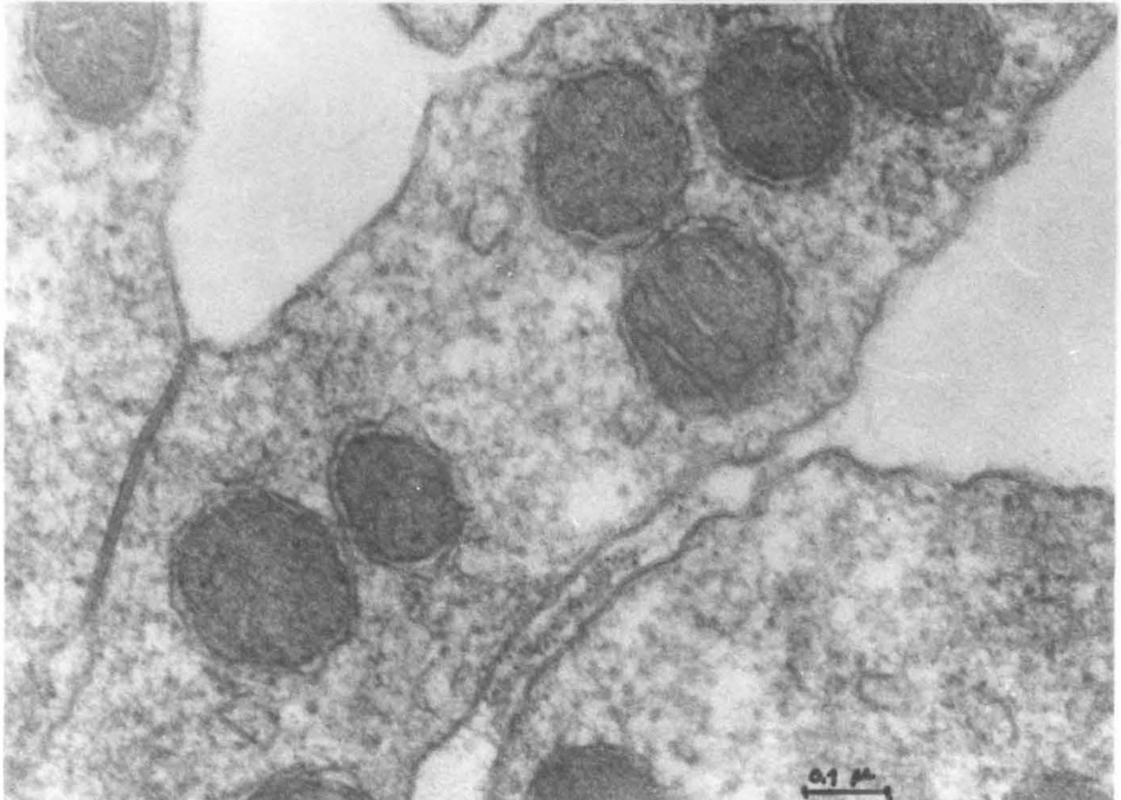
0.1 μ

Figure 26. The basal half of the central region of the cusp cells. The dorsal sinus is above. Note how the ferritin granules appear progressively more compact with increasing distances from the basal end of the cell.

X 36,400.

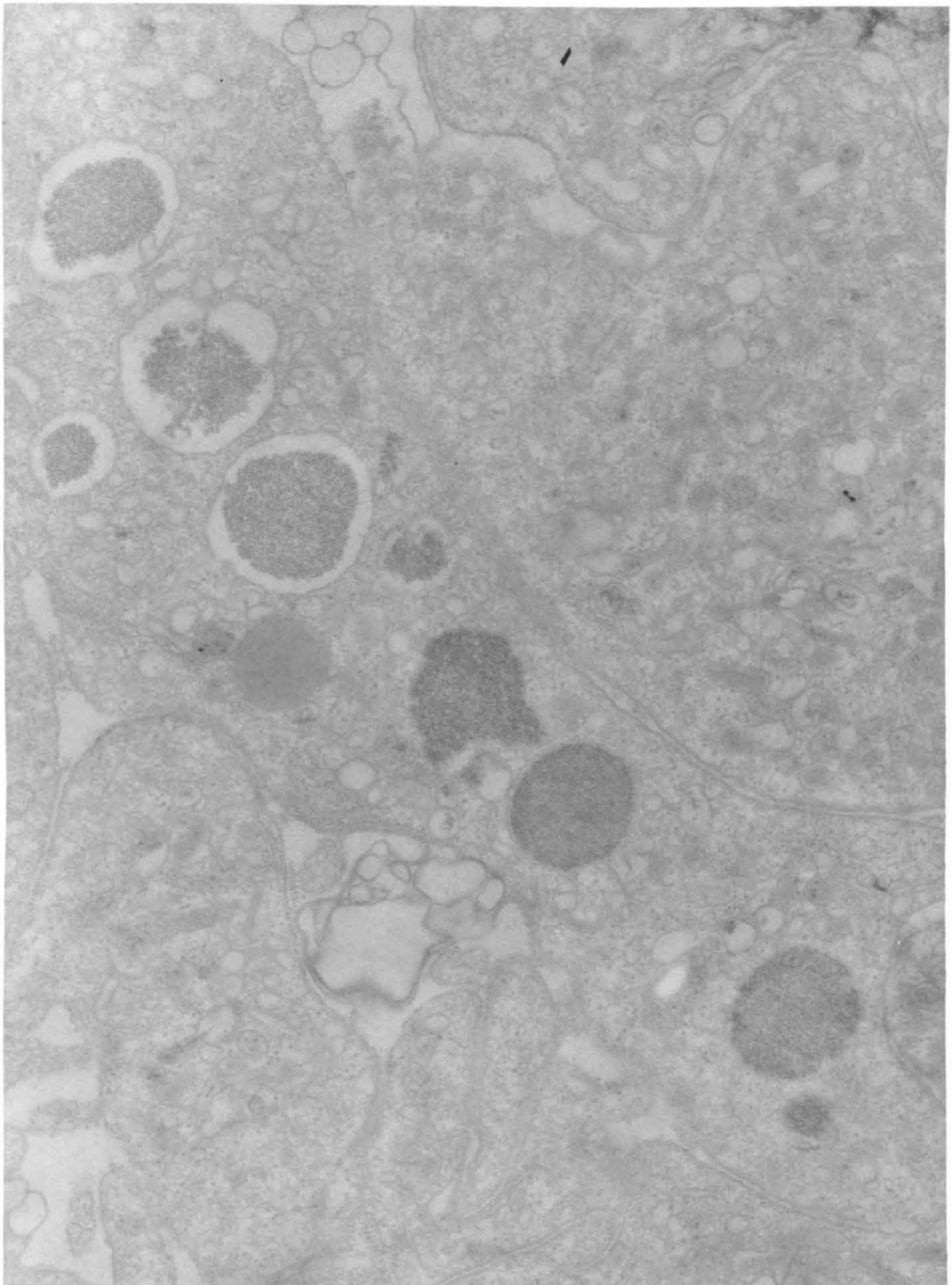

Figure 27. A transverse section through the cusp cells in the basal half of the central region. Note the interdigitation of the adjacent cells.

X 48,000.

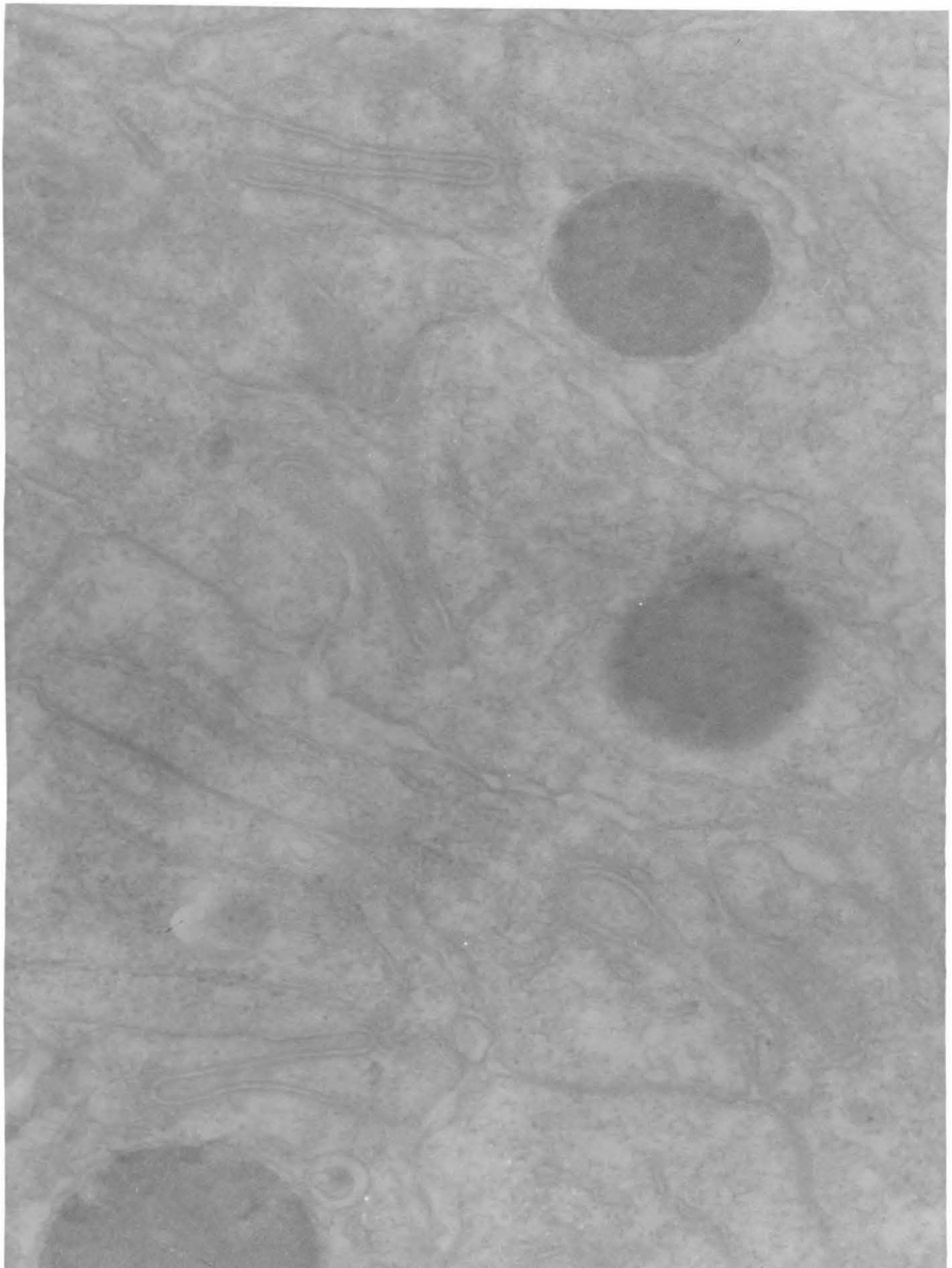

Cisternae of rough endoplasmic reticulum are present in increasing concentration towards the nucleus. Intercellular spaces, containing some ferritin molecules, can be seen throughout the central region (Figures 28,29), even at the level of the nuclei (Figure 30). In a few sections, we have observed small ferritin-filled vesicles, identical to the pinocytotic vesicles of the basal region, near the cell membranes in the central region (Figures 28,29). It is likely that there is a minor uptake of ferritin by the deeper-lying portions of the cusp cells.

The large oval nucleus is situated in the apical half of the cusp cell (Figure 6). In the perinuclear region, the rough endoplasmic reticulum is extensively developed (Figure 31). It often occurs as stacked sheets of cisternae, bearing 110 to 130 Å ribosomes on their outer surfaces (Figure 32). The interior cavities of the cisternae are generally filled with a moderately dense material. In Figure 33, several spiral arrays of ribosomes, presumably membrane-bound polysomes, can be seen on a tangentially sectioned endoplasmic membrane.

Beyond the apical end of the nucleus, the cytoplasm of each cell contains a well-developed Golgi apparatus, usually arranged parallel to the long axis of the cell (Figure 34). The Golgi apparatus is comprised of two to six flattened Golgi cisternae followed by several layers of swollen cisternae and Golgi vacuoles (Figures 34-37). The flat cisternae are about 300 Å thick (two 75 Å unit membranes and a ∿ 150 Å internal space) and contain some electron-dense material in their lumen. The larger cisternae and vacuoles are of lower internal density. Many smooth-surfaced vesicles (up to 1500 Å in diameter), which are probably

Figures 28 and 29. Longitudinal sections through the cusp cells in the basal half of the central region. Note the small ferritin-containing vesicles and the numerous ferritin molecules in the intercellular spaces.

Figure 28: X 108,000.

Figure 29: X 108,800.

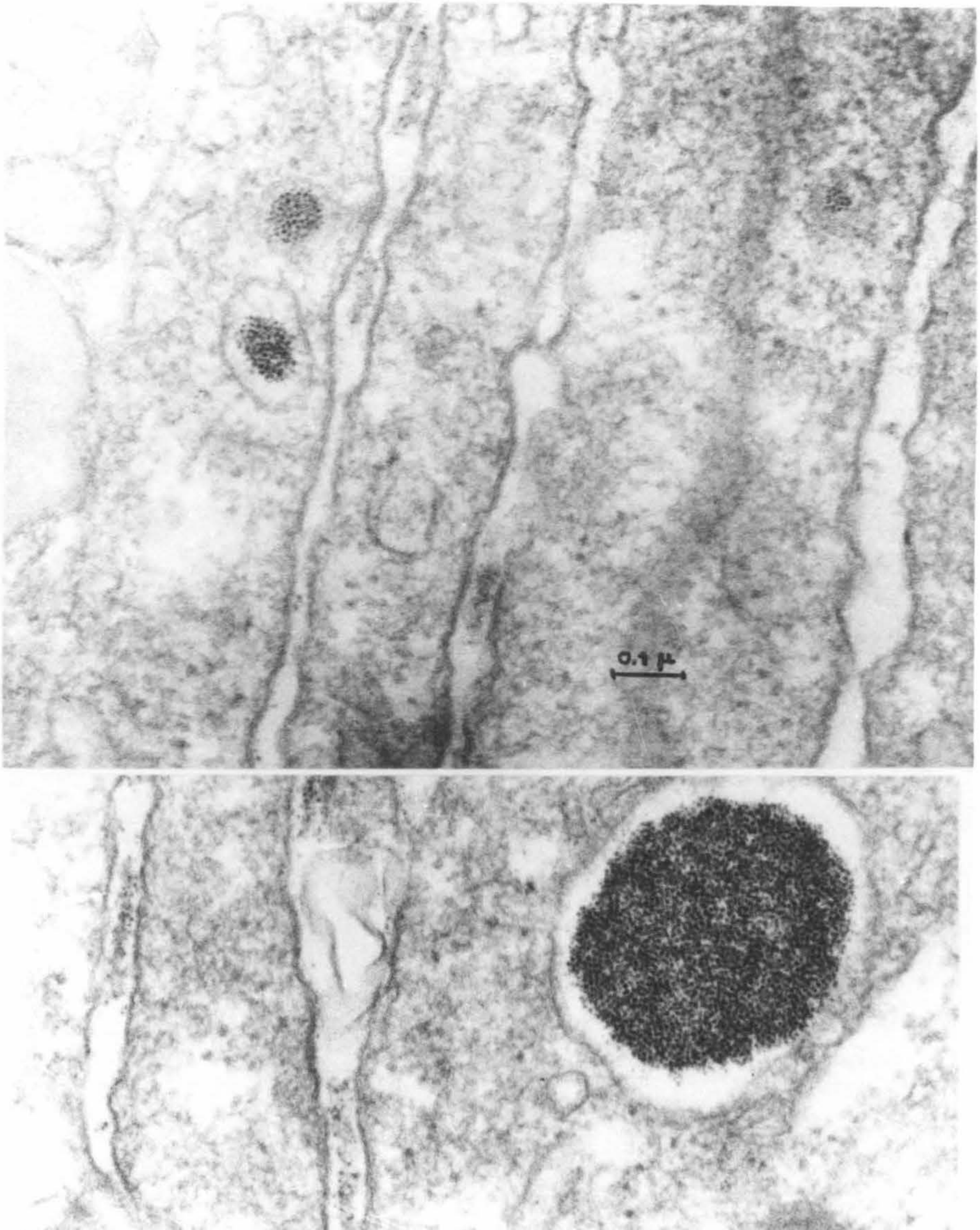
0.1 μ
0.1 μ

Figure 30. The central region of the cusp cell at the level of the nuclei. Note the ferritin micelles in the intercellular spaces.

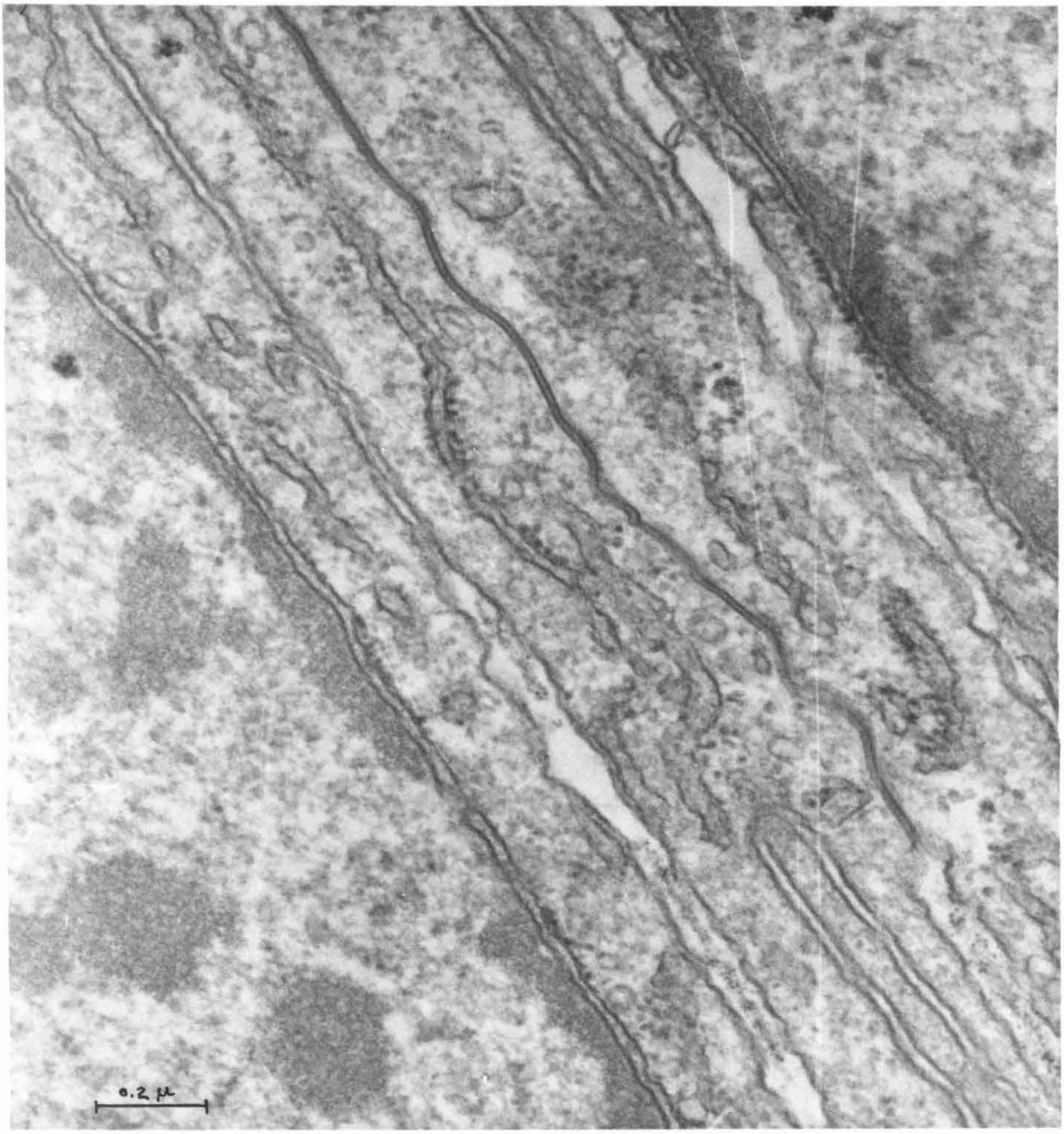
0.2 μ

Figure 31. The perinuclear cytoplasm of the cusp cell. Note the endoplasmic reticulum, bearing ribosomes, sometimes in curved arrays. The internal cavity of the endoplasmic reticulum cisternae contain electron-dense material. X 60,000.

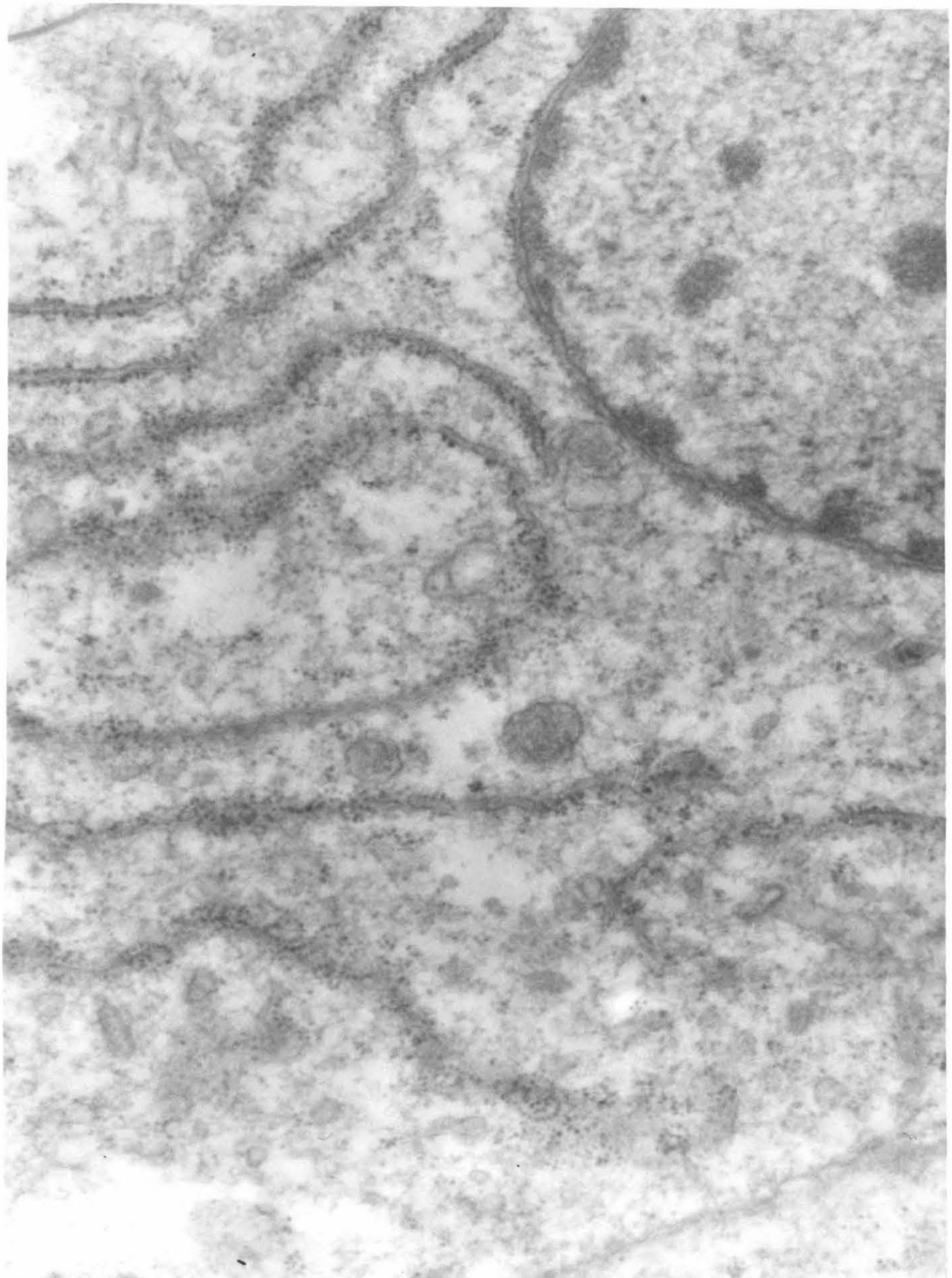

Figure 32. Stacked sheets of endoplasmic reticulum in the perinuclear cytoplasm. Note the material within the cisternae.

X 120,000.

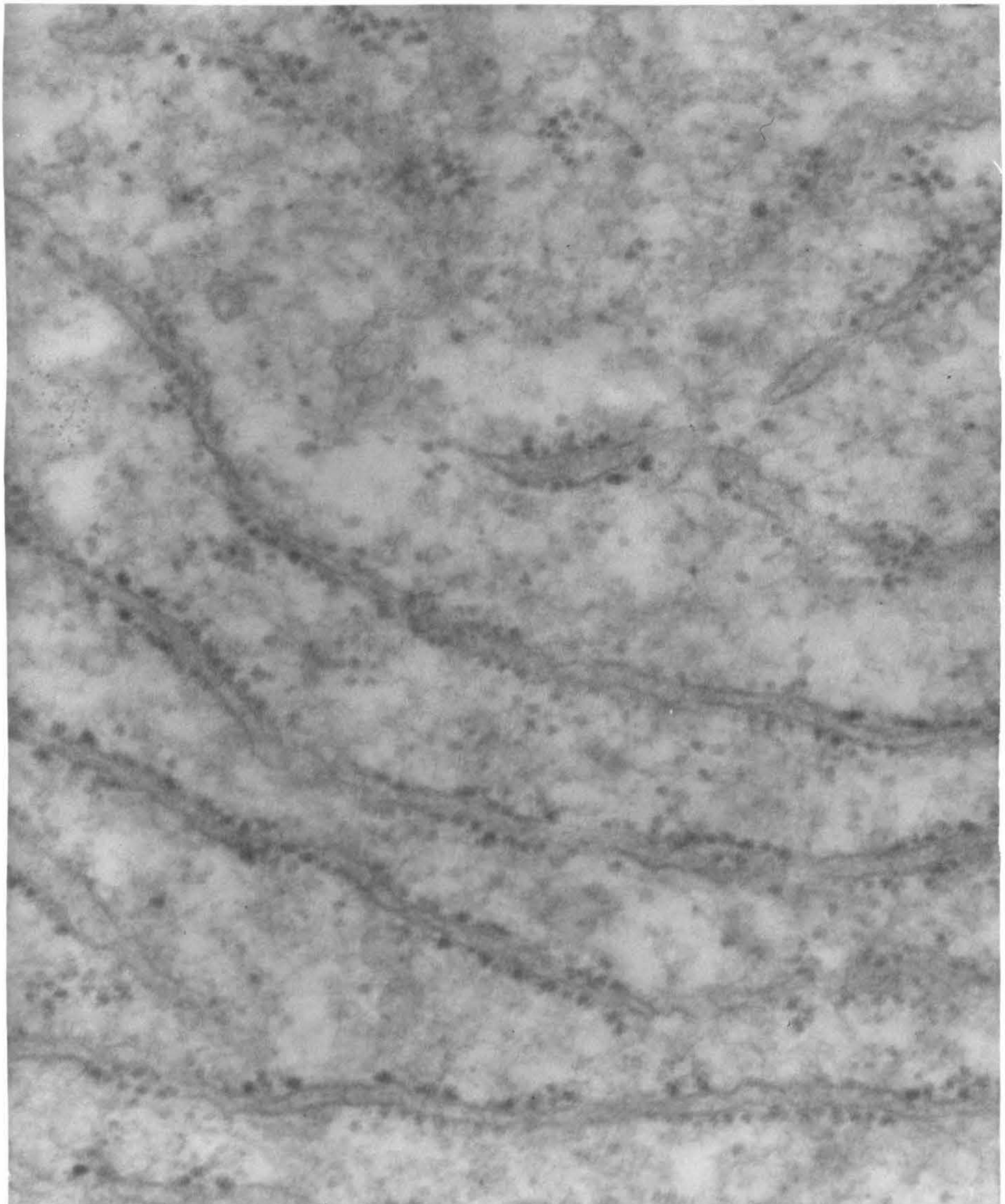
0.1 µ

Figure 33. Tangential section of endoplasmic reticulum. Note the membrane-bound polysomes.
X 88,400.

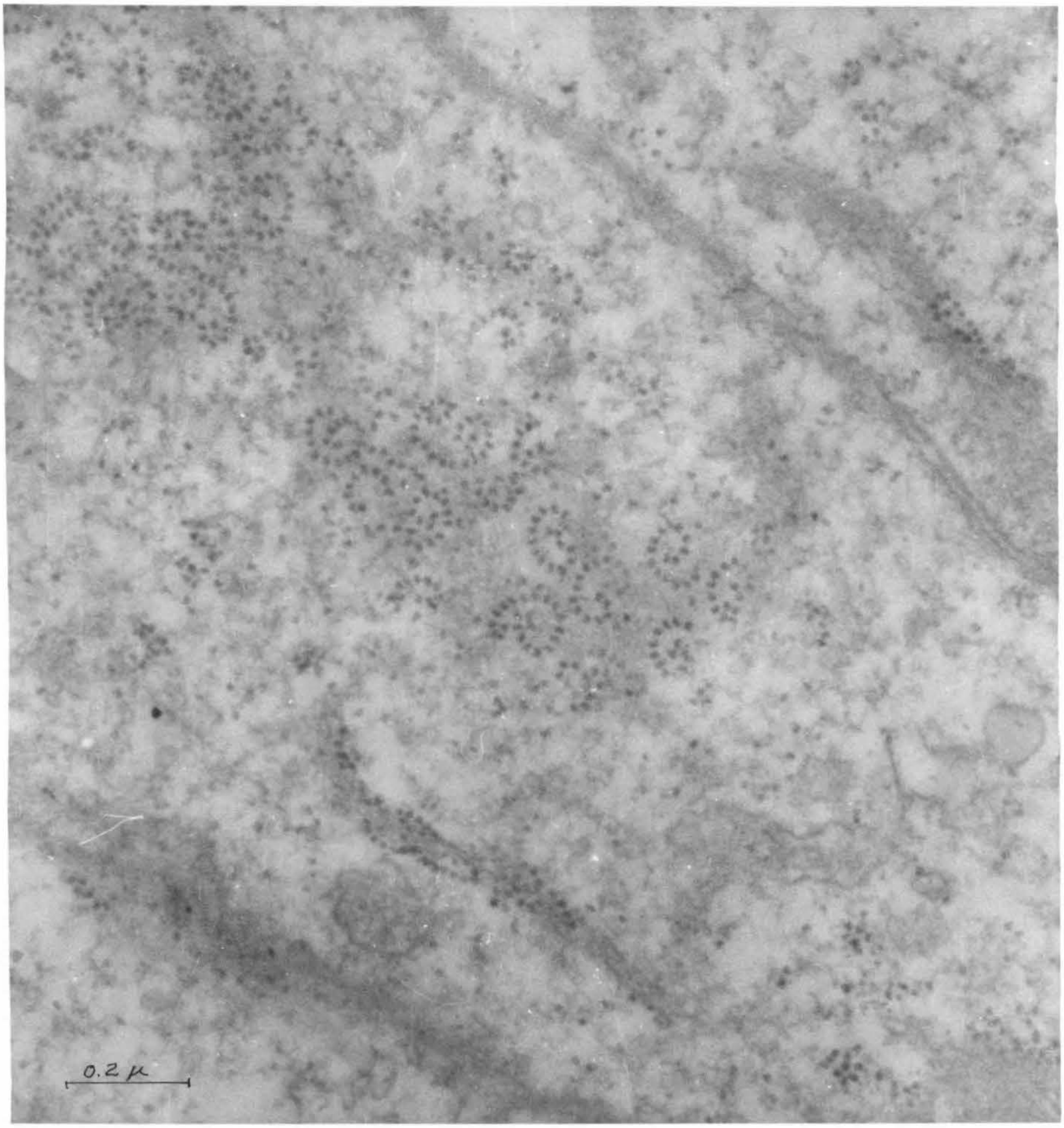
0.2 μ

Figure 34. Golgi region of the cusp cells, apical to the nucleus. X 24,000.

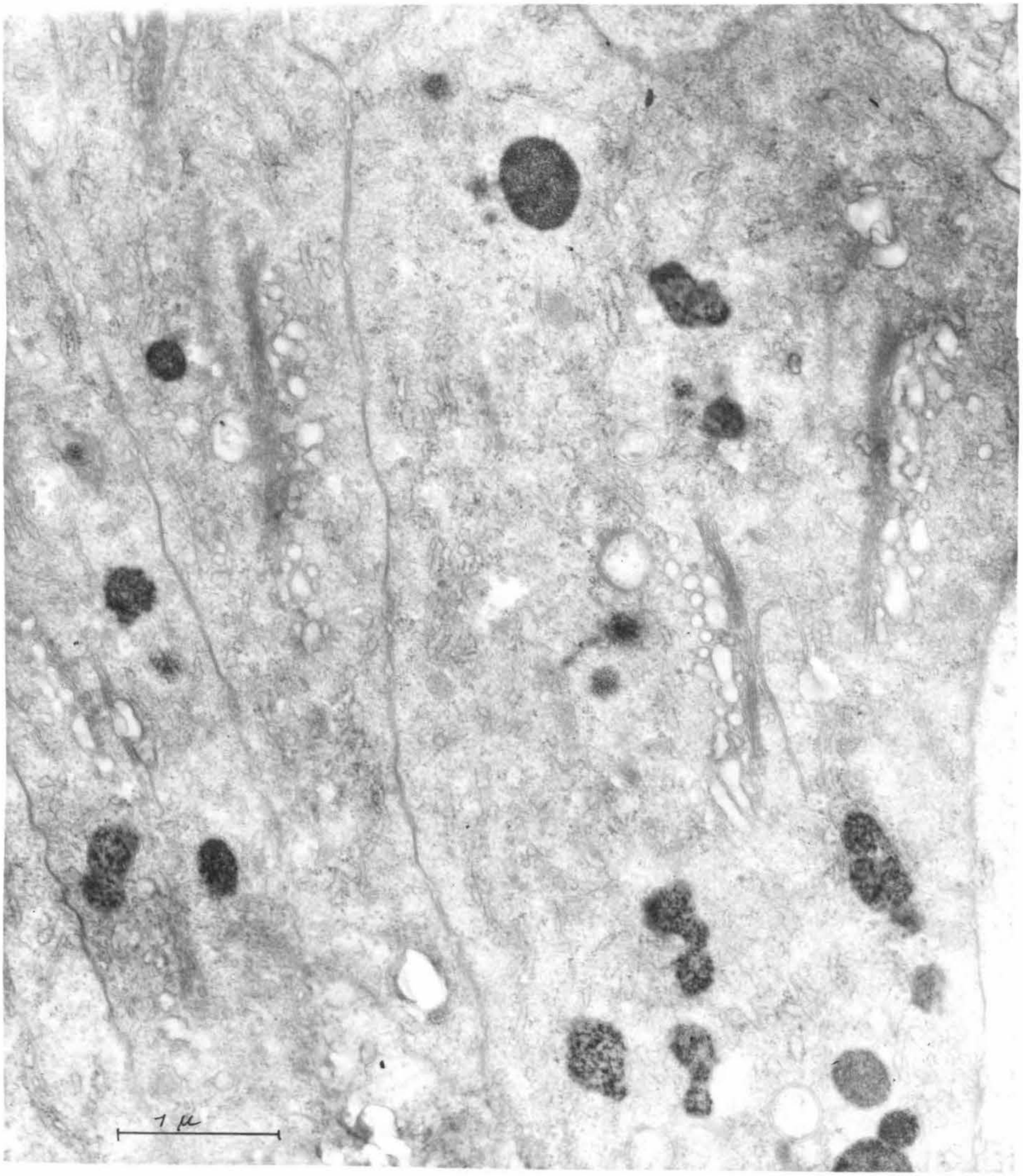
1 μ

Figure 35. Higher power view of the cusp cell Golgi apparatus.

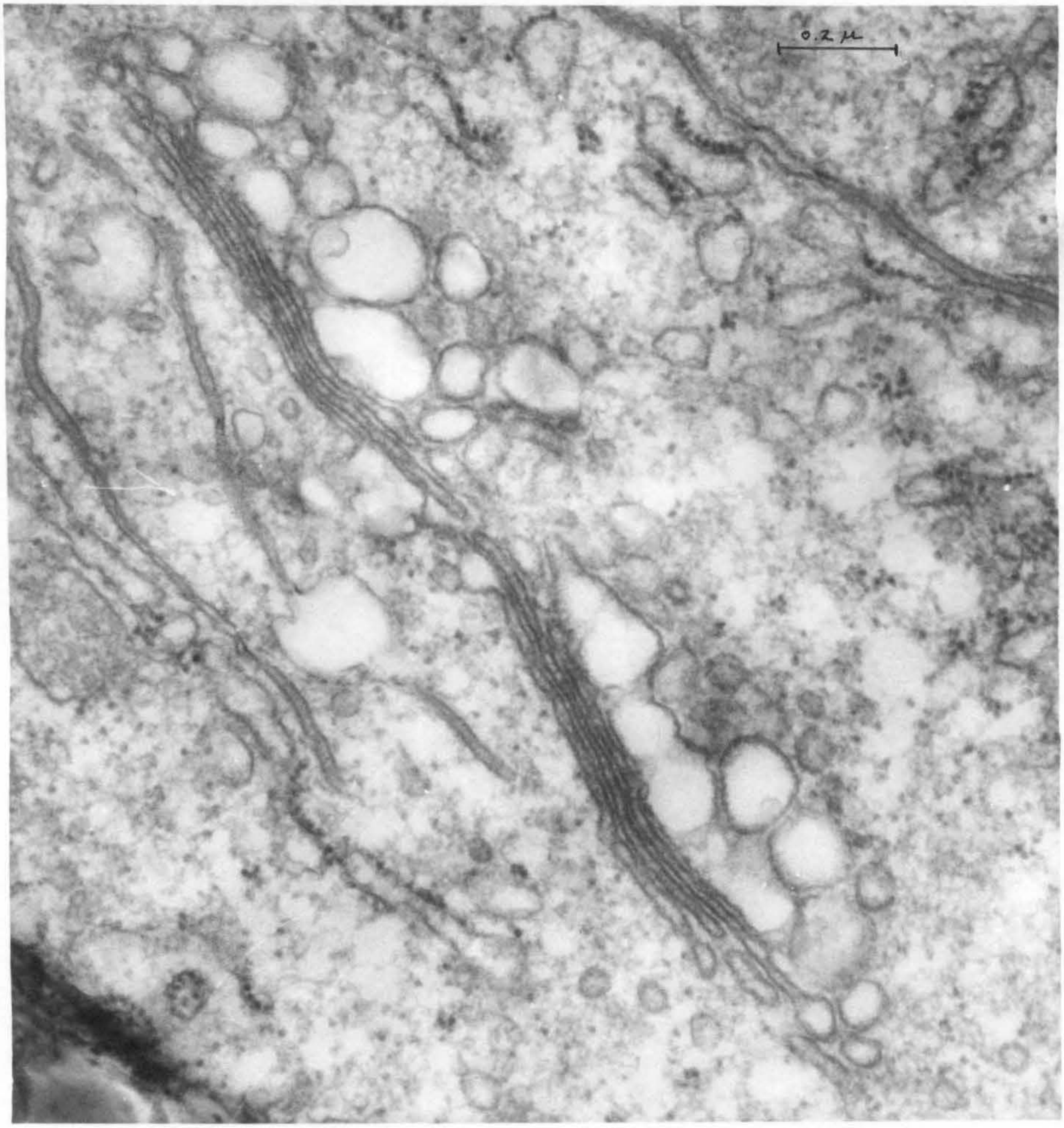
0.2 μ

Golgi vesicles, are scattered throughout the apical cytoplasm. Often, these vesicles are found near the membrane-bound iron-containing granules in this region (Figure 36). We have observed that some of the cusp cells contain more than one Golgi apparatus (Figure 37).

The Apical Pole of the Cusp Cells.

The apical ends of the superior epithelial cusp cells terminate directly on the surface of the major lateral tooth cusps. Hence, we assume that the apical poles of the cusp cells are intimately involved in the processes which eventually result in the impregnation of the cusps with the mineral magnetite. As we described in the Introduction, the initial step of mineralization is the deposition of a ferric oxide hydrate on the protein-chitin matrix of the cusp, resulting in the so-called brown teeth.

Figures 38 and 39 show representative longitudinal sections of the second brown tooth cusp and the apical half of the associated cusp cells from the radula sac of L. hartwegi (cf. Figures 4,6). The apical pole of each cusp cell can be divided into two distinct regions: the zone of iron-containing granules, and the zone of microvilli (Figure 39). In the following sections, we present our findings on the ultrastructure of these regions in the order in which they lie, from the nucleus to the cusp.

(a) The Granule Zone.

Starting at approximately the level of the Golgi apparatus, the

Figure 36. Golgi apparatus of the cusp cell. Note the Golgi vesicles near the ferritin granule.
X 56,000.

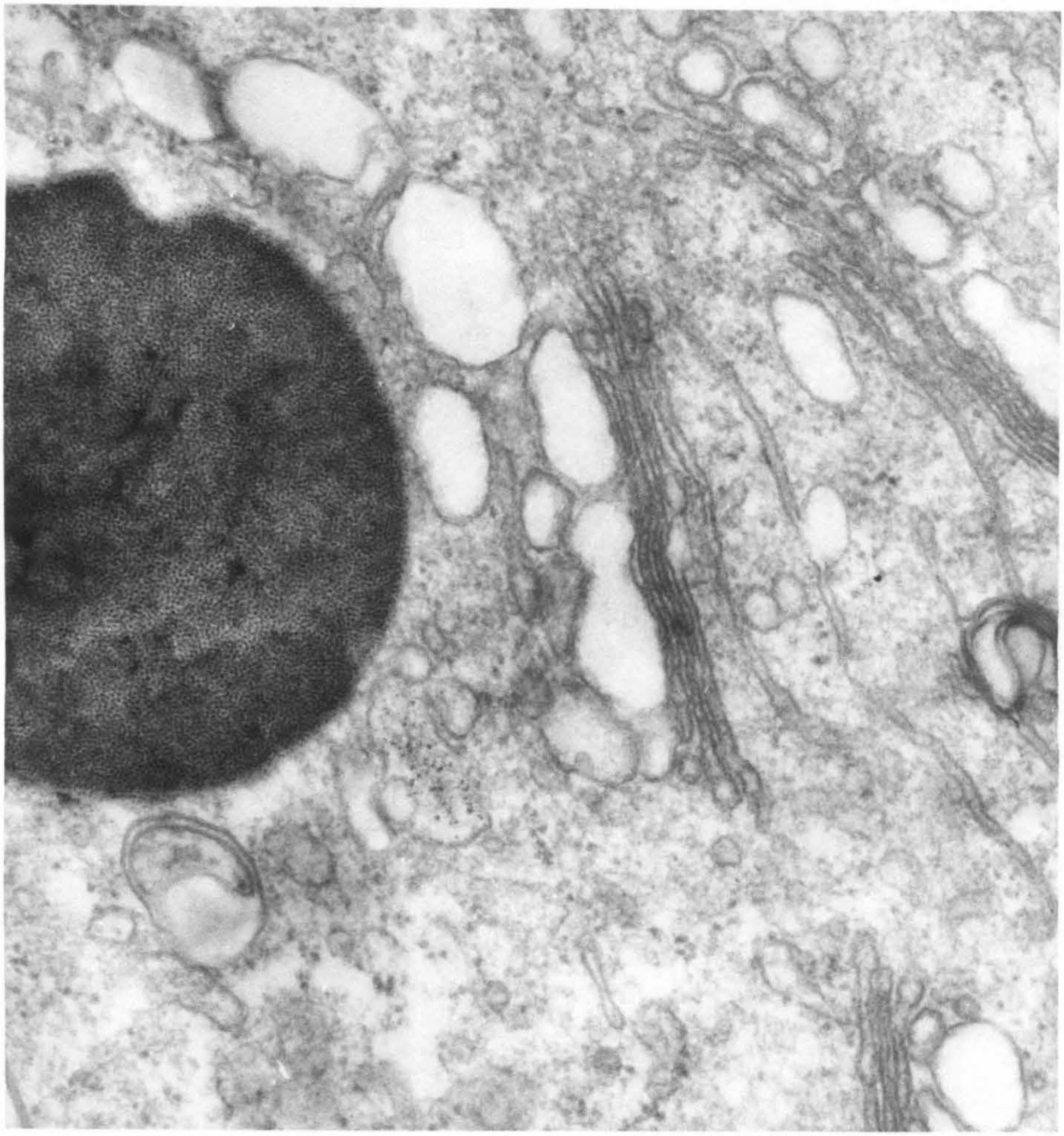

Figure 37. A cusp cell that contains two Golgi systems. Note the oblique section of the nucleus at the upper right. X 34,000.

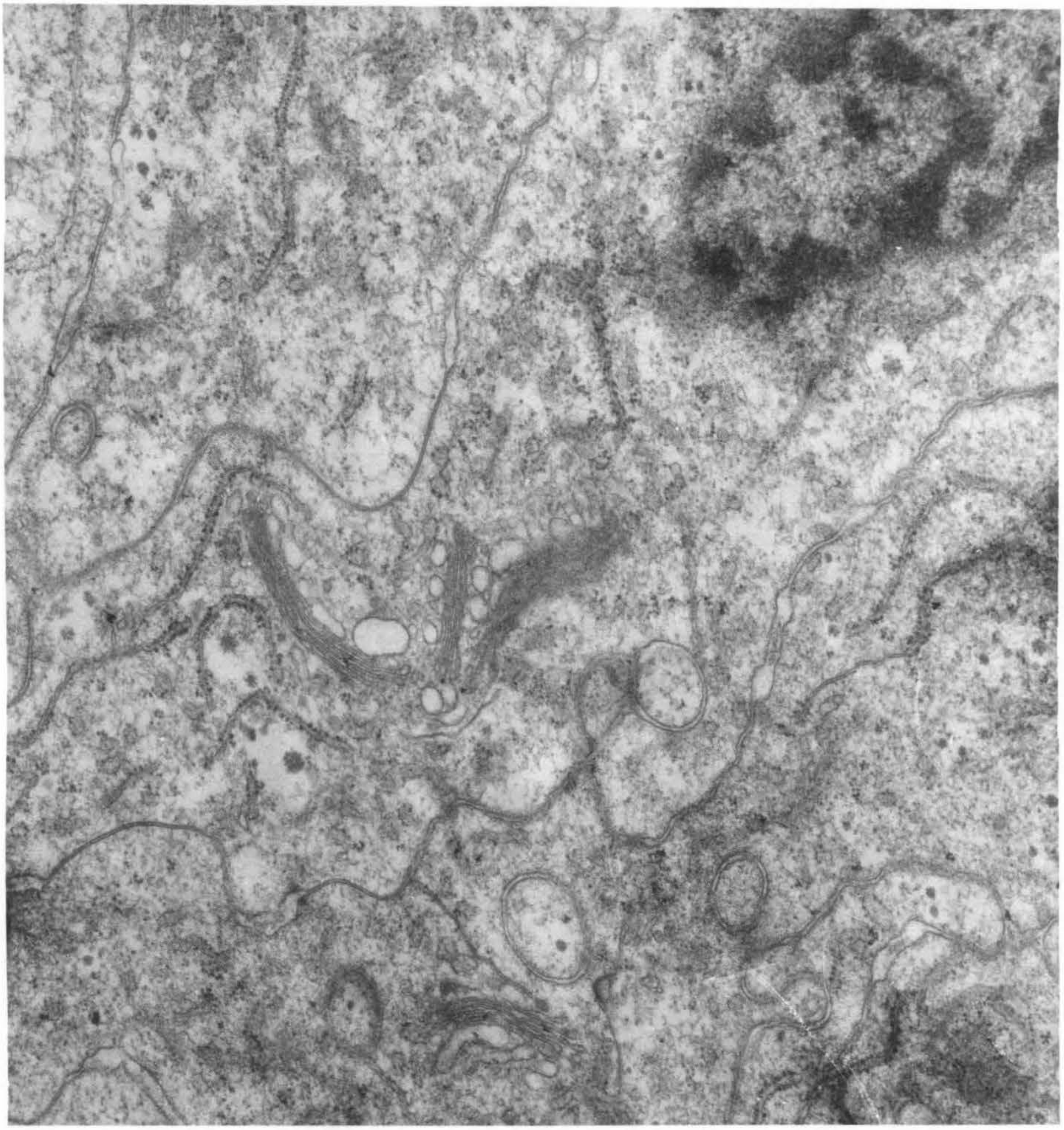

cytoplasm of the cusp cells contains a dense accumulation of iron-containing, electron-dense granules (Figures 38,39). The granule zone extends for about 10 to 20 μ and terminates at a distance of 5 to 10 μ from the apical tip of the cell.

Since the thickness of an ultrathin section (∿ 500 Å) is very small compared to the dimensions of an individual granule, every section through the granule zone should contain granules with a wide range of apparent diameters. The apparent size of a granule depends on the distance of its center from the plane of sectioning.

An estimate of the upper limit of granule diameter comes from measuring the largest granules in a section. This value is generally about 1.5 to 2 μ. A better estimate of granule size results from measuring the diameters of only those granules whose outer membrane appears to be sectioned nearly transversely (i.e., the membrane exhibits a clear tri-layered structure). By this method, the iron-containing granules range from 0.3 to 3.0 μ in diameter.

Even at low magnification, one can see that the granules are not all of equal electron-density (Figures 38,39,49). In fact, even some individual granules exhibit density inhomogeneity (Figures 39,49). At higher magnification (Figures 40-48), the variability in electron-density is revealed to be due to the presence of several classes of granules, each containing materials of different appearance.

In our examination of hundreds of sections through the granule zone, from a large number of individuals of L. hartwegi and M. muscosa, we have never detected a segregation or a concentration of any one class

Figure 38. A low power electron micrograph of the apical ends of the cusp cells. Note the brown tooth cusp at the bottom right. Also note the zone of concentrated iron-containing granules and the mitochondria-rich apical cytoplasm adjoining the microvilli zone.

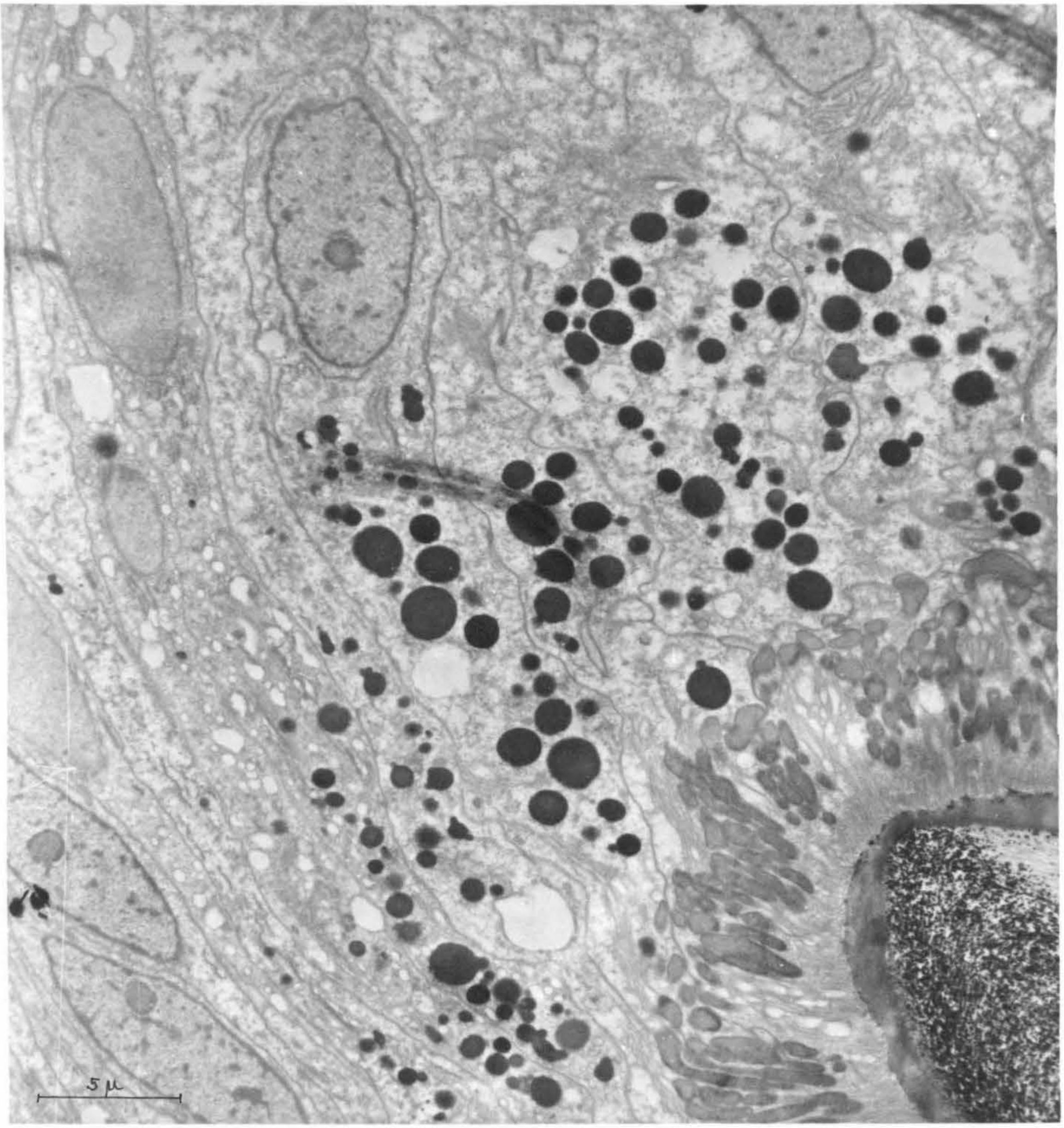
5 μ

Figure 39. Similar to Figure 38. Note the heterogeneous pattern of cusp mineralization.

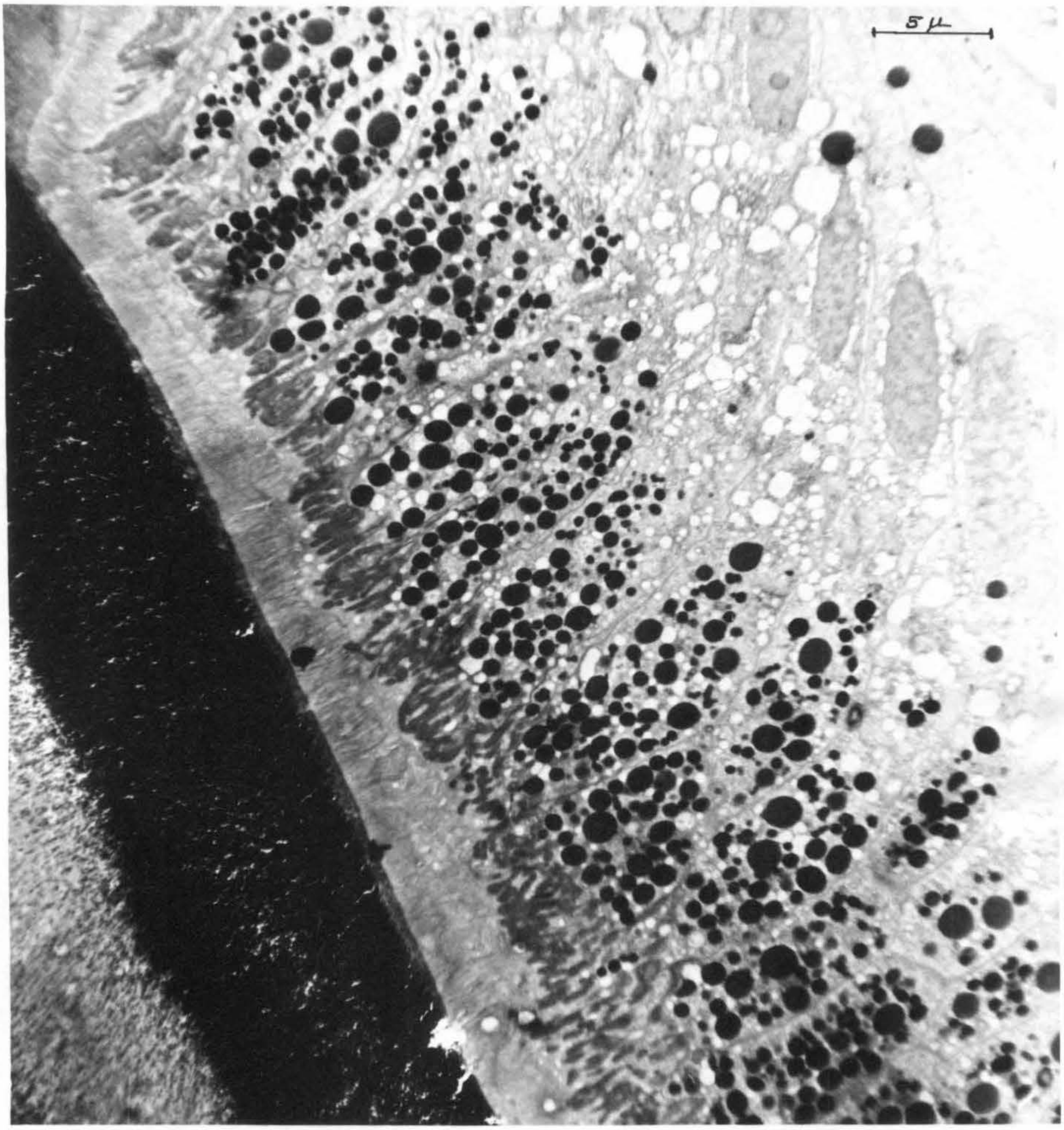
5 µ

of granules anywhere within the whole granule zone. Although we have not made any quantitative measurements, we suspect that the arrangement of the various classes of granules throughout the granule zone is random.

(i) Ferritin-Containing Granules.

The first group of granules to be considered are those which are filled with 60 Å micelles, which are characteristic of ferritin. As previously described (13,40), there are two classes of ferritin-containing granules, crystalline (Figures 40.41) and paracrystalline (Figure 42). The crystalline granules are composed of hexagonal-packed ferritin molecules with a lattice spacing of 95±5 Å. Most commonly, several crystalline domains are found in a single granule (Figure 40), but we have seen a few granules which appear to be single crystals (Figure 41). The crystalline ferritin granules are much less common in L. hartwegi than in M. muscosa, but even in the latter, they comprise no more than one-fiftieth of the ferritin-containing granules.

Several examples of paracrystalline ferritin granules are shown in Figure 42. They are most commonly about 1.0 μ in diameter, but a significant proportion are larger (up to ∿ 3 μ). For the most part, the molecules of ferritin do not exhibit any overall order, but there are often small regions, within a granule, in which ten or twelve micelles are arranged in short, parallel rows (Figures 42d,44). The average distance between unordered molecules, determined as the center-to center spacing between micelles, is 114±10 Å. If we assume that a ferritin molecule occupies a spherical volume 114 Å in diameter, then

Figure 40. Crystalline ferritin granules.

a. X 132,000.

b. X 154,000.

c. X 158,000.

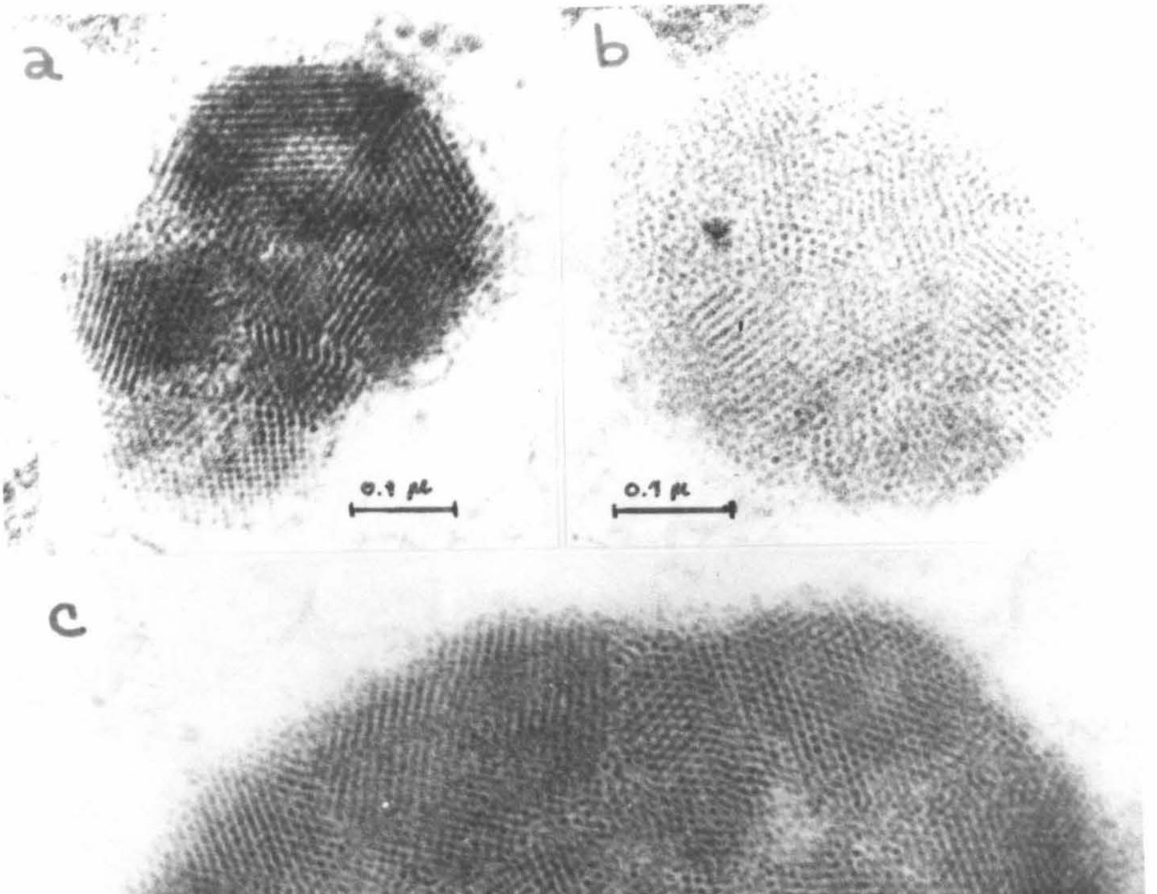
a
0.1 μ
b
0.1 μ
c
0.1 μ

Figure 41. A single domain crystalline ferritin granule.

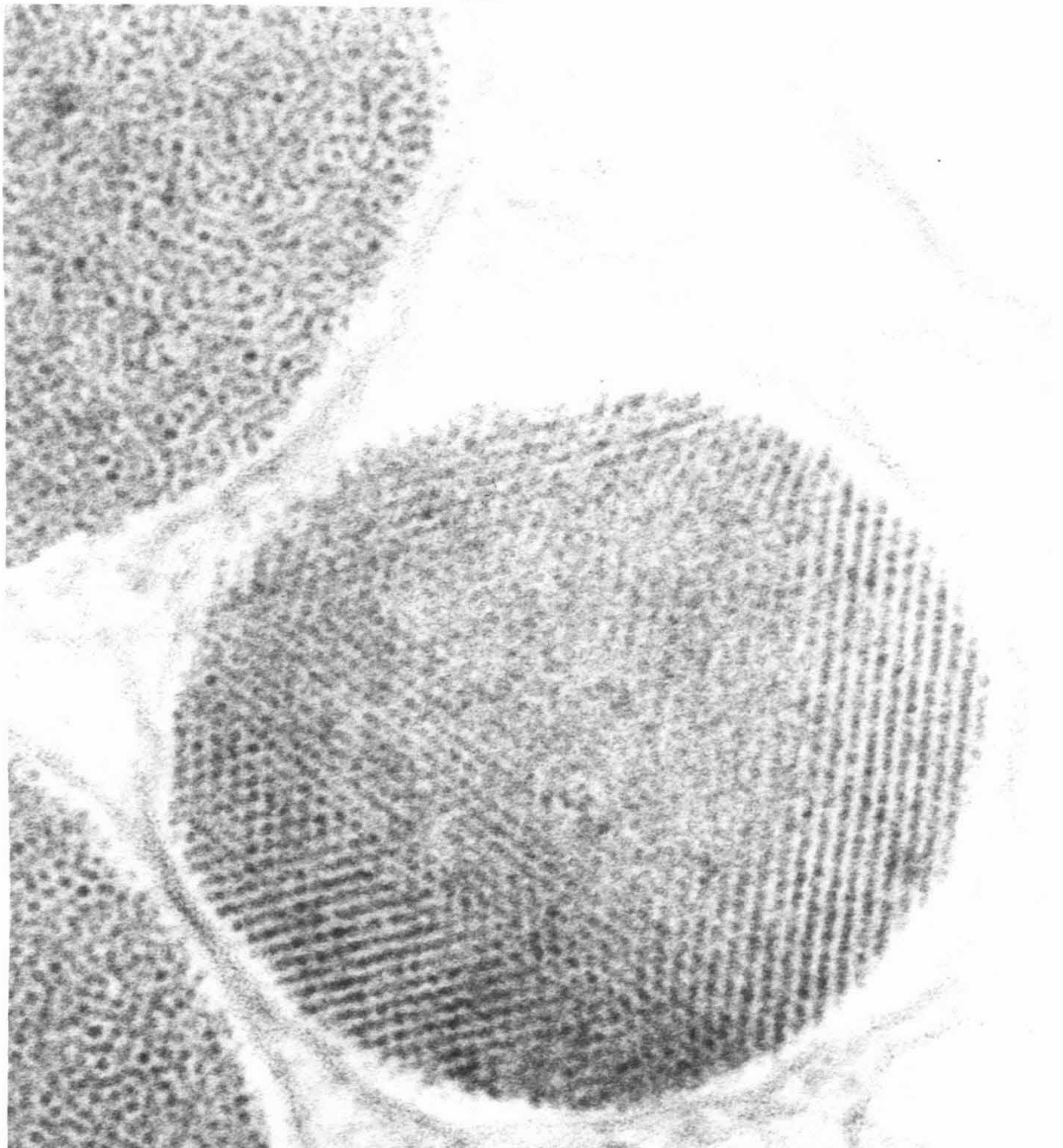
0.1 μ

Figure 42. Paracrystalline ferritin granules. Scale, 0.1 µ.

a. X 70,500.

b. X 83,200.

c. X 102,000.

d. Note the small areas of ordered micelles.
X 164,000.

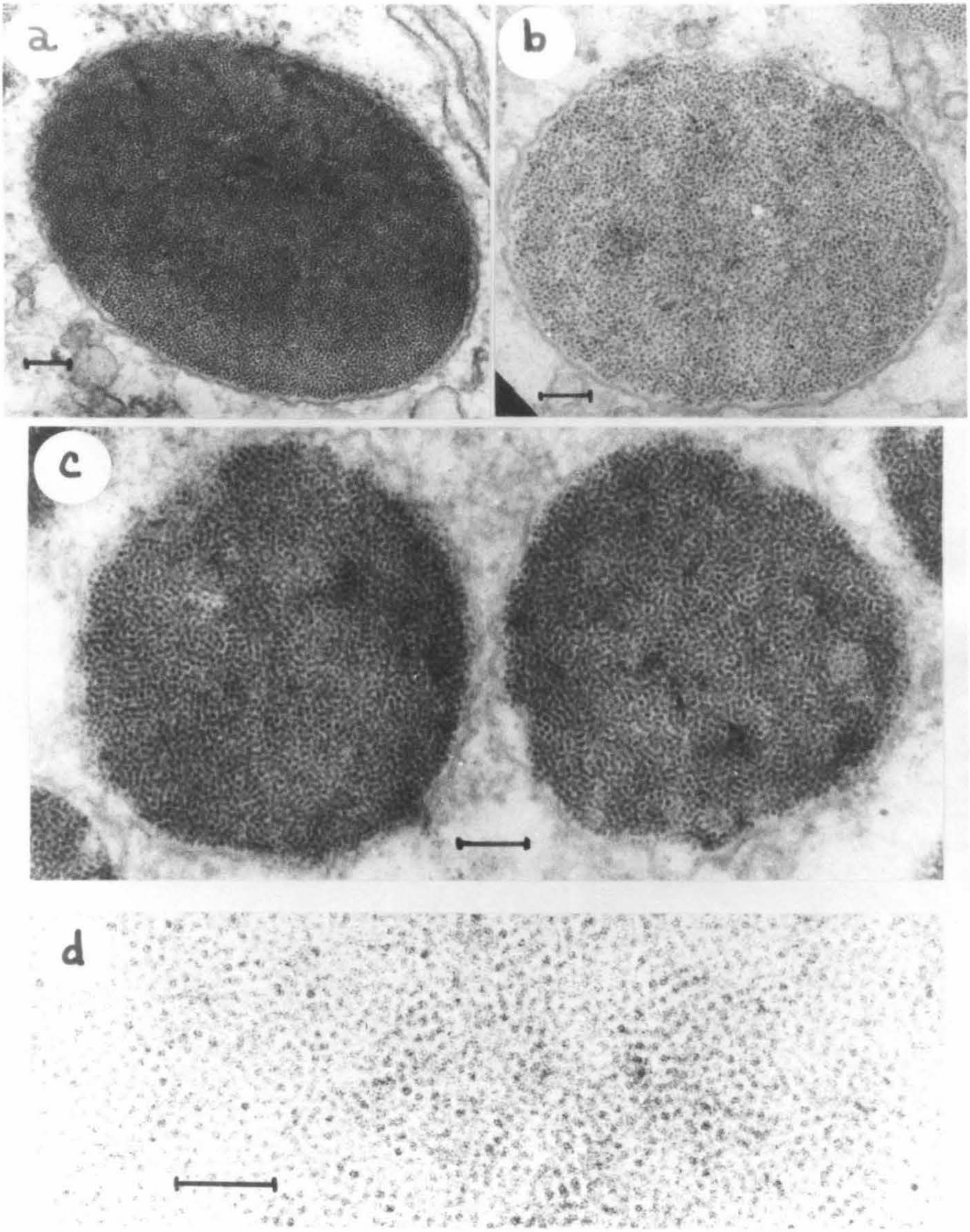
a
b
c
d

it can be readily calculated that a granule 1.0 μ in diameter contains over 6 x 10^6 molecules of ferritin. The paracrystalline granules make up an estimated one-third of the total granule population.

(ii) Ferruginous Granules.

The largest class of granules, comprising over one-half of the total, are filled with extremely small electron-dense particles which form aggregates of irregular shape and variable size (Figure 43). Even at very high magnification, it is difficult to discern, with certainty, the outline of individual particles within an aggregate. However, it is possible to state that the maximum size of the particles is about 20 Å, and that the majority must be appreciably smaller (Figure 44). These granules are similar morphologically to some published figures of the vertebrate iron-storage material, haemosiderin (77,78,87) which may be composed of a hydrated form of α-ferric oxide (79). We will refer to this class which has been observed previously (13), as ferruginous granules.

The ferruginous granules have an average diameter of about 0.7 to 0.8 μ (20 to 30 % smaller than the ferritin granules). We have observed that the granules of highest electron-density in low magnification microscopy are invariably ferruginous granules. However, the converse is not true; many ferruginous granules of very low density are also usually present.

(iii) Intermediate Granules.

The next class of granules to be described are the ones which

Figure 43. Ferruginous granules. Scale, 0.1 μ.

a. X 108,000.

b. X 98,600.

c. X 105,000.

d. X 72,000.

e. X 197,000.

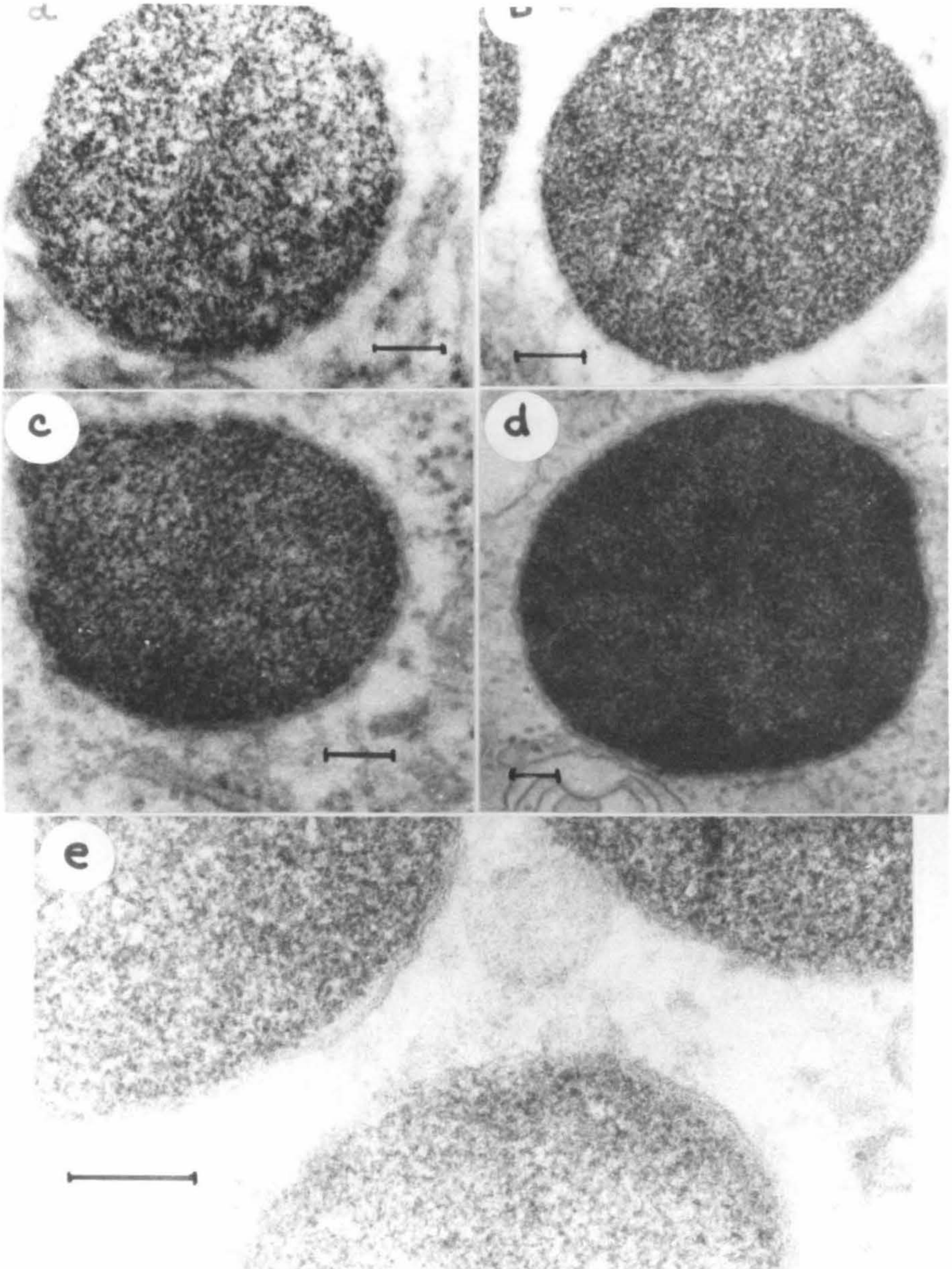
a
b
c
d
e

Figure 44. High resolution micrograph of a ferruginous granule and a paracrystalline ferritin granule.

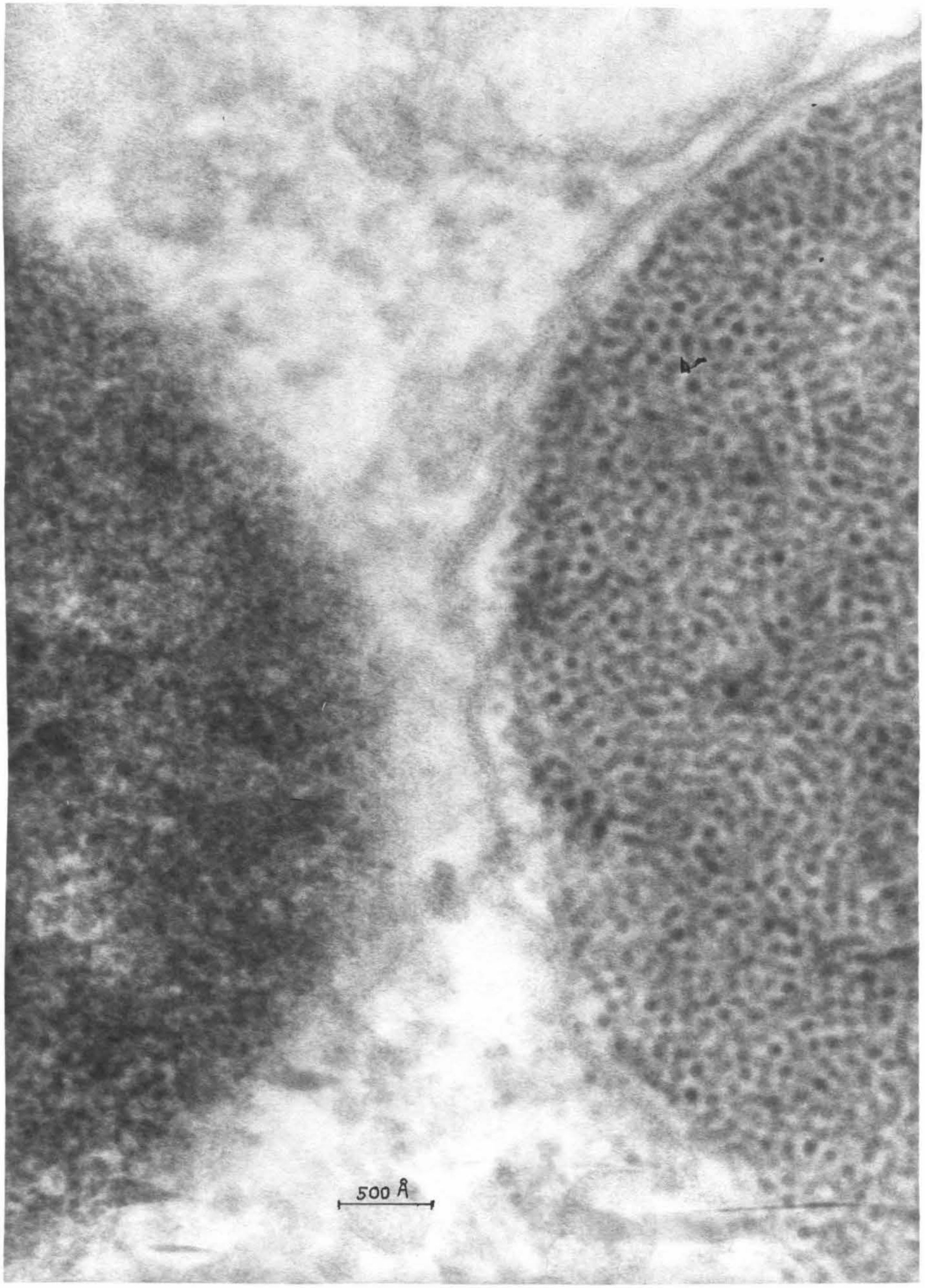
500 Å

appear to be heterogeneous in density at low magnification (Figures 39,49). We refer to this class as the intermediate granules. These granules are usually about 1.0 μ in diameter. They contain an internal core of paracrystalline ferritin and an outer shell of finely particulate material identical to the contents of the ferruginous granules (Figures 45,46). We have observed a continuous series of intermediate granules, which range from those with a ferruginous layer only a few hundred Ångstroms thick to those with only a tiny central core of ferritin.

Within the core region, it is usually apparent that the 60 Å ferritin micelles are embedded in a matrix of moderately dense material (Figure 46), which we presume to be the apoferritin protein moiety. At the junction with the ferruginous zone, there are frequently areas of much lower electron-density in which scattered aggregates of fine particles appear (Figure 46).

We estimate the size of the intermediate granule class to be about 3 to 5% of the total population of granules. However, this is undoubtedly a lower limit since a significant fraction of these granules will be scored as ferruginous granules if the plane of sectioning does not include the ferritin core.

(iv) Miscellaneous Granules.

The remaining granules have two features in common: a small diameter (generally 0.2 to 0.5 μ) and a moderately electron-dense, homogeneous matrix (Figures 47,48). In many of these granules, the matrix contains a low concentration of electron-dense material which is very

Figure 45. Intermediate granules. Scale, 0.1 μ.

a. X 67,600.

b. X 74,700.

c. X 88,700.

d. X 91,600.

e. X 80,200.

f. X 74,400.

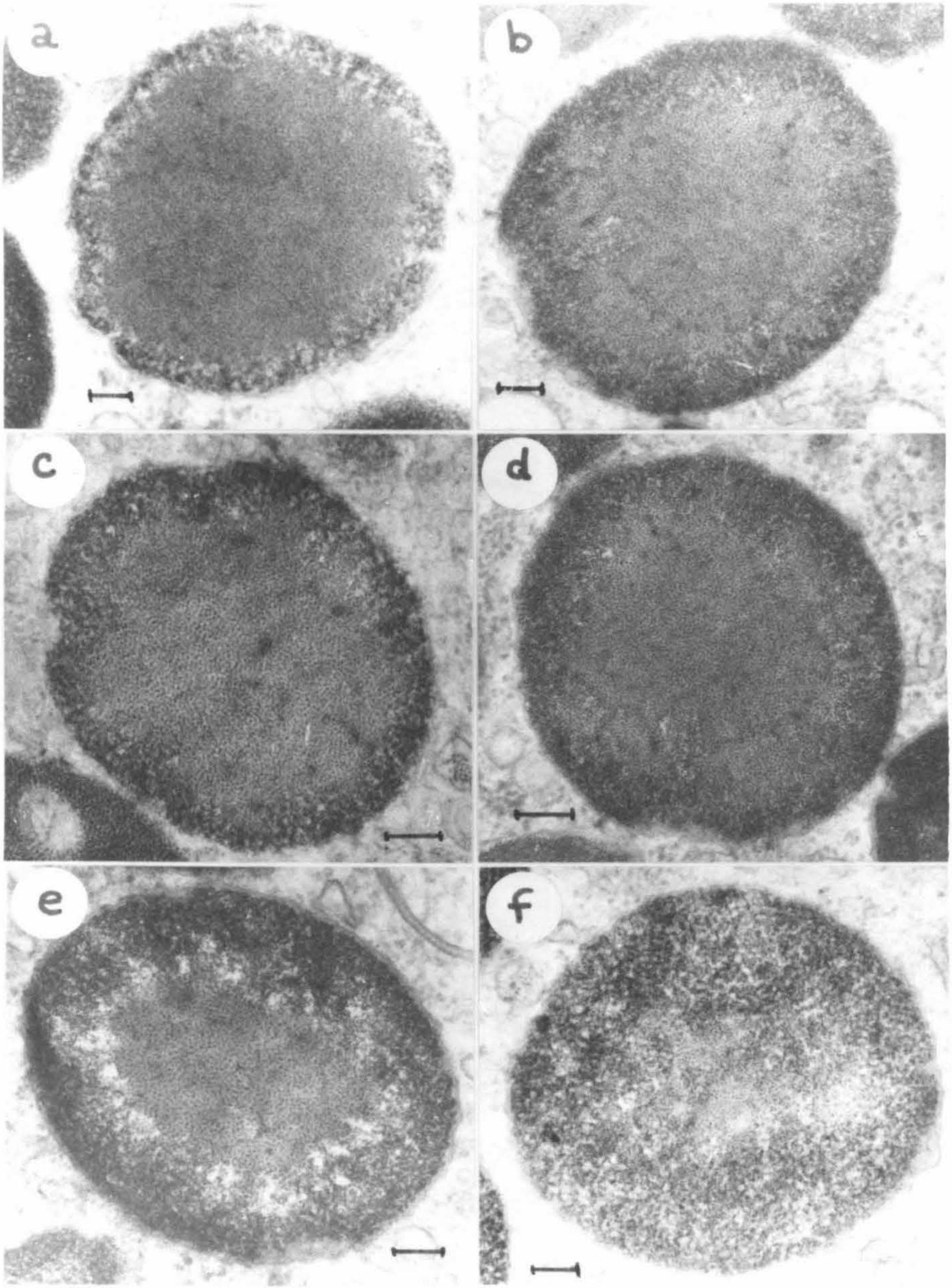
a
b
c
d
e
f

Figure 46. High resolution micrograph of the edge of an intermediate granule. Note the moderately dense material surrounding the ferritin micelles, and its absence at the junction of the ferritin and the ferruginous zones.

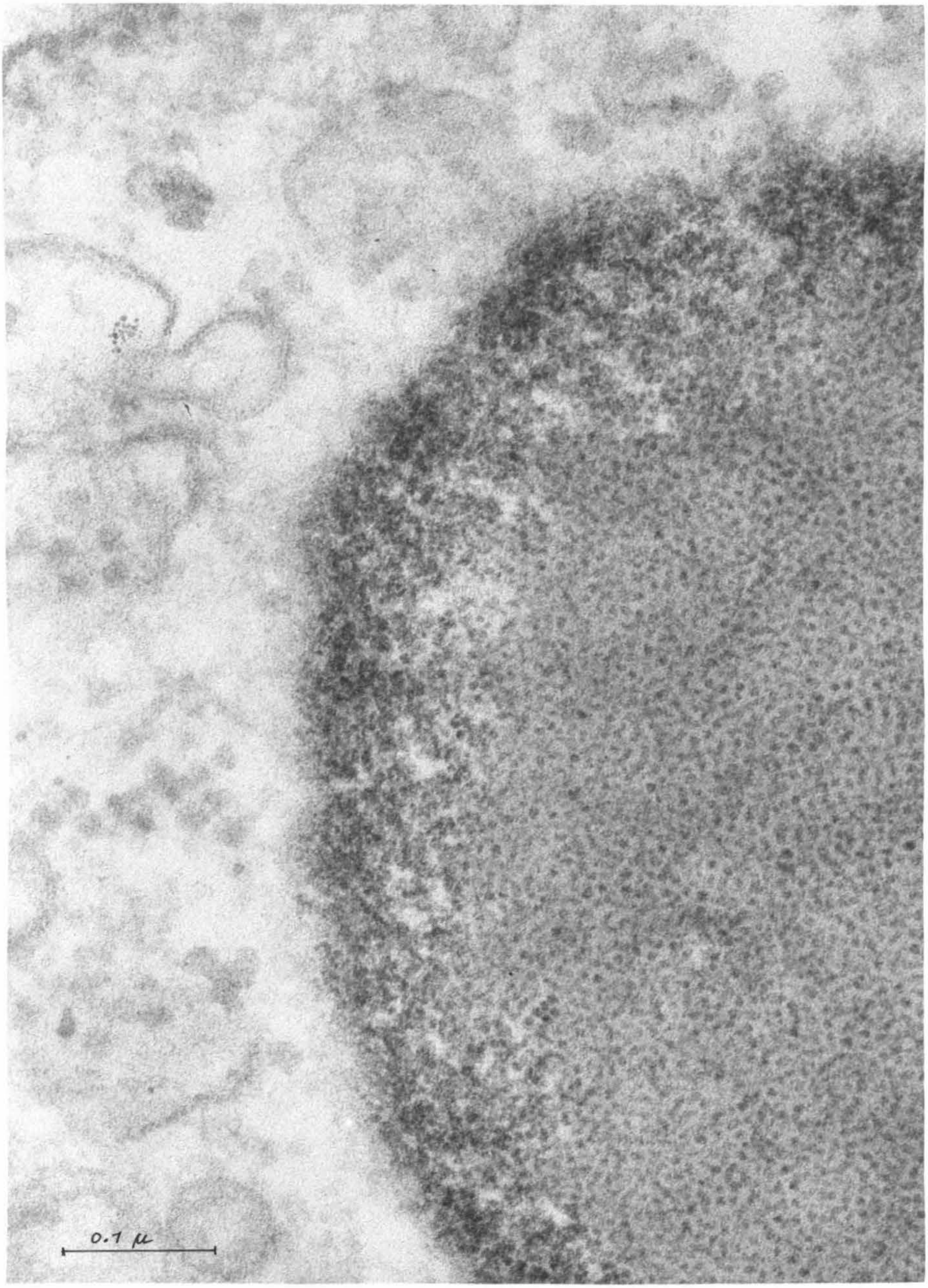
0.1 μ

similar to the particulate aggregates of the ferruginous granules (Figure 47). In the other small granules, the electron-dense inclusions appear less granular (Figure 48). Although their electron density is strongly suggestive, we have no direct proof that these "fluffy" inclusions contain any iron.

(b) The Microvilli Zone.

The apical end of each cusp cell is organized into a bundle of 500 to 1,000 microvilli which arise from the apical cytoplasmic mass and extend to the surface of the tooth cusp (Figures 49,50). The apical cytoplasm also extends nearly to the tooth surface as a thin shell which surrounds the entire bundle of microvilli of each individual cell. Commonly , one or more broad fingers of apical cytoplasm protrude towards the cusp from the central axis of the cell. Consequently, the microvilli of a single cell vary widely in length, depending on whether they arise from the cytoplasmic protuberances, the outer cytoplasmic shell, or the main body of apical cytoplasm (Figure 49). The length of most microvilli ranges from 2 to 6 μ, but some extend for up to 12 μ.

In transverse sections through the microvilli zone, the microvilli usually appear to be arranged in a tightly packed, hexagonal array (Figures 51,52,54-57). The microvilli are 80 to 120 mμ in diameter. Each microvillus is delimited by a single (tri-layered) unit membrane, approximately 60 Å thick (Figures 52-54,56,57). The outer surface is covered with a fuzzy coating of finely fibrillar material which may extend for 200 to 300 Å (Figures 52,53). The interior of the micro-

Figure 47. Miscellaneous ferruginous-like granules, which contain a low concentration of electron-dense material. Scale, 0.1 μ.

a. X 106,000

b. X 97,800

c. X 121,000

d. X 101,000.

e. X 102,000.

f. X 212,000.

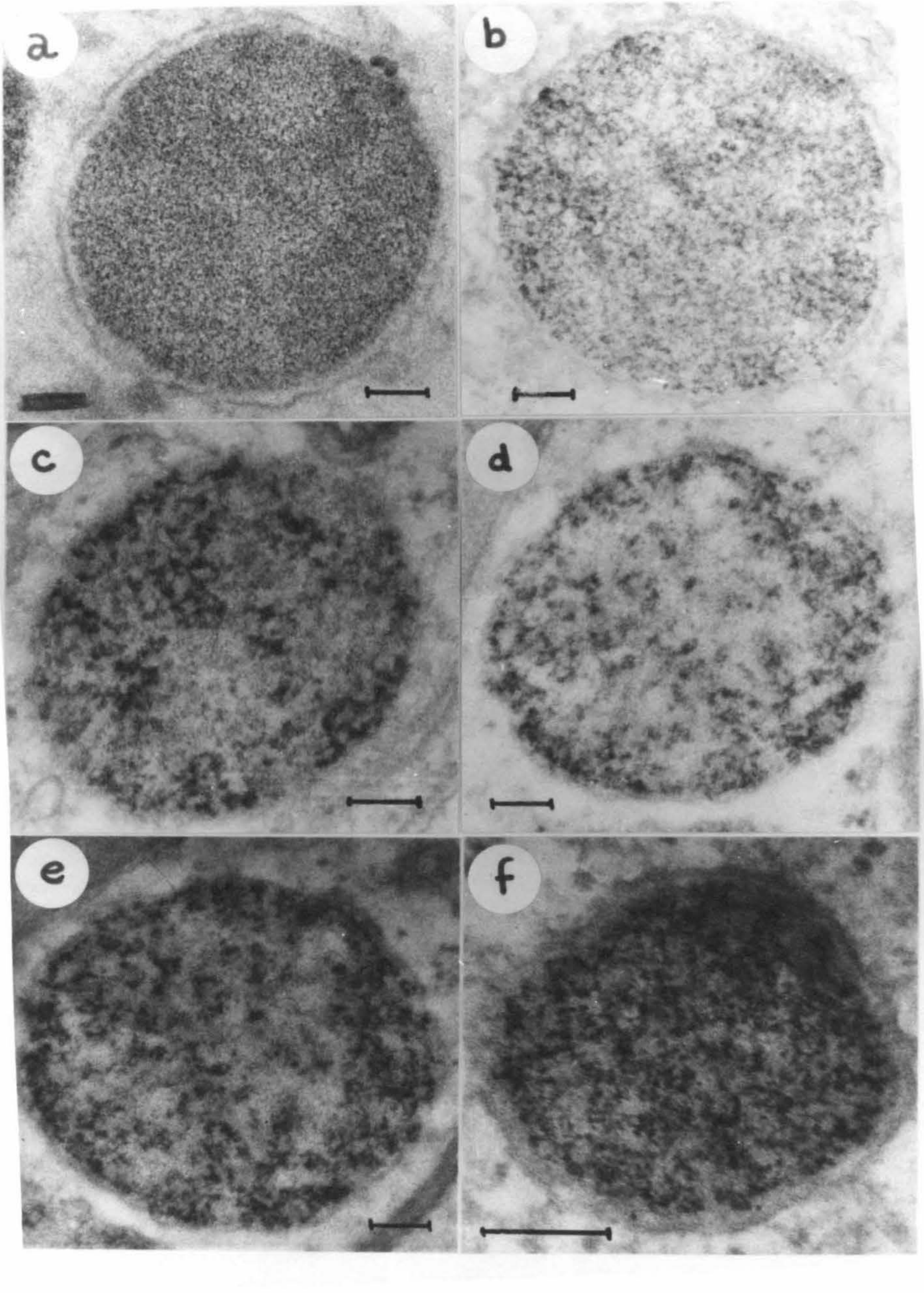
a
b
c
d
e
f

Figure 48. Miscellaneous "fluffy" granules. Scale, 0.1 µ.

a. X 187,000.

b. X 104,000.

c. X 221,000.

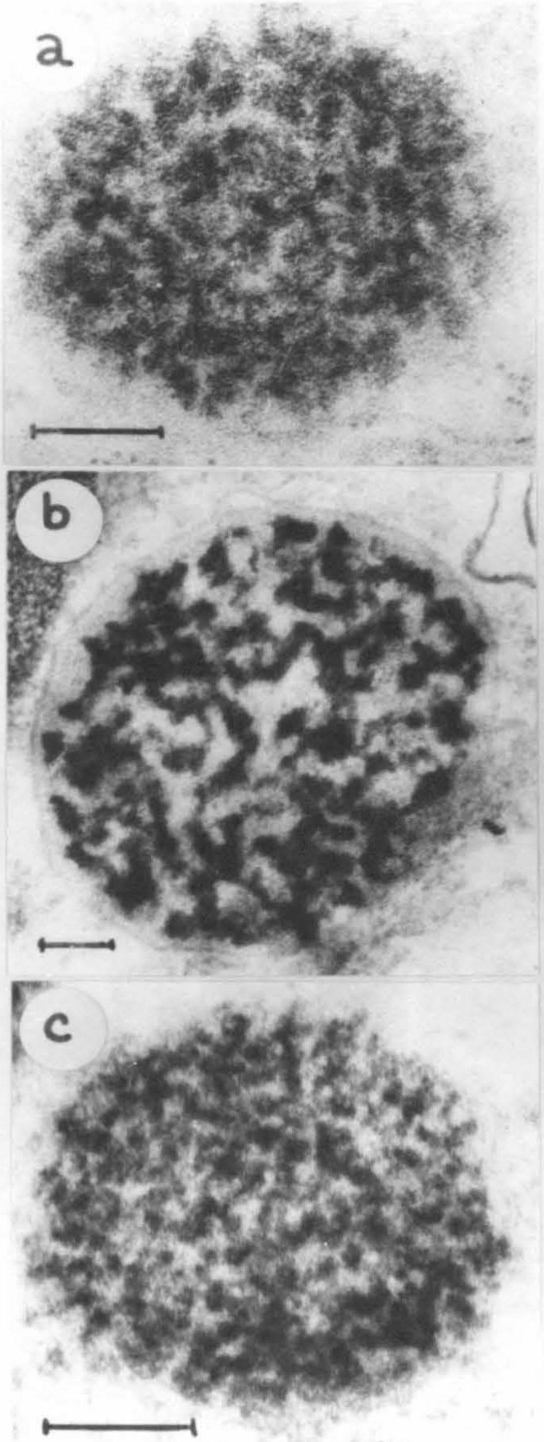
a
b
c

villi contains a loose network of thin fibers, 30 to 40 Å across, which tend to be arranged parallel to the long axis (Figure 53). In cross-sections the fibers are found to be located at the periphery of the internal spaces of the microvilli (Figures 52,54,56,57).

In the many sections of this region that we have examined, we have never seen any ferritin molecules or other highly electron-dense particles within the microvilli or in the extracellular space in which they lie. It should be emphasized, however, that neither the absence of detectable electron-dense material nor the negative histochemical tests for iron in the microvilli zone can be taken as evidence that the microvilli contain no iron: we would undoubtedly fail to identify any dense structures that are smaller than about 30 Å in the sectioned tissue, either in the electron microscope or by Prussian blue staining. We have not attempted any experiments which might affirm the presence of soluble forms of iron.

The mass of apical cytoplasm, from which the microvilli arise, is characterized by the presence of numerous mitochondria (Figures 38, 49-51,54,55,60), which accounts for the dense staining of this region in thick sections (Figures 4-6). The mitochondria-rich cytoplasm extends from the base of the granule zone to the microvilli zone. The highest concentration of mitochondria occurs in the shell of cytoplasm that surrounds the microvilli and within the cytoplasmic protuberances which approach the cusp surface (Figure 49). The mitochondria are highly variable in size and shape. Many, particularly within the surrounding shell, are long (4 to 6 μ) and sinuous structures which often appear

Figure 49. Apical region of the cusp cells. Note the long microvilli extending from the mitochondria-rich apical cytoplasm to the cusp surface. Most of the mitochondria are very long.

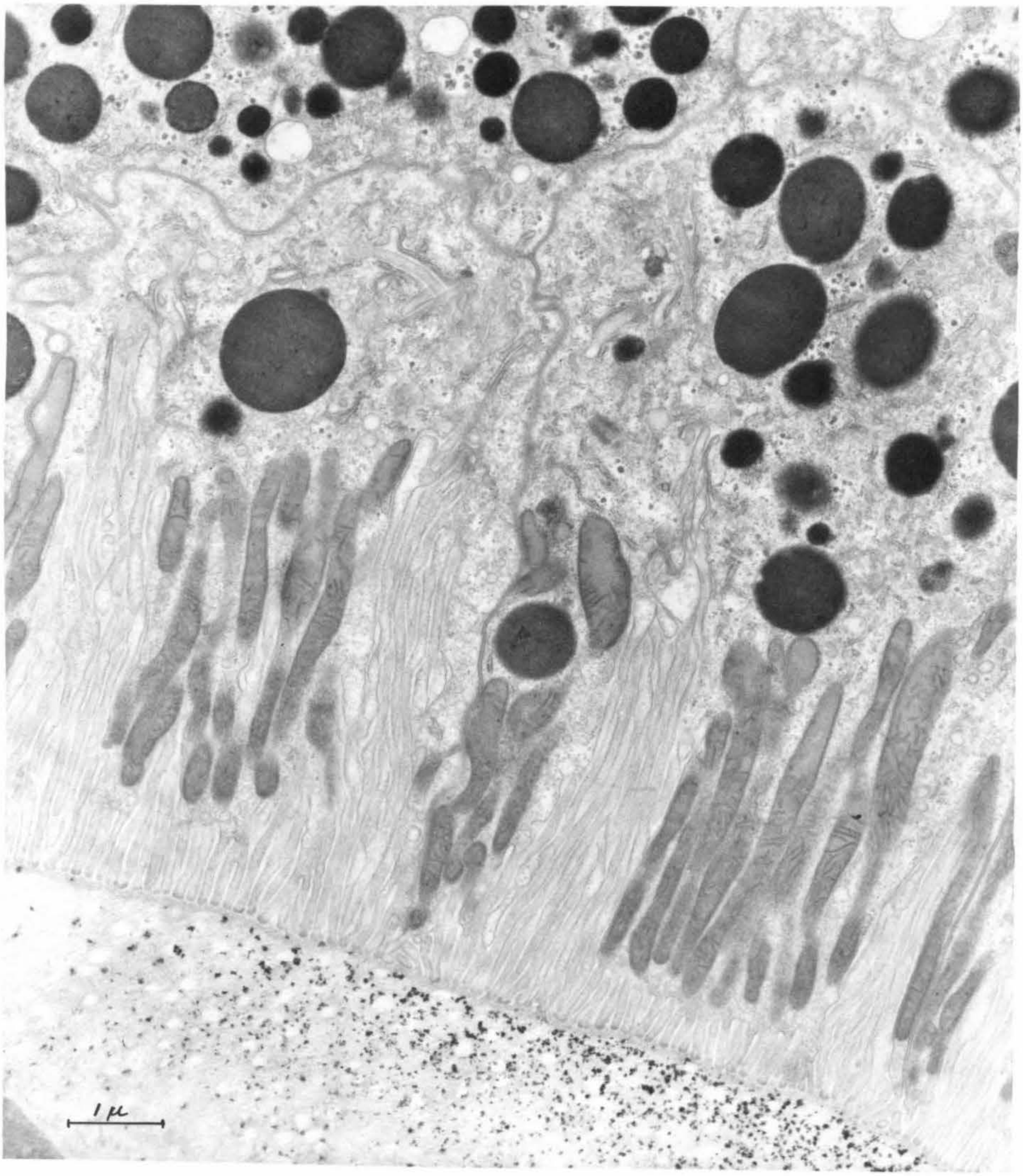
1 μ

Figure 50. An oblique section through the apical ends of the cusp cells. Note that the edge of the apical cytoplasm that lines the microvilli bundles is heavily stained near the granule zone.

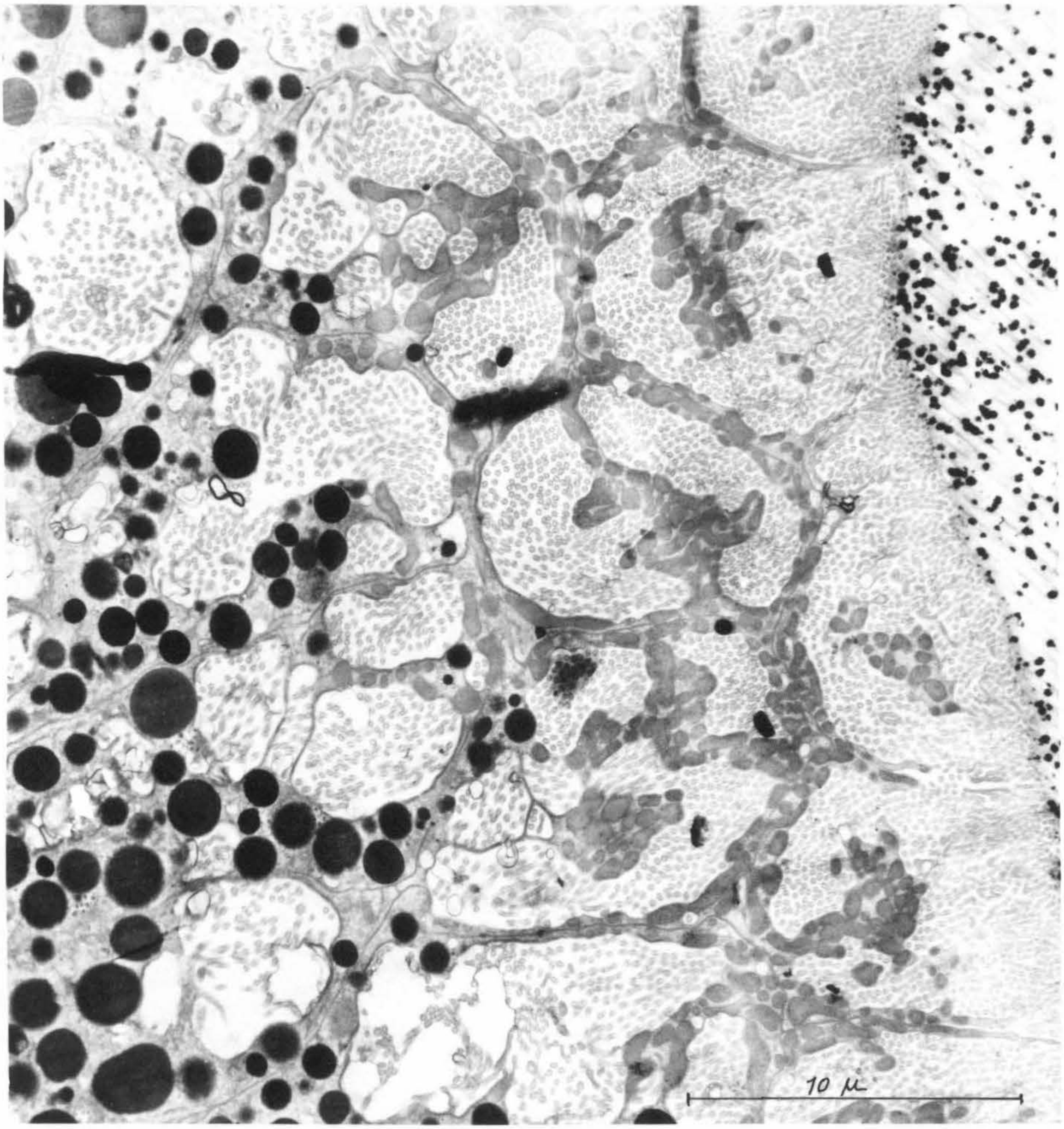
10 μ

Figure 51. Cross-section of the cusp cells through the microvilli zone. Note the cytoplasmic shell surrounding all the microvilli of an individual cell. Also note the cytoplasmic protuberances in the center of many microvilli bundles. The microvilli are tightly packed in a hexagonal arrangement.

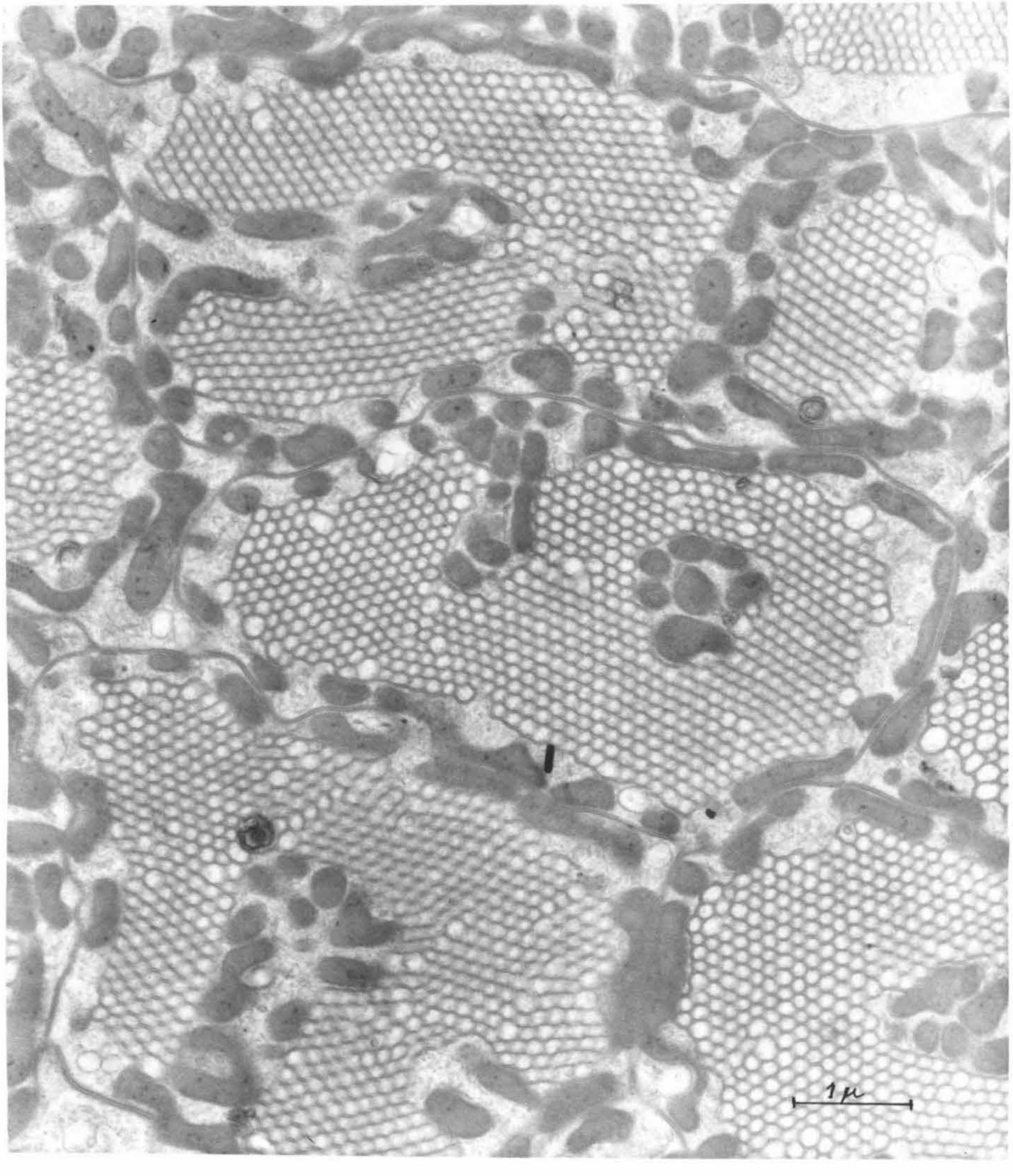
1 μ

Figure 52. High power view of the microvilli. Note the fibrillar material that coats the outer membrane. The tri-layered unit membrane structure is visible in many places. Also note the cross-sectioned fibrils within the microvilli. X 230,000.

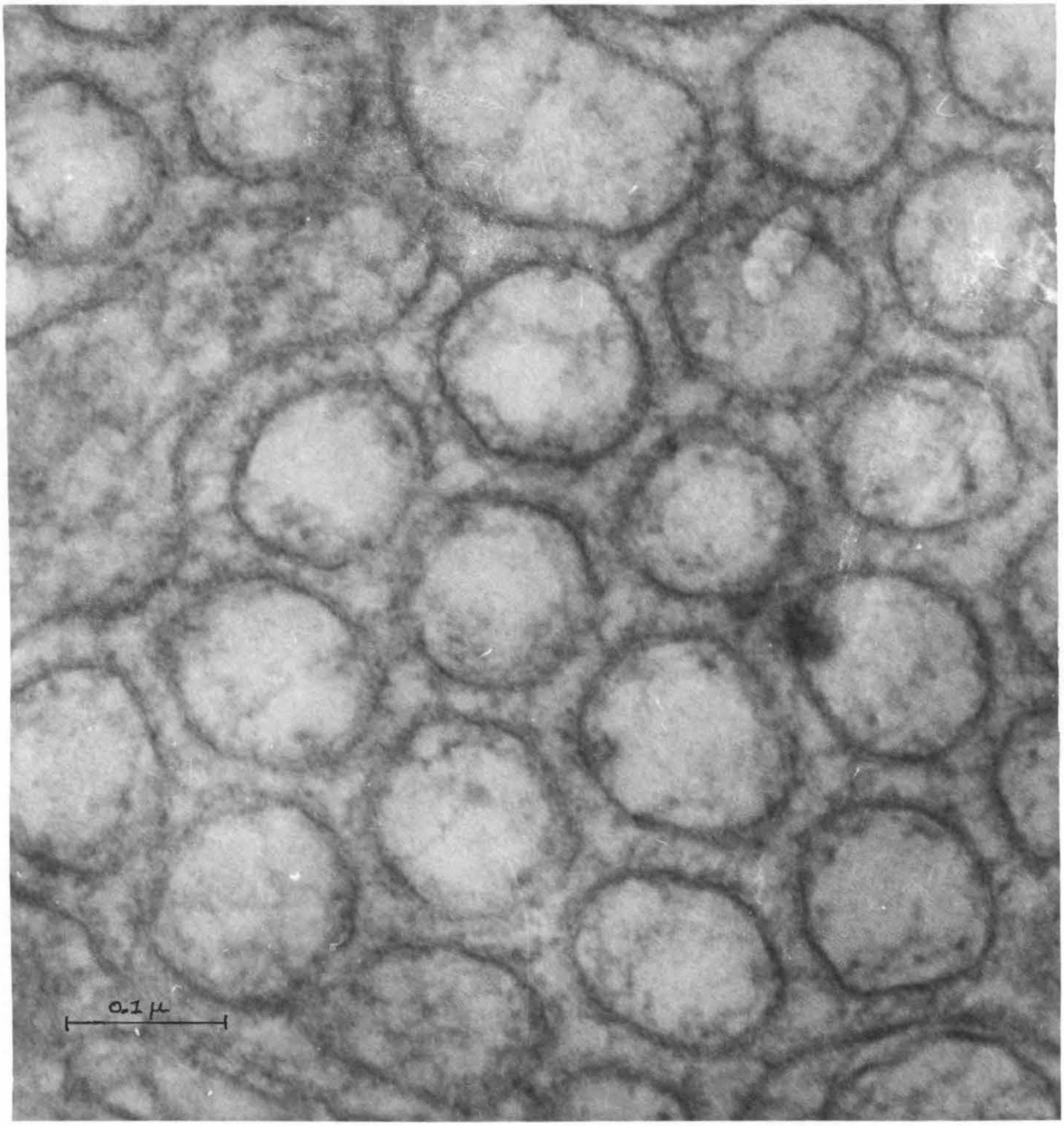
0.1 μ

Figure 53. Longitudinal high power view of the microvilli. Note the fibers on the interior and the fibrillar material coating the exterior of the microvilli.

X 124,000.

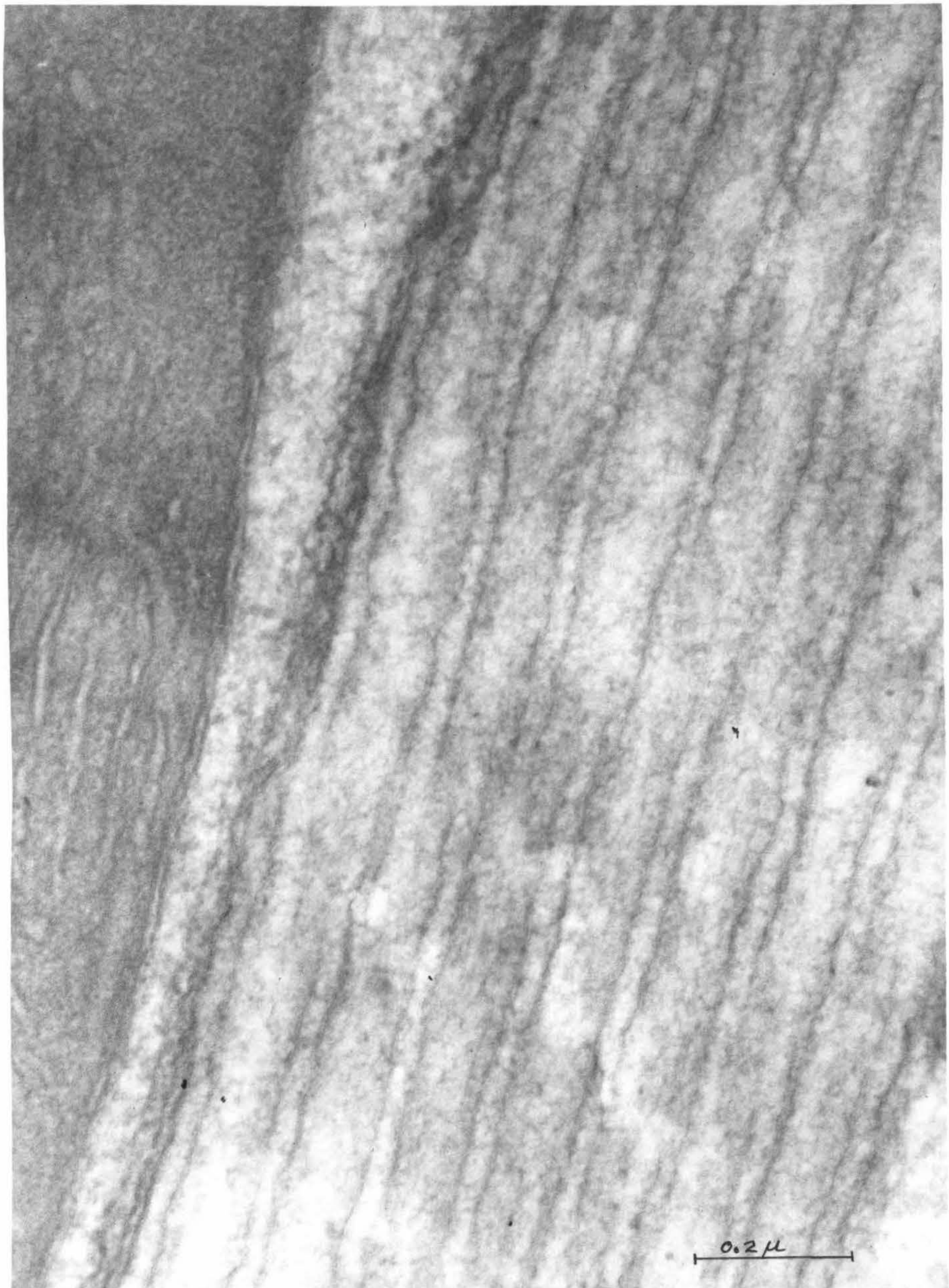
0.2μ

Figure 54. Higher power view similar to Figure 51. Note the fibers peripherally arranged within the hexagonally packed microvilli. Also note the branched mitochondrion. Note dense material between the microvilli.

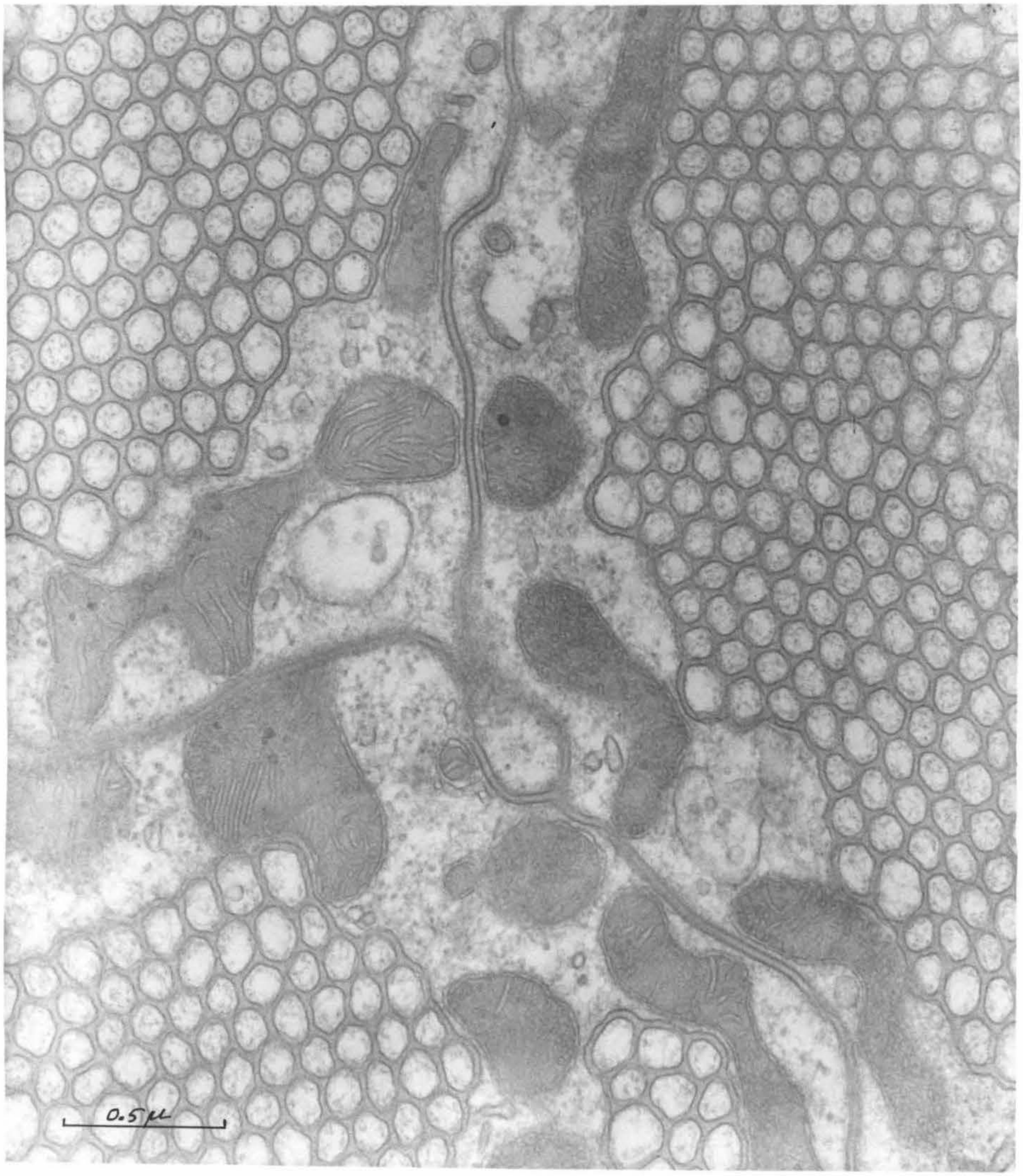
0.5μ

to be branched (Figures 54,55). Numerous short rod-shaped mitochondria, about 1 μ long and 0.3 μ in diameter, are also present. The internal matrix of the mitochondria is more densely stained than the ground cytoplasm.

The mitochondrial cristae exhibit a wide range of appearances, from flat sheets (Figures 53,54,61) to tubular processes (Figure 54). Opaque granules are commonly observed within the mitochondrial matrix (Figure 55).

In an oblique section through the apical region, one can see that there is a level at which the membrane-bound iron-containing granules in the apical cytoplasm are in close proximity to the microvilli (Figure 50). Almost exclusively at this level, a system of membranes is developed within the apical cytoplasm which lines the extracellular space in which the microvilli are situated (Figure 55). A double-membrane structure is apposed to the inner surface of the plasma membrane, which appears to be a normal unit membrane, approximately 75 Å across. The double-membrane system, which is situated 65 to 70 Å away from the plasma membrane, is composed of two 75 Å unit membranes separated by an irregular space which varies from 70 to 120 Å in width (Figures 56-58).

The double-membrane structures closely resemble cisternae of endoplasmic reticulum. The two membranes can often be seen to be joined at their ends (Figures 56-60). Often, 120 Å ribosome-like structures are attached to the surface of the interior-most membrane (Figures 56, 58). Longitudinal sections indicate that these structures sometimes

Figure 55. Oblique section through the upper end of the microvilli zone. Note the double membrane structures applied to inner face of the cell membrane of the cytoplasmic shell. Also note the branched mitochondria.

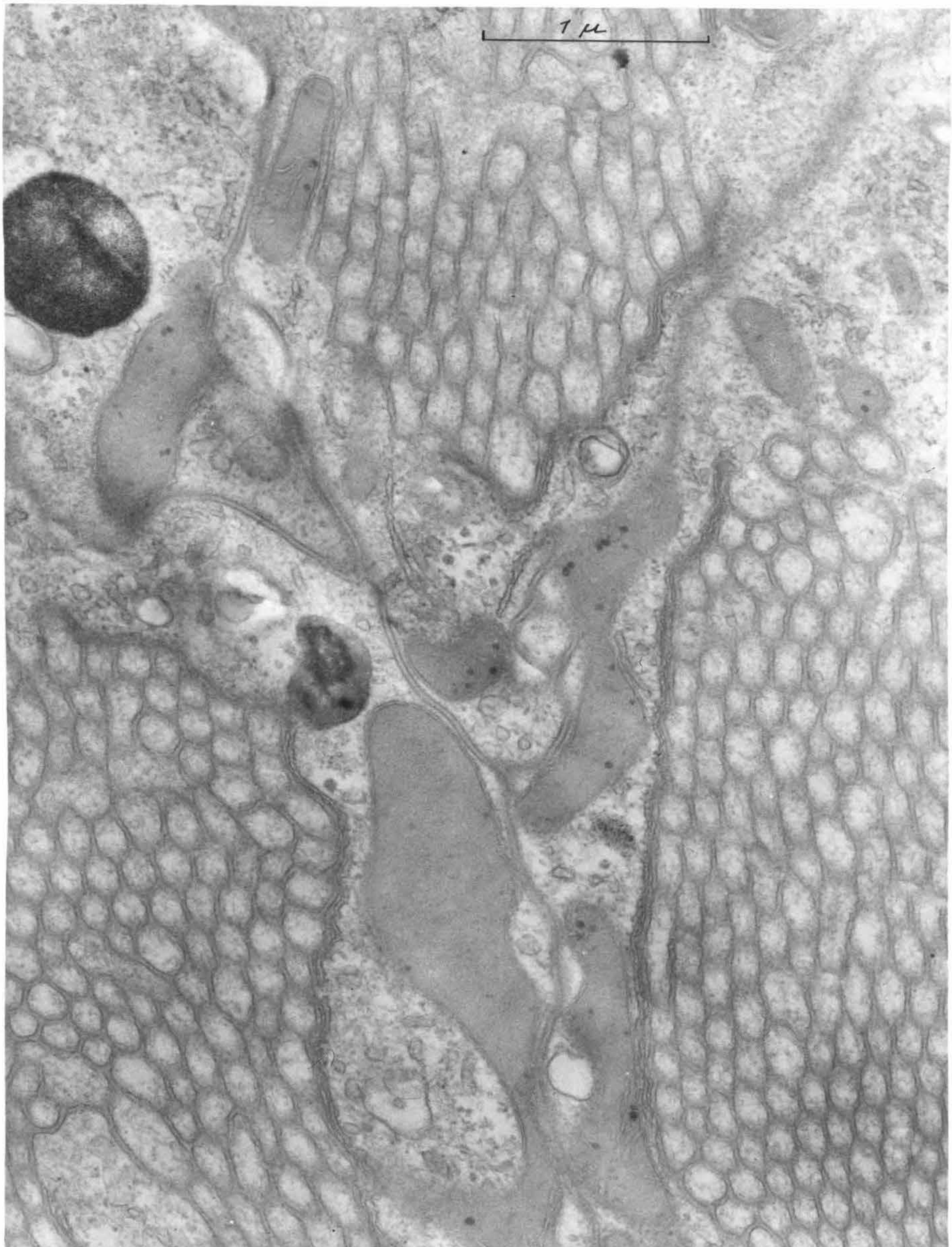
1 μ

Figure 56 and 57. The double membrane structure.

Figure 56. X 126,000.

Figure 57. Note that the two membranes are fused at the ends of the segments.

X 91,400.

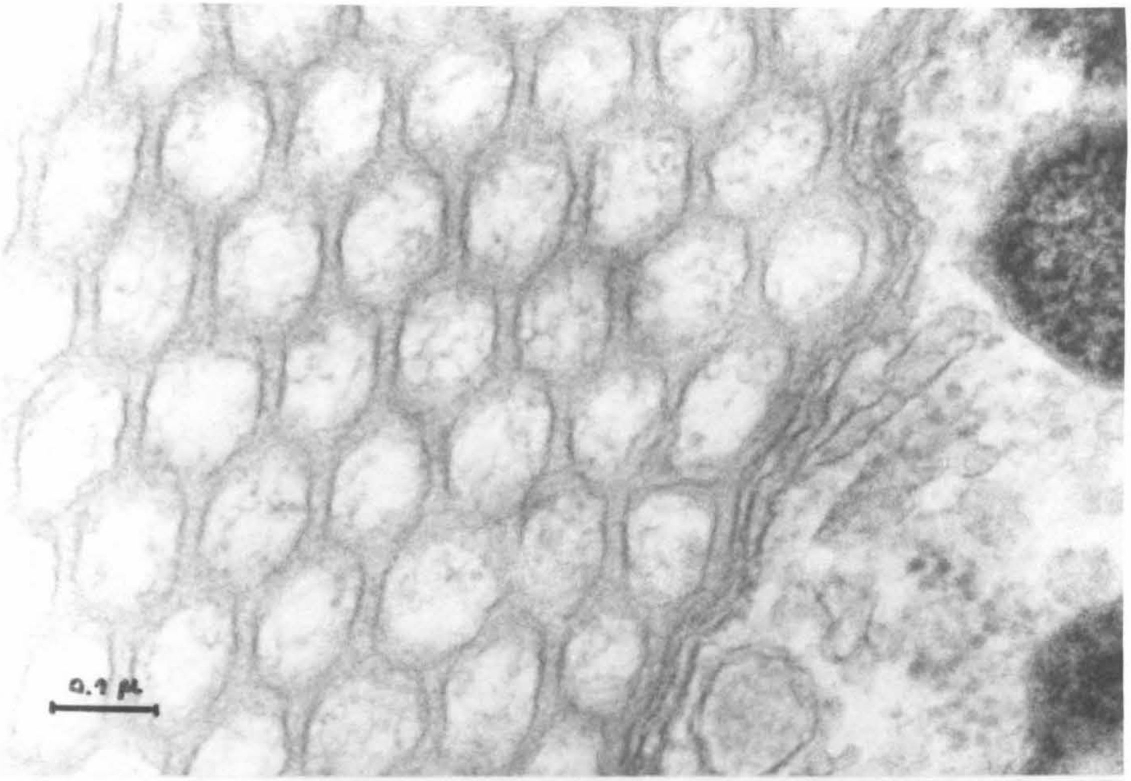
0.1 μ

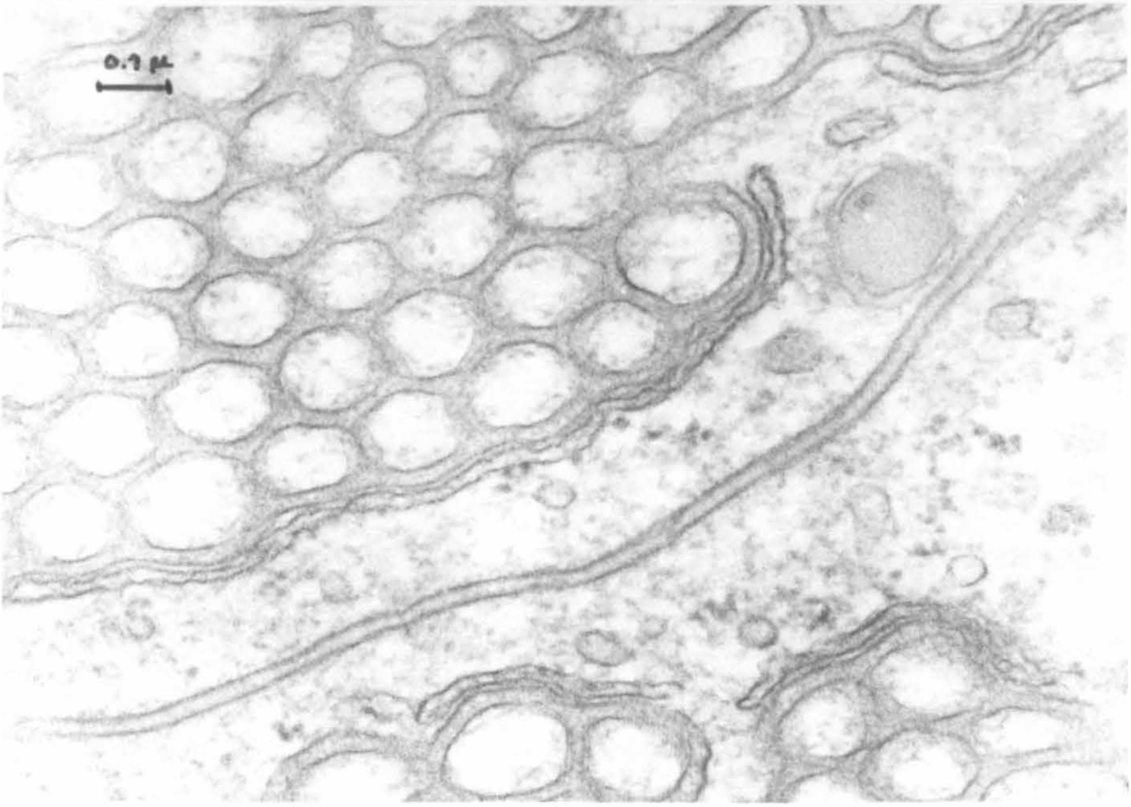
0.1 μ

Figure 58. Oblique view of the double-membrane structure. Note the 120 Å dense bodies attached to the inner surface.

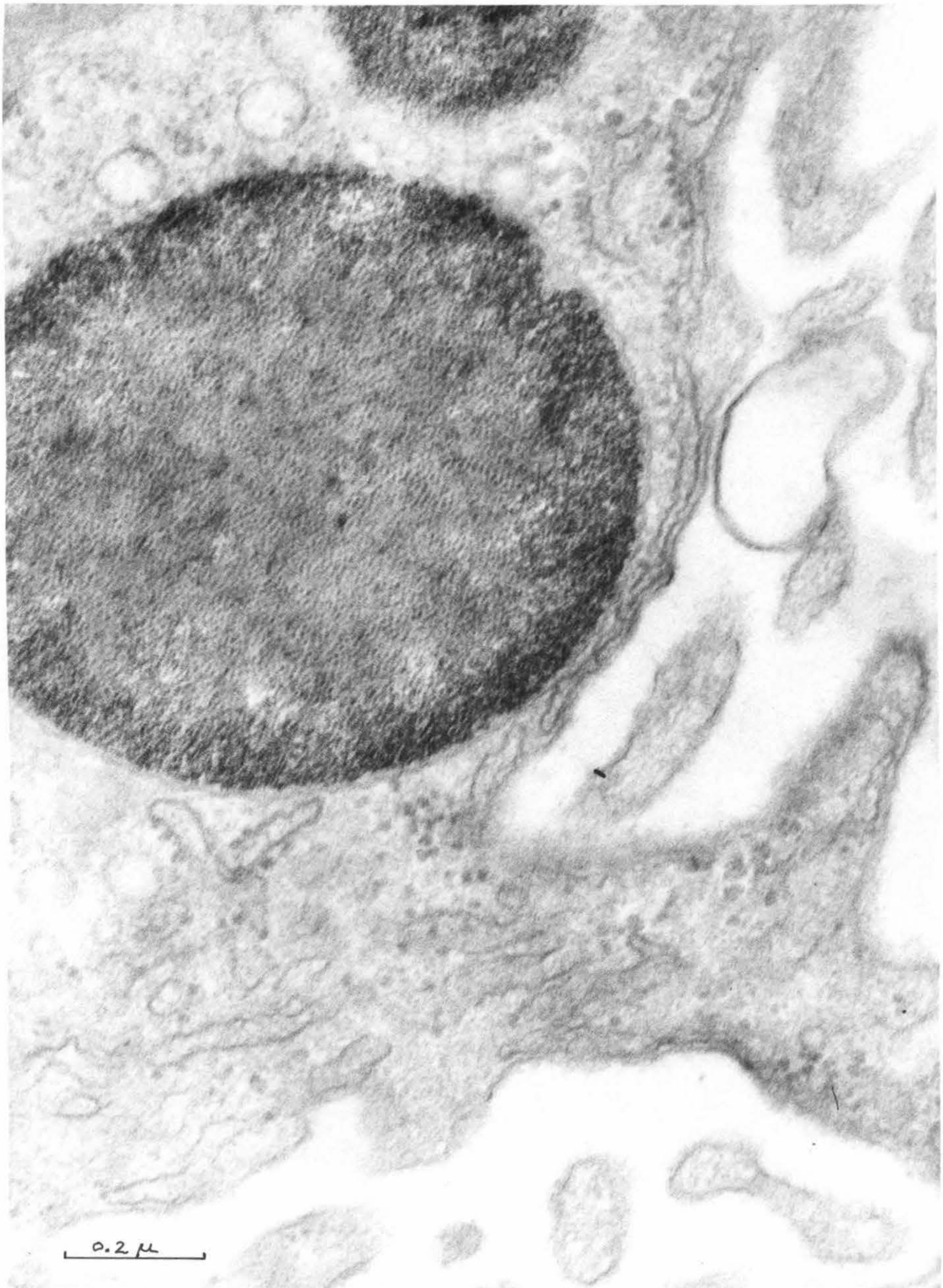
0.2 μ

extend a short way past the microvilli zone and become indistinguishable from endoplasmic reticulum (Figures 59,60). As shown in Figure 51, the double-membrane system does not extend along the plasma membrane very far into the microvilli zone. Apparently, it occurs only where iron granules can be found near the microvilli.

The iron-granules in the apical cytoplasmic mass always appear to be intact. We do not see any electron-dense material in the cytoplasm surrounding the granules, nor do we observe any granules with broken membranes.

In the microvilli zone, the areas of contact between adjacent cusp cells are highly modified, in comparison with cell junctions in the central or basal regions. In transverse section, the plasma membranes are asymmetric tri-layered structures approximately 75 Å thick (Figures 61,62). The internal dense layer of the membrane is thicker and more heavily stained than the outer dense layer. The apposed cell membranes are separated by a space 150 Å wide that is filled with a moderately stained substance. Many segments of the cell-to-cell junctions show additional substructure. In these areas, the interspace between the cell membranes contains repeated 100 Å wide structures which consist of two dark bands and a central light zone, each approximately 30 to 35 Å wide. These structures extend across the interspace perpendicular to the cell membranes. Generally, the cytoplasm in contact with these segments contains an electron-dense material which is closely applied to the inner surfaces of the apposed cell membranes. The appearance of the structures in Figure 62 suggests that they may

Figures 59 and 60. Longitudinal sections of the double membrane structures. Note the similarity to endoplasmic reticulum, where the structure extends into the apical cytoplasm.

Figure 59. X 67,000.

Figure 60. Note the unusual cell junction in the upper left corner.

X 46,700.

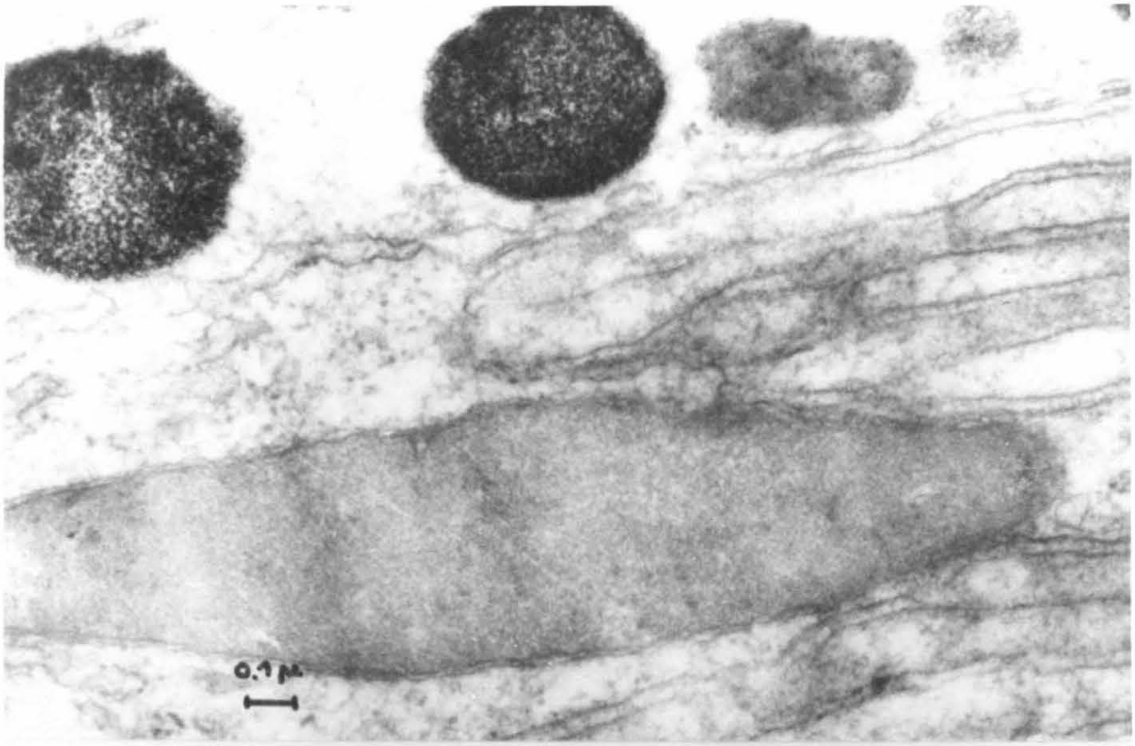
0.1 μ

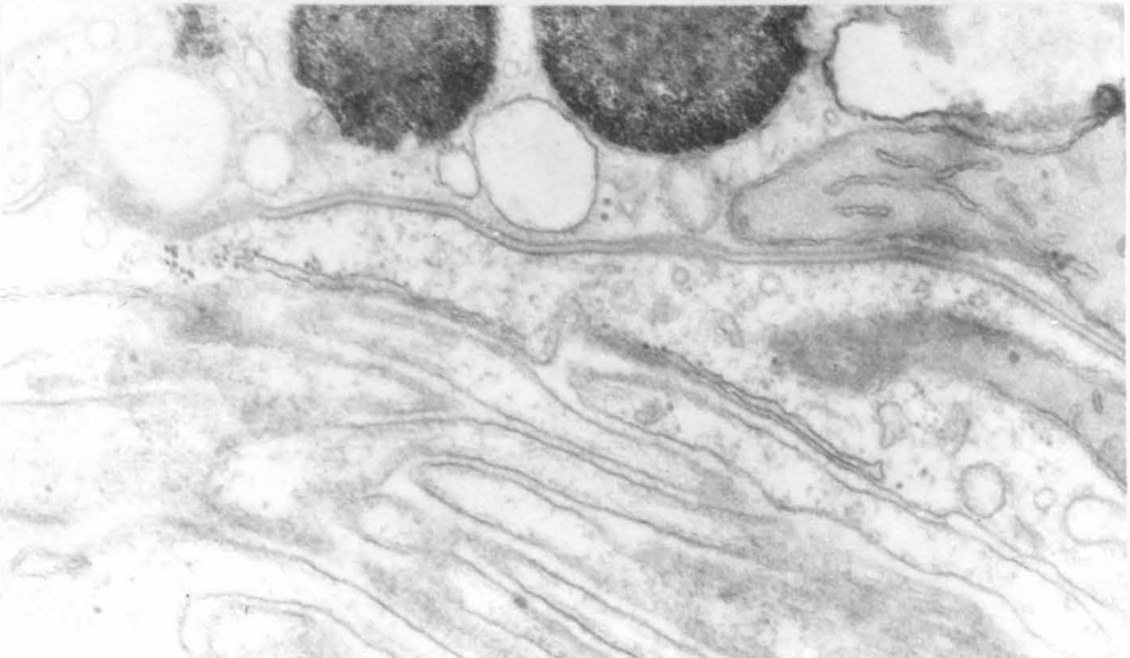
0.1 μ

Figures 61 and 62. Cusp cell apical junctions. Each apposed cell membrane is asymmetric. Note the areas of substructure within the interspace.

Figure 61. X 94,000.

Figure 62. Note the apparent connection of the cytoplasm of the adjoining cells *via* tubule-like structure.

X 96,800.

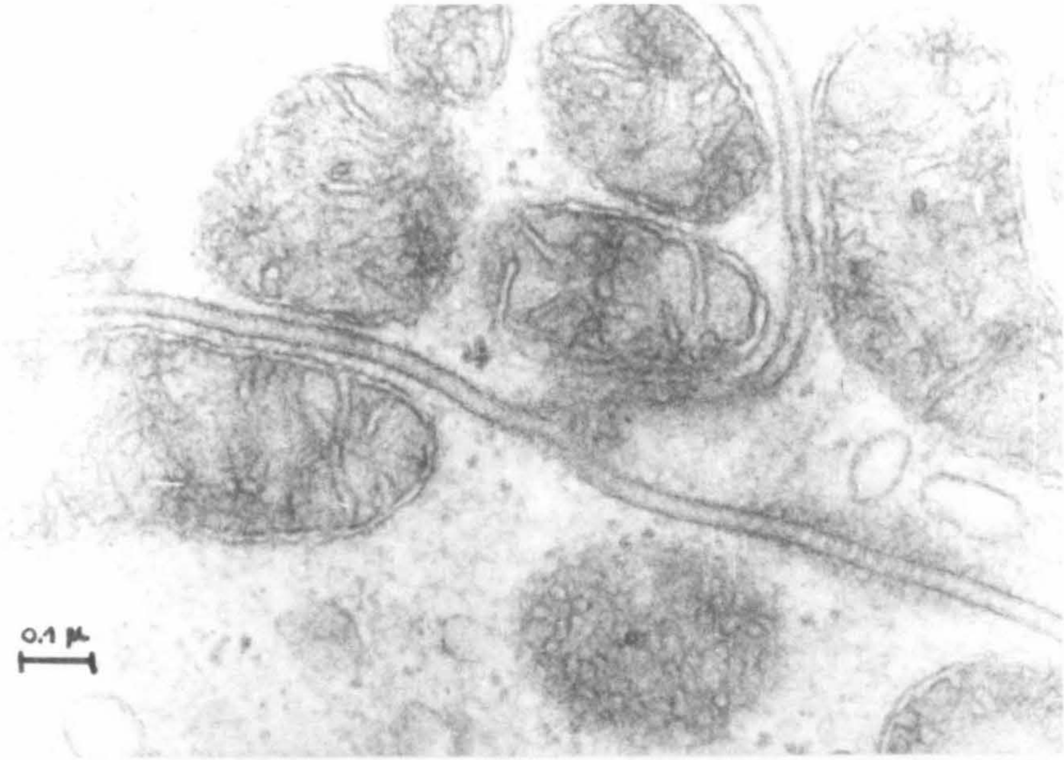
0.1 μ

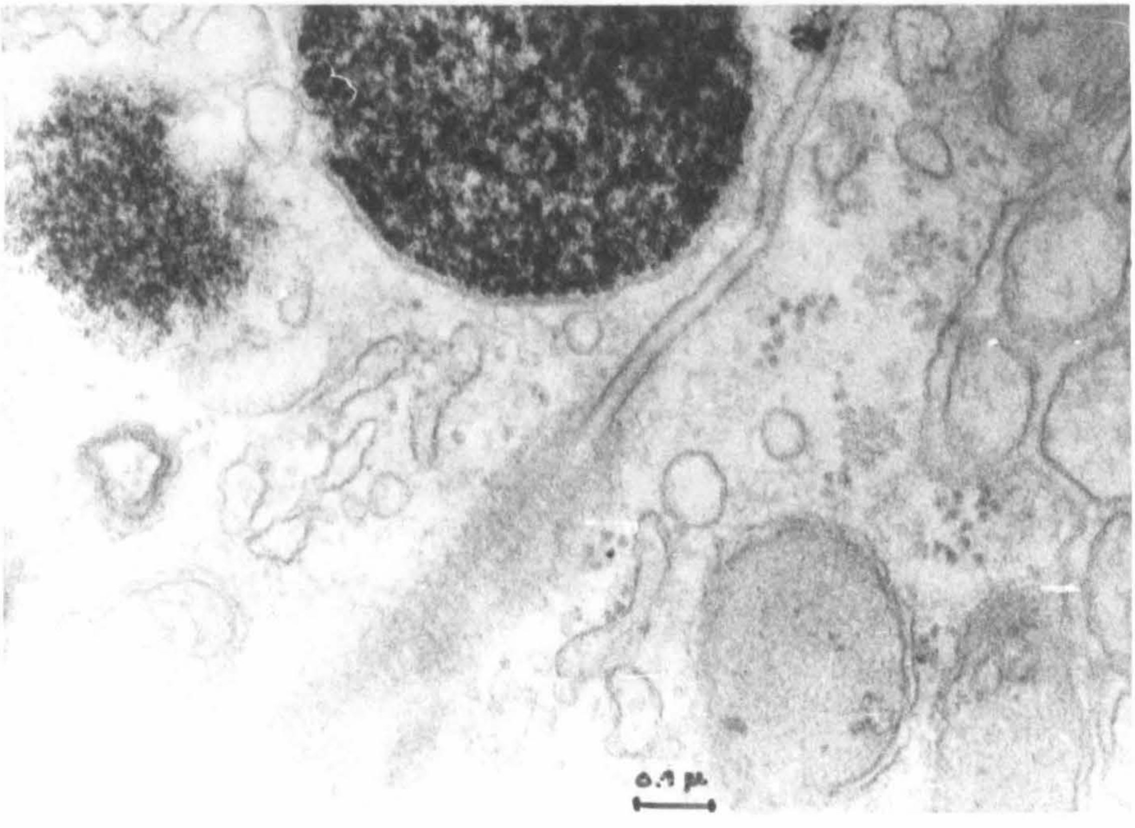
0.1 μ

be tubular intercellular bridges. At the present time, we do not have sufficient information to determine the function of these structures.

The Ultrastructure of the Tooth Cusps.

We have previously discussed the electron microscope findings of Towe and Lowenstam (13) on the major lateral tooth cusps of *Cryptochiton stelleri* (cf. General Introduction). Our observations on the structure of the cusps of *L. hartwegi* serve to support and extend their findings.

The protein-chitin material that comprises the matrix of the tooth cusps of *L. hartwegi* consists of fine fibrils (Figures 63,64). Where individual fibrils can be seen, they generally measure about 20 Å across, in contrast to the reported value of 50 Å for *Cryptochiton*. Examination of the published micrographs of *Cryptochiton* cusps (13) does not allow us to establish whether this difference is real.

The 20 Å fibrils are massed into long fibrous sheets, approximately 200 Å thick. The sheets are arranged to form the walls of an array of long cavities (Figure 65), which are roughly polygonal in cross-section (Figure 64).

It was suggested, but not fully demonstrated, by Towe and Lowenstam (13), that the initial deposition of iron-containing mineral in the brown tooth cusps occurs directly on the organic framework. Figure 65 fully documents the validity of their suggestion; we can see that the great majority of the spherules of hydrated ferric oxide are in intimate association with the fibrillar matrix. In regions where the spherules are relatively concentrated, their relationship with the matrix has an

Figure 63. Oblique section through the brown tooth matrix. The smallest fibrils are about 20 Å wide. The electron-dense spherules appear to be aggregates of smaller granules. X 192,000.

Figure 64. Transverse section through the polygonal cavities of a brown tooth cusp. X 185,000.

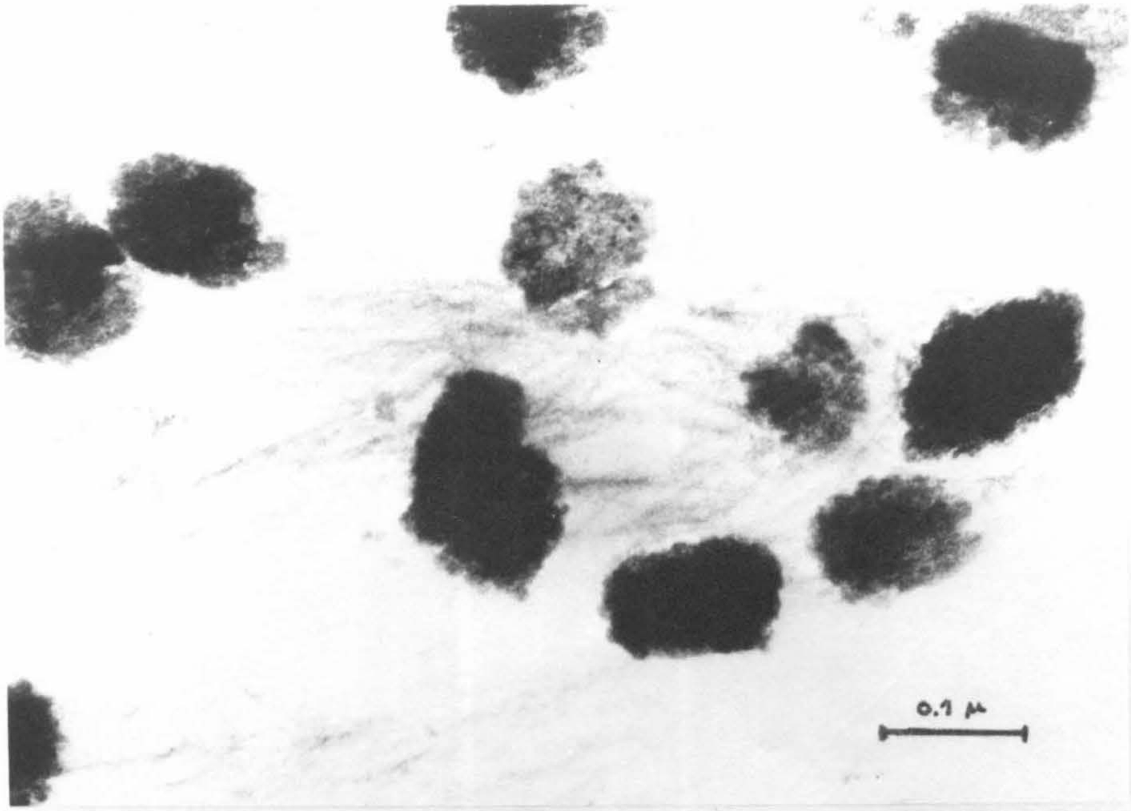
0.1 μ

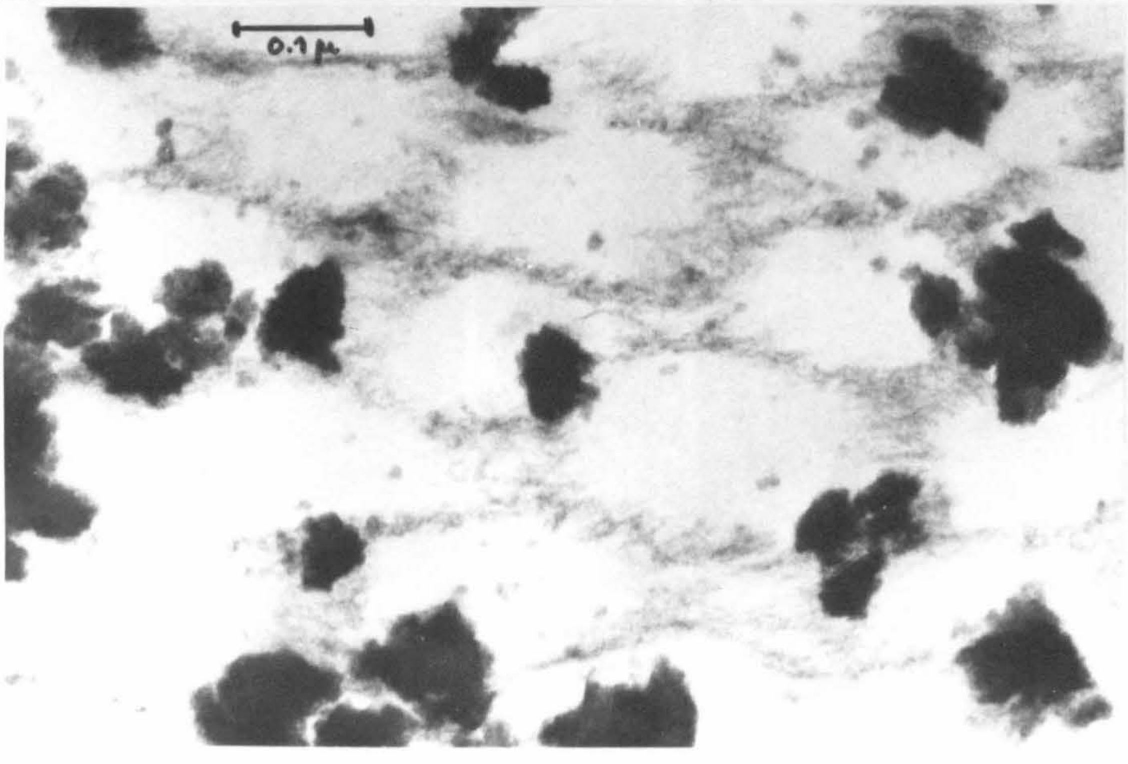
0.1 μ

Figure 65. A longitudinal view of a brown tooth cusp. Note the close association of the mineral spherules with the matrix fibers.

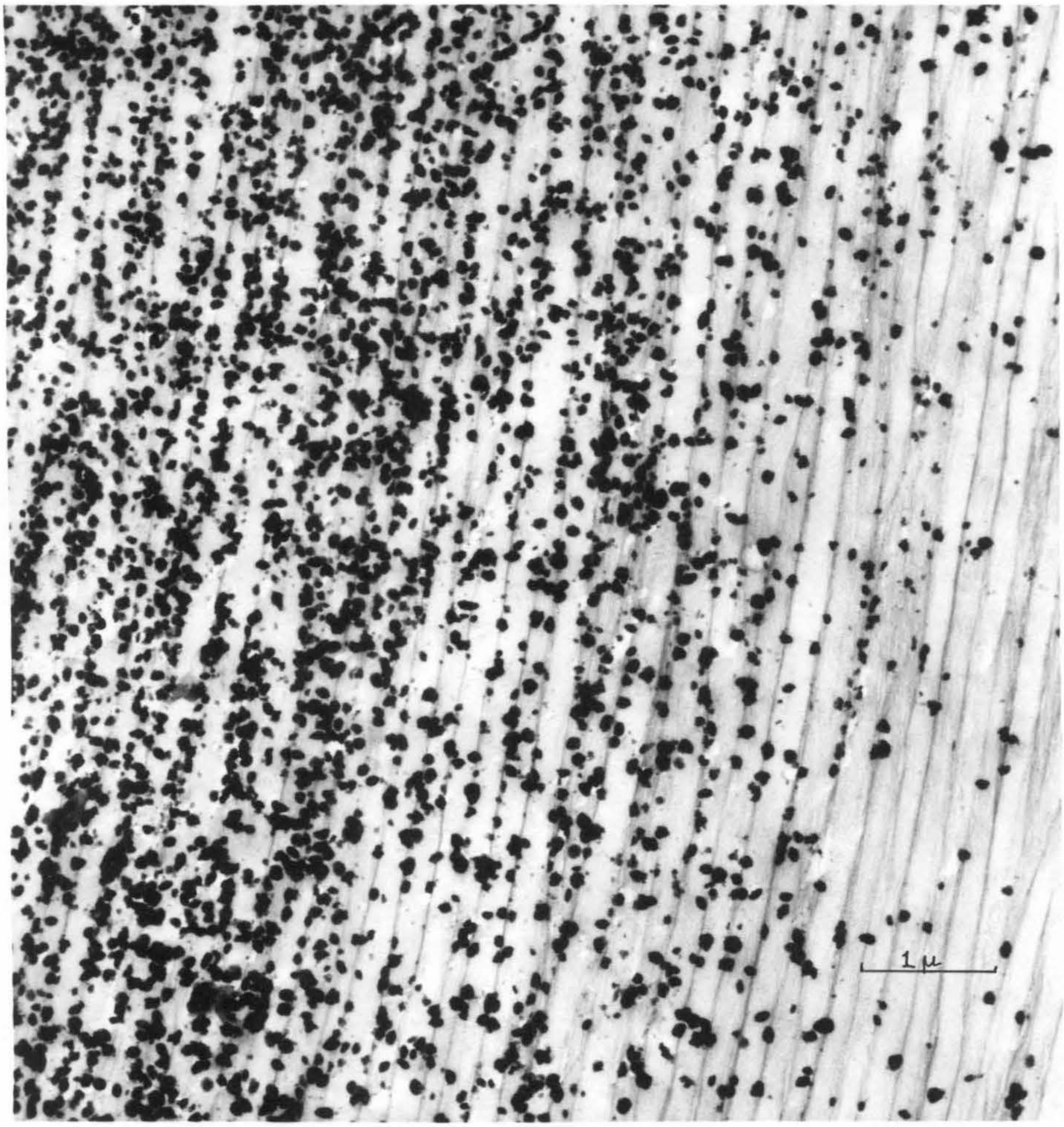
1 μ

appearance that resembles beads on a string. In slightly more mineralized regions, the spherules completely obscure the underlying matrix fibers.

Thus, in low magnification sections through the brown tooth cusps, the pattern of spherules serves to indicate the arrangement of the underlying organic matrix. In Figure 66, the entire visible area of sectioned tooth displays a high degree of order. In this almost transverse section through the cusp, the long axes of the polygonal cavities bounded by the organic matrix entend nearly parallel to the anterior surface of the tooth cusp. Internally, the array of cavities makes a nearly 180° turn so that the cavities abut the posterior face of the cusp at an acute angle to the plane of the surface. Further observations and analyses are needed to determine whether this matrix pattern is related to the mechanical stress pattern which is produced when the mature magnetite-impregnated cusps are used for the rasping process.

At the level of the brown cusps and the first rows of black teeth, mineralization of the cusp matrix does not appear to proceed evenly throughout the cusp (Figures 4,5,39,66). A 5 to 7 μ thick layer along the posterior face of each cusp contains, on the average, a much higher concentration of iron-containing minerals than does the anterior portion. However, localized patches of higher mineral concentrations are also commonly found in the anterior portion of the cusp, particularly within the first magnetite-containing tooth cusps.

The whole posterior surface of the brown cusps is covered with a layer of moderately dense material, about 150 to 200 mμ thick (Figure

Figure 66. Low power transverse view of a brown cusp. Note the layer of moderately dense material which forms a thin coat over the posterior surface and a thicker one over the lateral edge of the cusp.

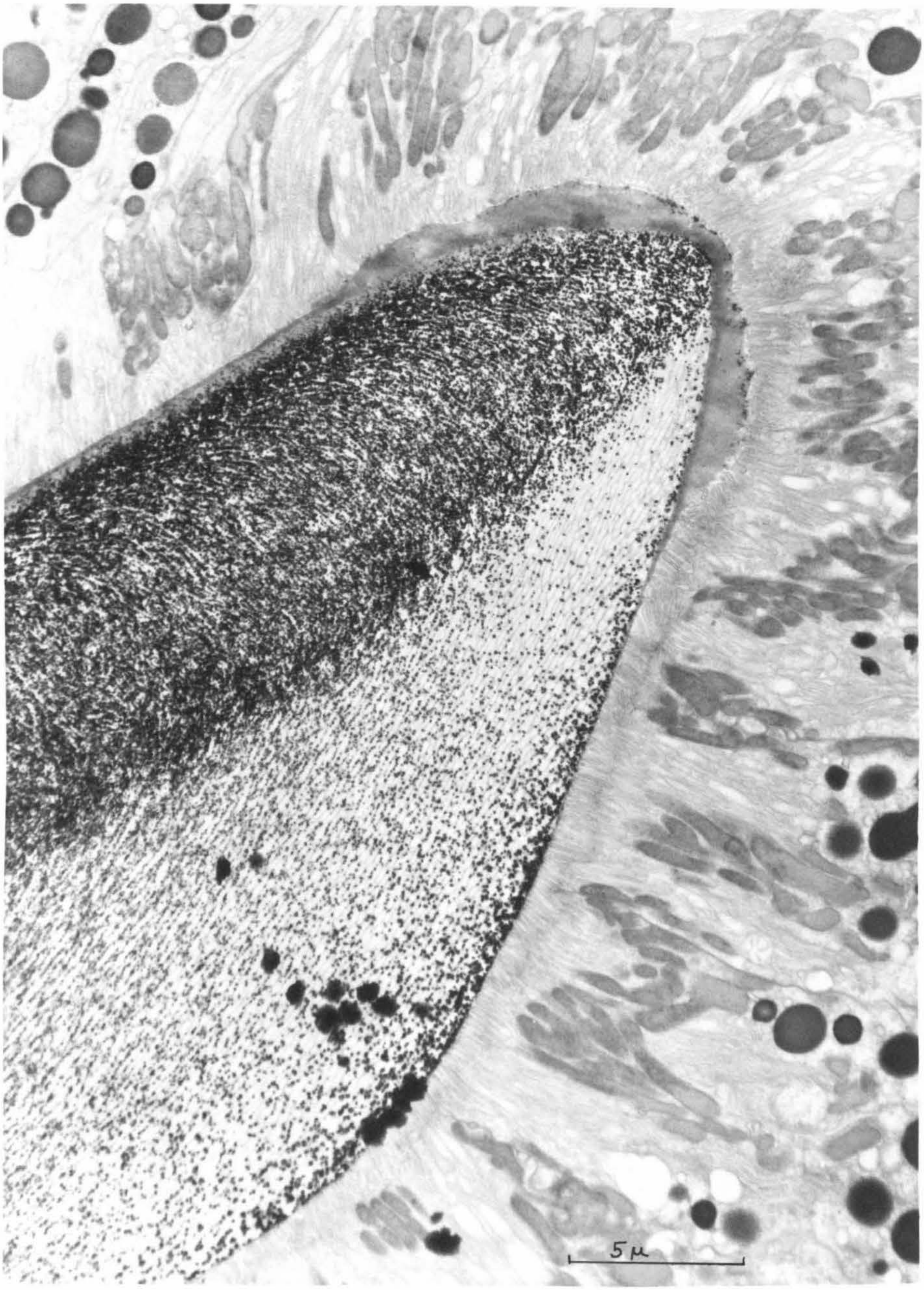
5 μ

39,66). This thin coating becomes much thicker in the space between the bases of the prongs of the tricuspid teeth of L. hartwegi and M. muscosa, as is shown in Figures 67 and 68a.

The coating material appears amorphous and quite homogeneous, even at high magnification (Figure 68b). The coating layer also contains a number of ∿ 200 mμ electron-dense spherules, which consist of aggregates of very small particles; these spherules are morphologically similar to the brown mineral spherules observed within the matrix of the brown cusps (cf. Figures 63,64). In regions where the coating material is thick, the spherules are concentrated towards the outer surface (Figure 67,68a). Selected-area electron diffraction studies of the amorphous layer indicate that the spherules are composed of the same hydrated ferric oxide mineral that is present within the brown teeth.

We have examined several sections which include the edge of a tooth cusp that contains, in addition to the spherules of brown mineral, a number of small, rod-like or plate-like electron-dense structures which commonly lie at an acute angle to the walls of the matrix cavities (Figure 69). Selected-area diffraction of these cusp sections gives a series of diffraction lines which appear to be a superimposition of the diffraction pattern of hydrated ferric oxide and of magnetite (Table 1). Hence, we conclude that the generally rectangular structures are crystals of magnetite. The cusp that is seen in Figure 69 must be the first of the magnetite-containing teeth, since the cusp of the row immediately posterior contains only brown mineral. We have been unable to establish with certainty whether the first appearance of magnetite crystals occurs

Table 1. RESULTS OF ELECTRON DIFFRACTION ON THE FIRST MAGNETITE-CONTAINING TOOTH CUSP

d (Å) Tooth Cusp	d (Å) Ferric Oxide Hydrate	d (Å) Magnetite
2.99	--	2.97
2.55	2.54	2.53
2.23	2.24	--
2.10	--	2.10
2.00	1.98	--
1.71	1.725	1.71
1.61	--	1.62
1.50	1.515	(1.48)
1.47	1.47	(1.48)
1.29	(1.34)	(1.33)(1.28)

The d-spacings in the first column are from the present investigation. The ferric oxide hydrate values are from Towe and Bradley (56), and the magnetite spacings are from Berry and Thompson (107).

Figure 67. The tip of one prong of the brown cusp. Note the massive layer of material in which it is embedded. Also note the presence of electron-dense granules within the outer portion of this material.

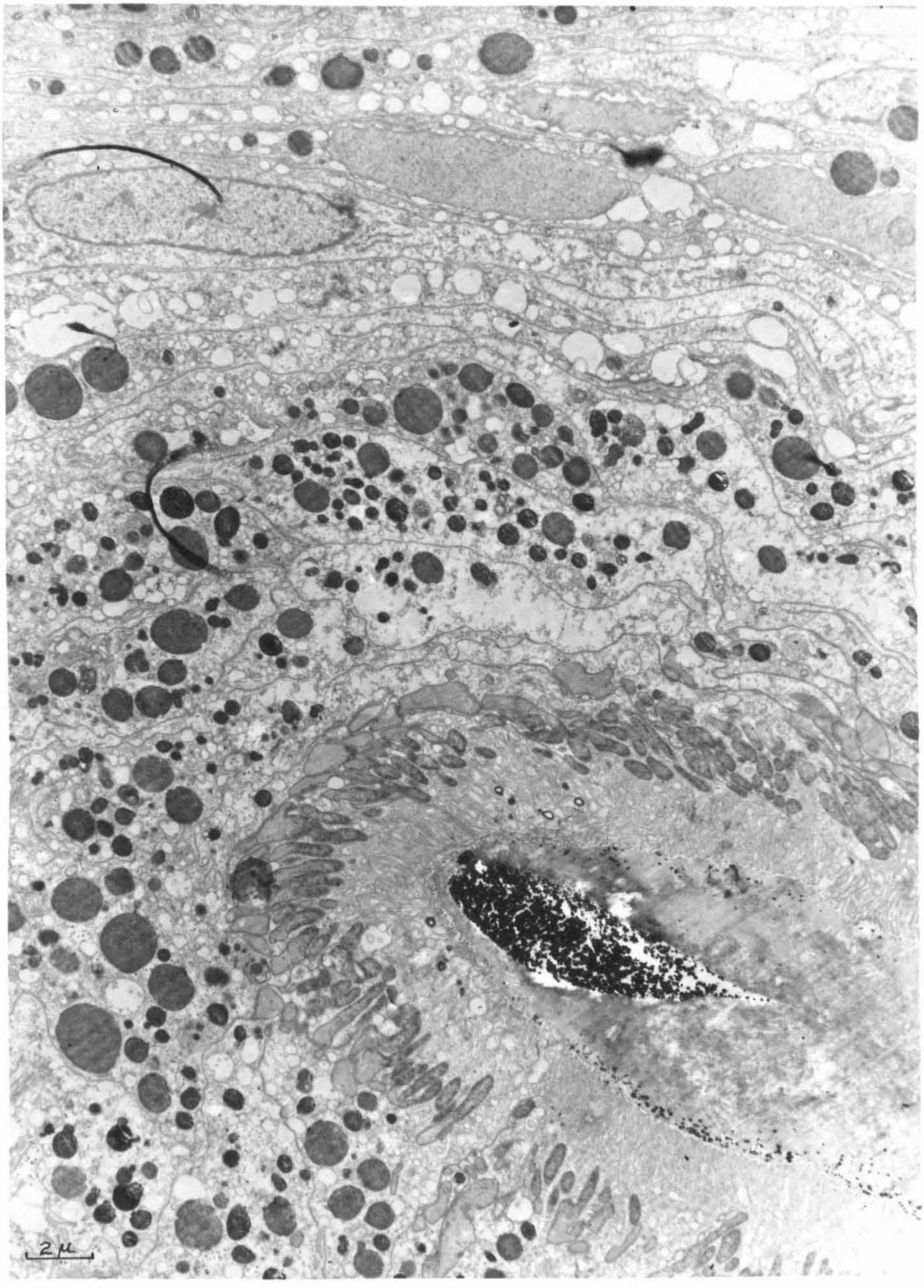
2 μ

Figure 68. The amorphous coating of the tooth cusp.

a. Lower power view. Note the concentration of dense spherules towards the outer surface of the amorphous layer.

b. Higher magnification of the amorphous layer. The spherules are composed of small electron-dense particles.

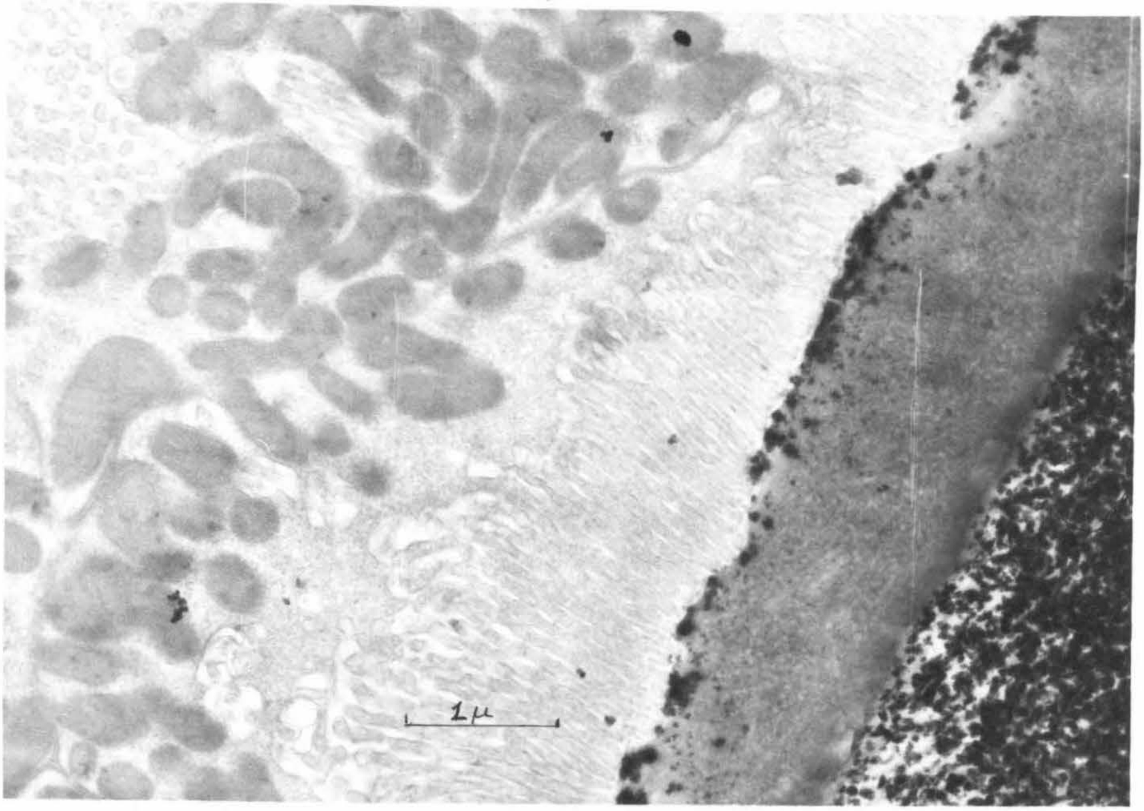
1μ

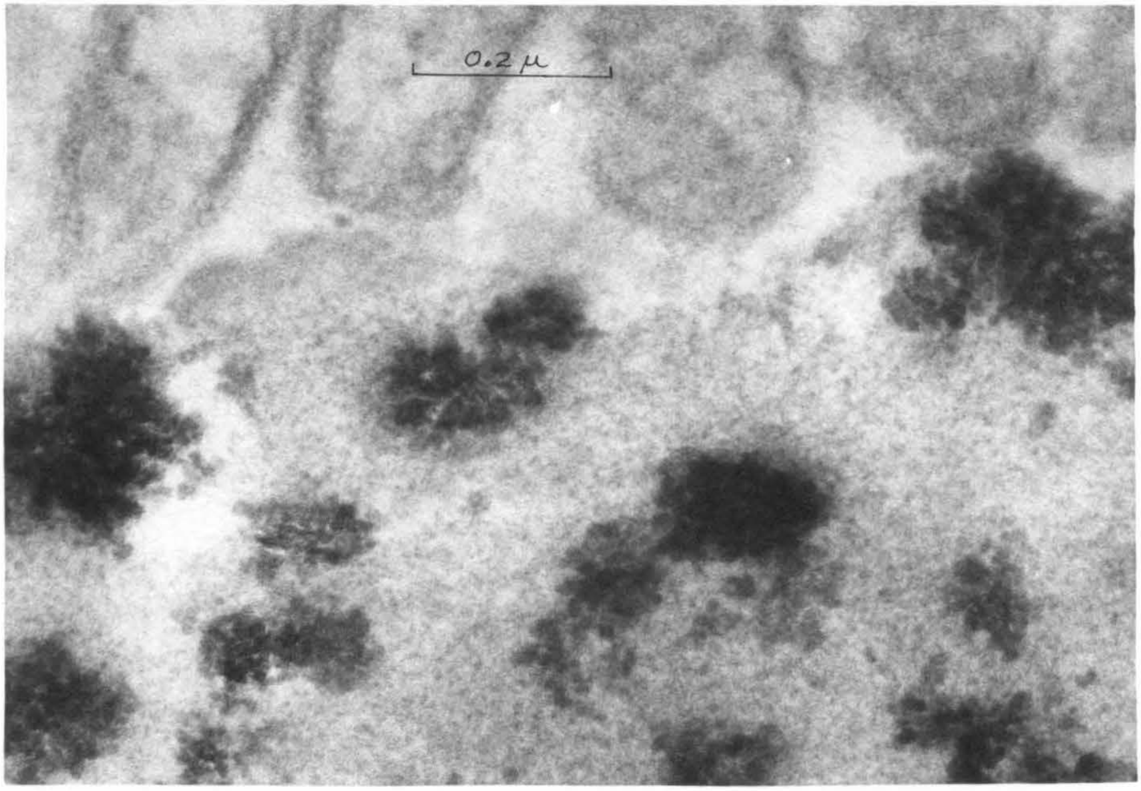
0.2 μ

Figure 69. The first magnetite-containing cusp. Note the arrangement of the angular crystals, with respect to the fibrous matrix. X 70,000.

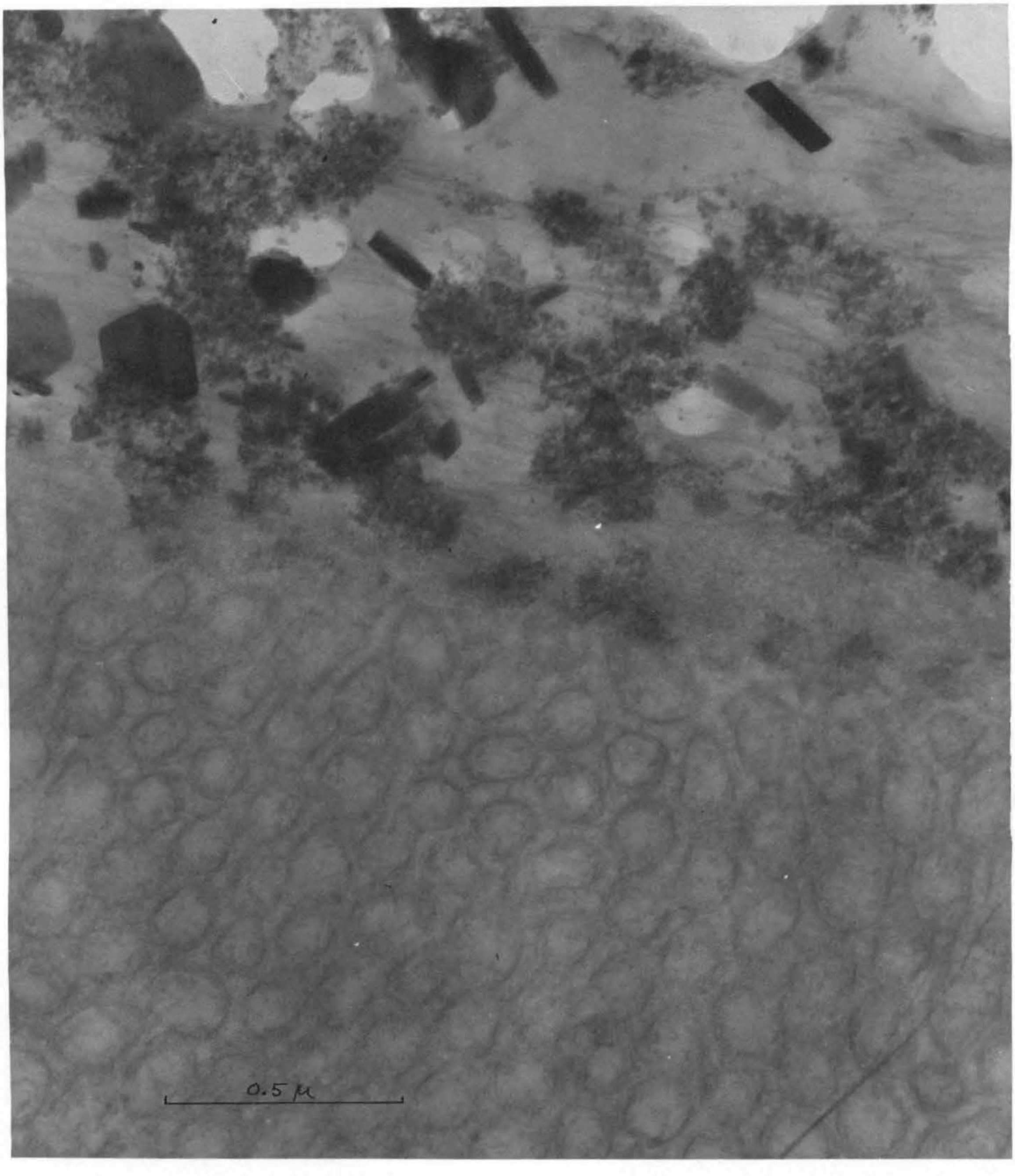
0.5 μ

near the surface or deep within the cusp. Except for a slightly higher concentration of iron-containing granules, the cusp cells which contact the first magnetite-containing cusps are identical to those of the preceding tooth rows.

The Apical Region of the Minor Cells.

The minor superior epithelial cells terminate on the surfaces of the styli and the minor radula teeth. We have encountered great difficulty in cutting sections of material which contain these minor teeth. Apparently, the teeth are not impregnated with the embedding material; they almost inevitably shatter or pull away from the surrounding tissue as they are being cut. In the few cases where we have been able to examine the teeth, they appear to be composed of a relatively homogeneous brittle material which is without any resolvable substructure (Figure 70,71). The apical ends of the minor cells which contact the minor teeth are formed into numerous interdigitating processes which have no detectable preferred orientation with respect to the tooth surface. The processes contain ground cytoplasm and a few small membrane-bound vesicles. The nearby cytoplasm contains segments of rough endoplasmic reticulum, various sized vesicles, and sometimes a few ferritin-containing or ferruginous granules. In Figure 71, two Golgi systems can be seen. These few observations are enough to indicate that the minor cells are quite different from the cusp cells, not only at their basal poles, as we have previously discusses, but also at their apical ends.

Figures 70 and 71. The apical ends of the minor cells. Note the thick interdigitating processes at the tooth-cell junction. A few scattered iron-containing granules are present in the cytoplasm.

Figure 70. Note the endoplasmic reticulum and the numerous vesicles.

X 25,000.

Figure 71. Note the two Golgi systems.

X 94,900.

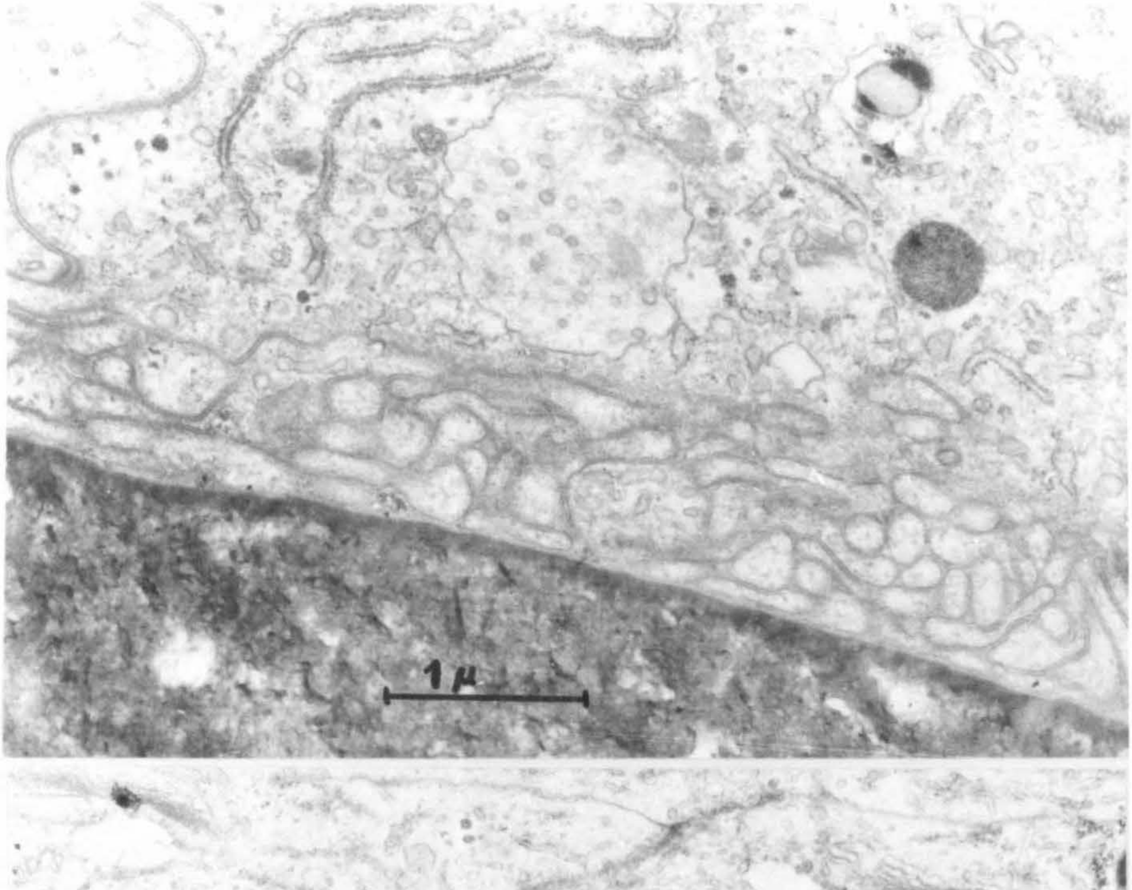
1 μ
1 μ

DISCUSSION

Since the publication of Prenant's cytological studies on the cells of the superior epithelium of the Polyplacophoran radula sac (18), it has been the accepted view that these cells are intimately involved in the transport and secretion of iron into the major lateral tooth cusps. Our electron microscope investigations of the radula sac tissues of two California species of chiton, Lepidochitona hartwegi and Mopalia muscosa, have revealed the existence of a number of highly specialized regions and organelles within the cusp cells and in their vicinity. In the following discussion, we place the major emphasis on the functions of the observed structures and on their possible roles in the processes which result in the formation of magnetite-impregnated tooth cusps.

We have discovered that a large dorsal sinus extends posteriorly within the radula sac, passing through the mineralization zone to the posterior blind end of the sac. From the appearance of its endothelial lining and the contents of its lumen, we have tentatively concluded that the dorsal sinus is a blood sinus. It is presumably connected with the haemocoel-type circulatory system at some point towards the anterior end of the radula sac.

The basal ends of the superior epithelial cells all appear to terminate in close proximity to the dorsal sinus. The cusp cells are separated from the lumen by a thick layer of basement material and a thin single-cell layer of endothelial lining tissue. Some of the endothelial cells contain small vesicular structures filled with material which closely resembles the ferritin-containing aggregates found in the dorsal sinus. Several studies on capillaries of many mammalian tissues have shown that the transport of ferritin across the capillary endothelial cells occurs within plasmalemmal vesicles (80,81, 82). In these cells, the ferritin-containing vesicles are formed by a pinocytotic process, move across the thin cells, and empty their contents into the area of the basement membrane. We suggest that a similar process is performed by the endothelial lining cells of the dorsal sinus of the radula sac. It may be argued that there are too few vesicles visible in the endothelial cells to account for the large accumulation of ferritin molecules in the basement layer and the basal regions of the cusp cells. However, we must emphasize that, in the absence of efficient methods for rapid perfusion of fixative into the sinus, the preservation of the delicate pinocytotic invaginations is likely to be poor. Further, since, in the early stages of fixation, we excise the radula, the presumed circulatory fluid within the dorsal sinus can easily escape through the cut end. The loss of ferritin from the lumen would undoubtedly cause a decrease in pinocytotic activity of the endothelium.

The molecules of ferritin within the basement material are concentrated into a highly ordered pattern. The electron microscope findings do not allow us to establish any structural basis for the observed arrangement. We are unable to distinguish between the possible presence of preformed channels through the basement material or the existence of preferential binding sites within the basement layer. We have not encountered any reports which describe similar examples of highly ordered substructure within the basement layers of other tissues. We are unable to determine whether or not this orderly arrangement is indicative of a special mechanism for the transport of ferritin molecules through the basement material to the epithelial cells.

Our findings strongly indicate that ferritin molecules are incorporated into the cusp cells at their basal pole. The uptake occurs by a process which seems identical to the process termed rhopheocytosis by Policard and Bessis (76). Rhopheocytosis refers to a phenomenon in which a cell takes up macromolecular substances in a process closely related to pinocytosis. Molecules are bound to regions of the plasma membrane and are incorporated into intracellular vesicles by the invagination and pinching off of the cell membrane. The plasmalemmal structures which we have observed in the basal region of the cusp cells are morphologically identical to the rhopheocytotic structures described by Bessis and his co-workers in vertebrate erythroblast cells (77,78).

The large ferritin-filled membrane-bound granules of the basal region are apparently formed by the fusion of the smaller rhopheocytotic vesicles. Similar fusion phenomena have been reported to occur during ferritin uptake by renal epithelial cells (83), by human epidermal cells (101), and by Erlich ascites tumor cells (84). In the latter case, it was found that the uptake and aggregation of ferritin take place under anaerobic conditions. The absence of mitochondria in the basal portion of the cusp cells suggests that ferritin rhopheocytosis in chitons may also be an anaerobic process.

From our observations, we conclude that the major source of iron for the cusp cells is ferritin, which is rhopheocytoticly incorporated mainly in the basal region and to a much lesser extent in the central region.

The next phase of the cellular iron transport is presumably the migration of the large ferritin-containing granules to the apical pole of the cusp cells. Out electron microscope studies do not provide any direct proof that the ferritin granules move to the apical region. However, the accumulation of granules in the apical granule zone and the occurrence of granules within the central cytoplasm, often arranged in rows within an individual cell, strongly suggest that such migration occurs. The relatively low concentration of granules in the central cytoplasm of the cusp cells may indicate that the ferritin granules are rapidly transferred from the basal region to the apical pole. Although many examples of intracellular movement of vesicles in specific directions have been studied, nothing is yet known about the mechanisms which control such migrations.

From the basal region to the level of the nucleus, all of the iron-containing granules within the cusp cell cytoplasm are filled with ferritin. At the level of the Golgi apparatus, near the basal edge of the granule zone, granules filled with other types of electron-dense iron-containing material first appear. If we accept our interpretation that the cusp cells take up iron primarily in the form of ferritin, it appears probable that the ferritin-containing granules are the source from which the other types of granules arise. A comparison of the ultrastructure of the various classes of granules leads us to suggest a developmental sequence which can account for the appearance of the several types of granules.

The key finding upon which we have based our scheme of granule transformation is the morphology of the intermediate granules. We interpret the intermediate granules as being representative of intermediate stages in the transformation of the ferritin-containing granules into ferruginous granules. The appearance of the intermediate granules strongly suggests that the iron-containing mineral micelle is released from the ferritin molecules by the degradation or removal of the apoferritin protein moiety. The micelles either spontaneously fall apart or are somehow broken down into the smaller electron-dense particles characteristic of the ferruginous granules. From the data at hand, we are unable to determine the chemical or mineralogical composition of the iron-containing material of the ferruginous granules. Our attempts to study this material by electron diffraction have been unsuccessful. However, diffraction studies of similar appearing ferruginous or "haemosiderin" granules in other organisms suggest that the iron-material may be a partly hydrated α-ferric oxide ($\alpha Fe_2O_3 \cdot nH_2O$) (79,102). We cannot exclude the possibility that the chiton ferruginous granules contain some ferrous iron. The negative results of histochemical tests for ferrous iron do not preclude the presence of Fe^{2+} in a masked form.

The average size of the ferruginous granules appears to be 20 to 30% smaller than the ferritin granules. This observation further indicates that some material, presumably the apoferritin protein, is lost from the membrane-bound granules during the transformation. We have no information on the subsequent function or path of the released apoferritin.

Similar conversions of ferritin into ferruginous or "haemosiderin" iron oxide deposits have been reported to occur in many vertebrate tissues (85,86). These deposits have been generally interpreted as being a means of storing excess iron. Some workers have suggested that the iron of haemosiderin is less readily mobilizable than ferritin iron (86). However, in the cusp cells, it appears that the ferruginous granules are the source of the iron which is secreted into the tooth cusps.

We suggest that the granules that contain a low concentration of small electron-dense particles are ferruginous granules which are in the process of releasing their iron. We are unable to distinguish whether the intact membrane-bound vesicles lose their iron in a soluble form or by the release of extremely small (less than 25 Å) particles of iron oxide.

The various classes of granules are distributed randomly throughout the granule zone. If the sequence of granule transformations that we have proposed is correct, then it appears necessary to postulate that the cusp cells have some means of recognizing the various types of granules, so as to carry out and control the processes which lead to the release of iron from the granules for secretion into the teeth. Several findings suggest that the Golgi system may be involved in the transformation processes; the non-ferritin granules make their first appearance at the level of the Golgi apparatus, and numerous vesicles that may be of Golgi origin are generally observed throughout the granule zone. However, the appearance of the intermediate granules suggests that the breakdown of ferritin is brought about by cellular products (perhaps proteolytic enzymes) which diffuse directly from the surrounding cytoplasm into the ferritin-containing granules. Direct proof of the proposed sequence of transformation and elucidation of the mechanisms of granule transformation and iron release are problems which can only be resolved by further study. The relation between the various types of granules can be investigated by following the path of radioactive iron within the cups cells. Biochemcial studies on cell-free preparations of iron-containing granules may provide information on the mechanisms involved in the processes of transformation and iron release.

We have noted that no free micellar or particulate electron-dense material is observable within the cytoplasm in the granule zone or within the microvilli. We must conclude that the iron occurs either in soluble form or within extremely small particles during the final phase of intracellular iron transport (i.e., from the presumed site of release at the outer surface of the ferruginous granules to the probable site of iron secretion at the surfaces of the microvilli). We do not know the chemical state of this cytoplasmic iron. This final phase of transport may occur by an active iron transport mechanism or simply by diffusion. Possible support for the latter process comes from the presence of a double-membrane structure, presumably a modified segment of endoplasmic reticulum, that is closely applied to the plasma membrane of the shell of cytoplasm that surrounds each bundle of microvilli. This structure is usually found only where iron-containing granules lie within the cytoplasmic shell. It seems possible that the double-membrane structure serves as a diffusion barrier which prevents the cytoplasmic iron from reaching the plasma membrane of the surrounding cytoplasmic shell. Because of its location, the structure may tend to increase the diffusion of iron into the microvilli.

The fact that the microvilli of the cusp cells terminate directly on the surface of the tooth cusps is quite unusual. Microvilli are typically found on the surfaces of cells which form the walls of a lumen (e.g., the epithelial lining of the intestinal tract, the brush border cells of the mammalial renal tubule, etc.). In such locations, the microvilli undoubtedly function to increase the surface area for the purpose of absorption of substances from the lumen. In the cusp cells, the most likely function of the microvilli is to increase the surface area for the purpose of iron secretion into the tooth cusps.

We suggest that the outer membranes of the microvilli contain a large number of sites at which iron is actively secreted from the interior of the microvilli into the tooth cusps. The concentration of iron in the extracellular spaces (i.e., the interior of the tooth cusps) must be high enough to allow the precipitation of ferric oxide, in the early phase of mineralization, and the formation and growth of magnetite crystals, in the later stages of mineralization. It is highly probable that the secretion of iron by the microvilli occurs against a concentration gradient. Hence, the iron must presumably be pumped out of the microvilli by an energy-requiring active transport system situated in the microvilli membrane. The characteristic accumulation of large numbers of mitochondria in the cytoplasm that surrounds the microvilli undoubtedly serves as a source of energy for the process of iron secretion.

As we have previously pointed out, the initial phase of mineralization consists of the deposition of hydrated ferric oxide on the organic matrix of the cusps. Since it appears that the iron taken up by the cusp cells is in the same chemical and mineralogic form (i.e., the hydrated ferric oxide micelle of ferritin), one might conclude that the cusp cell microvilli secrete ferric iron, either in a soluble form or in the form of particulate ferric oxide. The deposition of the brown mineral on the cusp matrix would then occur either by the *in situ* precipitation of soluble ferric iron or by the aggregation of particles of ferric oxide. However, an additional possibility is that the ferritin iron is reduced to Fe^{2+} within the cusp cells and is secreted as ferrous iron by the microvilli. It is well known that, in the process of iron uptake by the mucosal cells of mammalian intestinal epithelium, only ferrous iron is able to cross the cell membranes of the mucosal microvilli (cf. (104,105)). If the iron secreted by the cusp cells is in the ferrous state, it must first be converted to Fe^{3+} before it is deposited as ferric oxide within the cusps, either by oxidizing agents released from the cells or by oxidative activity of the matrix material itself. The intimate association of the brown mineral spherules with the organic framework of the tooth cusps suggests that the matrix material plays an important role in the early mineralization, perhaps containing nucleation sites for ferric oxide crystallization, analogous to the role of collagen in calcification (cf. (106)), or possibly possessing enzymatic (oxidative) activity.

In the later phase of mineralization, the first crystals of magnetite are formed in proximity to the brown mineral within the cusps. The role of the cusp matrix material and of the cusp cells in the processes involved in the transformation of ferric oxide hydrate to magnetite and the continued growth of the magnetite crystals are problems which require further study.

PART II

STUDIES ON CHITON BLOOD

INTRODUCTION

The process of tooth mineralization in the Polyplacophora requires that a continual supply of iron reach the superior epithelium of the radula sac. The most likely route of transport of iron from its site of absorption, in the digestive gland or the intestine (4,39), to the radula is the semi-closed (haemocoelic) circulatory system (88).

The blood (or haemolymph) of chitons contains a low concentration of formed elements, predominantly ameoboid cells (75). In the plasma of Cryptochiton stelleri, the amount of protein in solution varies between individuals, but generally ranges from 1.0 to 3.5% by weight (89,90). The major protein component (ca. 60%) has been reported to be haemocyanin (89,91), a copper-containing protein which is the characteristic respiratory pigment of the Mollusca (92). Although some workers have noted the presence of other plasma proteins, from velocity sedimentation and electrophoresis studies (89), these components have not been further characterized.

Carefoot (15) has analyzed the blood of a single specimen of Cryptochiton stelleri, and has found it to contain 83 µg. of iron per milliliter. He also stated that 93% of the iron was in the ferrous state.

The investigation presented in this section was undertaken in an attempt to identify the iron-carrying component of the blood of Mopalia muscosa.

MATERIALS AND METHODS

Animals.

Large (6-10 cm.) specimens of Mopalia muscosa are collected and maintained as described in Materials and Methods, Part I.

Blood Sampling.

Two methods are used to obtain samples of blood for investigation.

a) Blood can be sampled directly from the heart which is situated postero-dorsally, beneath the sixth and seventh valves. A hypodermic needle is inserted at a shallow angle into the connective tissue band between valves 6 and 7 or valves 7 and 8. If the needle penetrates the dorsal wall of the heart, samples of 1 to 2 ml. can be withdrawn into a syringe. This method is not reliable because of the extremely delicate, membranous nature of the heart.

b) Numerous shallow longitudinal incisions are made in the ventral surface of the muscular foot. The animal is then placed in a funnel which drains the blood into a collecting tube. The volume of blood obtained in this method is 1 to 3 ml.

All samples are immediately spun for 10 minutes in a clinical centrifuge to remove the cells and other debris. The samples are stored at -20° C.

Radioactive Iron Labeling.

Many of the animals were injected with trace amounts of radioactive iron-59 (Fe^{59}), from five to thirty days prior to blood sampling.

The iron is obtained (from New England Nuclear Corporation) in the form of $Fe^{59}Cl_3$ in 1.0N HCl. After neutralization with 10N NaOH, the stock is diluted with filtered sea-water. Appropriate volumes (0.1 to 0.2 ml), containing from 3 to 50 microcuries (μc) of Fe^{59}, are injected into individual animals. The site of the injection is either directly into the heart (i.e., between valves 6 and 7), or into the abdominal cavity through the foot.

Iron Assay.

Total iron is measured by a slight modification of the technique of Fischer and Price (93), which is a colorimetric assay based on the formation of a colored complex of ferrous iron with 2,4,6-tripyridyl-s-triazine (TPTZ).

Sample aliquots of 0.1 or 0.2 ml are heated to dryness (two hours at 110° C.). 0.1 ml of 6N HCl is added, and the samples are heated to 100° C. for 15 minutes to release the protein-bound iron. After the addition of 1.0 ml of distilled water, the samples are spun for 10 minutes in a clinical centrifuge to remove the insoluble material (mostly denatured protein). Then, 1.0 ml of the supernatant is thoroughly mixed with 0.5 ml of buffered chromagen reagent. The color reagent is prepared from: 1 part of 10% hydroxylamine hydrochloride ($NH_4OH \cdot HCl$); 2 parts of 50% ammonium acetate; and 1 part 0.004M TPTZ (purchased from Nutritional Biochemicals Corporation) in 0.001M HCl. The samples are allowed to stand for 10 minutes before their optical density at 593 millimicrons is determined with a Zeiss Spectrophotometer, Model PMQII.

For each set of assays, we routinely run several blank controls, containing no initial sample, as a measure of iron contamination of the reagents. Also, we determine a standard curve with samples containing known amounts of iron (0.5 to 10μg), prepared from a stock solution of ferrous ammonium sulfate (100μg Fe/ml).

The assay provides a measure of total iron.

Measurement of Radioactivity.

Determination of Fe^{59} radioactivity is carried out on samples (up to 1 ml in volume) mixed with 10 ml of Bray's solution (94). Radioactivity is measured with a Packard liquid scintillation counter. The background for Fe^{59} is about 25 counts per minute (cpm).

0.5 ml aliquots of the final iron assay samples are counted in order to measure the specific activity of the iron. Control samples indicate that the chromogen does not cause detectable quenching.

Agarose Gel Column Fractionation.

Total sample volumes of 0.4 to 1.2 ml are applied onto 50cm x 1.5cm columns of Bio-Gel A-1.5m agarose gel beads (50 to 100 mesh) (purchased from Bio-Rad Laboratories). The column is previously equilibrated with column buffer: 0.05M phosphate buffer (pH 6.00) containing 0.15M NaCl.

Generally, 10^9 to 10^{10} particles of bacteriophage MS-2, a spherical virus 260 Å in diameter (molecular weight 3.6×10^6) (95), are added to the input sample to serve as a marker of the column void volume. For some studies, 0.1 ml of a 10% solution of Blue Dextran 2000 (obtained from Pharmacia) is also added to the input sample.

The column buffer is run through at a flow rate of 24 ml per hour. Samples of 2.0 ml are collected with an automatic fraction collector.

Radioactivity is determined on a 0.5 ml sample of each fraction. MS-2 is measured by the plaque assay technique, as described by Davis and Sinsheimer (96). Blue Dextran is assayed by determining the optical density at 620 mμ with a Zeiss PMQ II Spectrophotometer.

Sucrose Gradient Sedimentation.

5% and 20% (w/v) sucrose solutions, in 0.05*M* phosphate buffer (pH 7.4) containing 0.1*M* NaCl, are used to prepare linear sucrose gradients, by a procedure similar to that described by Britten and Roberts (97). Gradients of 5ml are formed in cellulose tubes at 4° C.

0.3 ml samples, containing approximately 2×10^4 cpm of Fe^{59} and 10^9-10^{10} particles of bacteriophage MS-2, are layered on the top of the gradients. In some cases, 0.1 ml of a 10% Blue Dextran 2000 solution is also contained in the 0.3 ml sample. The tubes are spun for 120 minutes in a SW-50 rotor at 37,000 rpm (at 4° C.) in a Spinco Model L Ultracentrifuge.

Gradient fractions of 20 drops are collected directly into scintillation vials which are assayed for radioactivity. The twenty-first drop, of the first ten fractions, is assayed for MS-2 infectivity.

Absorption Spectra.

Absorption spectra of blood and ferritin are obtained with a Cary Model 15 recording spectrophotometer.

Electron Microscopy.

Copper-mesh grids are covered with a Formvar supporting film prepared from 0.25% Formvar in ethylene dichloride, and are lightly carbon-coated in a vacuum evaporator.

A droplet of sample is directly applied to the grid, the excess is drawn off with filter paper, and the sample is air-dried. For negative-stained preparations, a droplet of 4% phosphotungstic acid in 0.4% sucrose (pH 7.0) is applied to a grid prepared as above, but before the sample has dried. The excess is then drawn off and the grid is allowed to air-dry.

Grids are observed in a Philips EM-200 electron microscope operated at 80 kV, with a 50 μ objective aperture.

Purification of Ferritin.

a) Blood: Samples of *M. muscosa* blood are heated to 75° C. for 5 minutes. After cooling to room temperature, they are centrifuged at 10,000 x *g* for 20 minutes to pellet the heat-coagulated proteins. The supernatant is then spun for 90 minutes in a SW-50 rotor at 47,000 rpm in a Spinco Model L Ultracentrifuge to pellet the ferritin. The pellet is then resuspended in a small volume of water or buffer.

b) Tissue: The whole radulae and radula sheaths are removed from four individuals of *M. muscosa*. 15 ml of distilled water is added to the tissue and the sample undergoes five cycles of freezing and thawing. Then, it is treated for 10 minutes in an L + R Ultrasonicator, Model 312, to further break up the cells. The sample is spun in a clinical centrifuge for 10 minutes to remove the large debris. The supernatant is then treated exactly like a sample of blood as described in the previous paragraph.

Other Materials.

A purified preparation of rabbit ferritin was obtained as a gift from K. M. Towe.

Equine spleen ferritin (cadmium-free) was purchased from Calbiochem.

RESULTS

Studies on Whole Blood.

Oxygenated blood of *Mopalia muscosa* possesses a bluish-green color, caused by the presence of the blue haemocyanin-oxygen complex. In a nitrogen atmosphere, or upon standing, the blue color fades and a faint orange hue becomes apparent. Redmond (91) observed an orange color in the blood of *Katherina* and *Chiton*, but he assumed it was due to carotenoid pigments.

The absorption spectrum of whole blood is quite similar to that of haemocyanin alone: a protein absorption peak at 280 mμ, a large peak at 350 mμ, and a smaller absorption peak at 550 mμ (89).

(a) Iron Content.

The blood of ten individuals of *Mopalia muscosa* were analyzed for iron content. Table 2 shows the measured values of iron concentration. The ten animals have an average content of about 65 μg of iron per milliliter of blood, but there is a nearly three-fold difference between the lowest and the highest values of iron concentration. The value of 83 μg Fe/ml reported for the blood of *Cryptochiton stelleri* (15) falls within the range observed in *Mopalia*.

(b) Agarose Gel Filtration.

The first approach to understanding the nature of the blood iron was the use of agarose gel fractionation to estimate the number and sizes of the iron-containing components.

Table 2. IRON CONCENTRATION OF *MOPALIA* BLOOD

Results are expressed as μg of Fe/ml of blood. Each value is an average of at least two determinations.

41.9
44.6
47.6
51.1
51.5
60.7
64.2
70.5
88.0
113.0

Figure 72 shows the results of size fractionation of Fe^{59}-labeled blood by chromatography on a Gio-Gel A-1.5 m agarose column. Since the size of bacteriophage MS-2 exceeds the exclusion limit of the agarose gel, it is added to the blood sample to serve as a marker of the void volume of the column.

About 95% of the Fe^{59} appears in a single sharp peak which elutes in a volume only slightly larger than the void volume. The small, but reproducible, retardation of the peak of radioactivity suggests that the blood iron is contained in a homogeneous, large component (possibly a product of aggregation) of a size barely within the fractionation range of the gel.

In a number of further sutdies, MS-2 was replaced as a marker by Blue Dextran 2000 (BD). In every one of these runs, the peak of radioactivity coincided with the position of the BD. Under these conditions, the radioactive material appears to be completely excluded from the agarose gel.

(c) Sucrose Gradient Sedimentation.

In order to explain the discrepancies in the gel column data, and to investigate the possibility of aggregation, the same blood was analyzed by sucrose gradient velocity sedimentation.

Two aliquots of blood, one containing added MS-2, the other containing both MS-2 and BD, were layered onto sucrose gradients and centrifuged simultaneously. Visual examination of the BD-containing gradient revealed a broad blue band near the top of the tube and a dark blue pellet at the bottom. No pelleted material was observed in the

Figure 72. Bio-Gel A-1.5 m agarose column chromatography of Fe^{59}-labeled *M. muscosa* blood. Blood is obtained from an animal 12 days after it is given 10 µc Fe^{59}. The cells are spun out, and an 0.05 ml sample is added to 0.4 ml column buffer containing approximately 5 X 10^9 particles of MS-2. The sample is layered onto the column and 2 ml fractions are collected and analyzed as described in Materials and Methods.

Radioactivity: —●—●—●—

MS-2 Infectivity: -○--○-○--

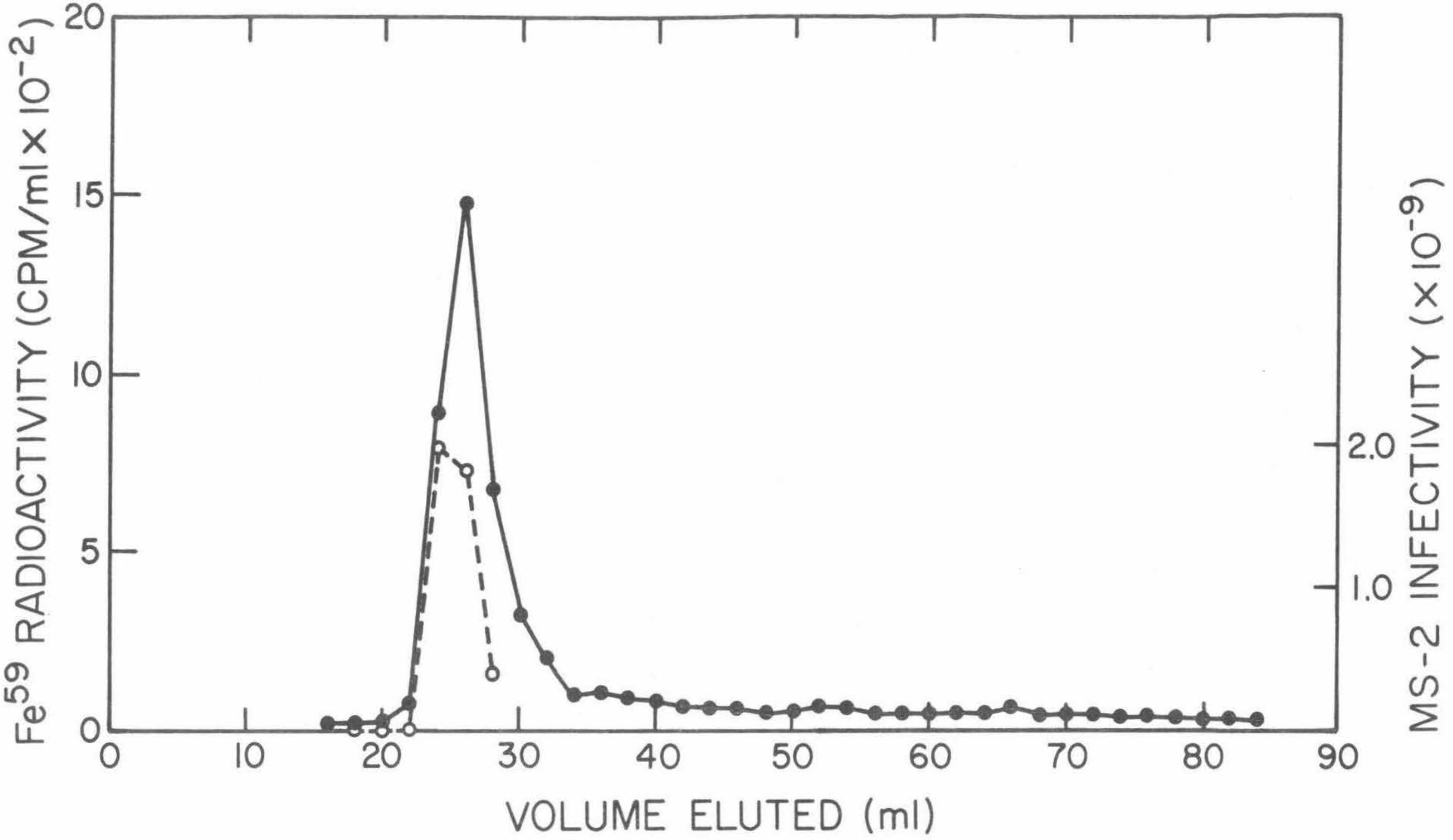
Fe^{59} RADIOACTIVITY (CPM/ml × 10^{-2})
20
15
10
5
0
MS-2 INFECTIVITY (× 10^{-9})
2.0
1.0
0
10
20
30
40
50
60
70
80
90
VOLUME ELUTED (ml)

absence of BD. On comparison of the two sedimentation patterns of radioactivity (Figure 73), it is apparent that only a negligible fraction of the input radioactivity is recovered in the presence of BD (Figure 73b). The pelleted material could not be redissolved, but a portion of the pellet was resuspended and found to contain a large fraction of the input radioactivity.

These findings strongly indicate that Blue Dextran 2000 combines in some way with the iron-containing material to form a complex which sediments very rapidly. The formation of an aggregate also provides an explanation for the observed co-elution of radioactivity and BD from the gel column.

In the absence of BD (Figure 73a), the radioactive material sediments in a very broad band, slightly behind the peak of MS-2 activity. A rough estimation of the range of sedimentation coefficients, $S^{o}_{20,w}$, of the iron-containing material can be calculated, as outlined by Martin and Ames (98), by using MS-2 as a sedimentation marker of 81S (95).

The material at the relatively sharp front of the radioactivity peak has an $S^{o}_{20,w}$ of approximately 66S. However, a significant amount of the radioactive material appears to move more slowly. The sedimentation coefficient of the slowest trailing material decreases to 30S or lower.

The findings up to this point indicate that the iron-containing material of Mopalia blood is a large substance of relatively homogeneous size but of widely heterogeneous S value. The heaviest material is

Figure 73. Sucrose density-gradient analysis of M. muscosa blood. Analytical details are given in Materials and Methods. The S values are calculated from the position of the peak of MS-2 infectivity by the method described by Martin and Ames (98).

a. Without Blue Dextran 2000.

b. With Blue Dextran 2000.

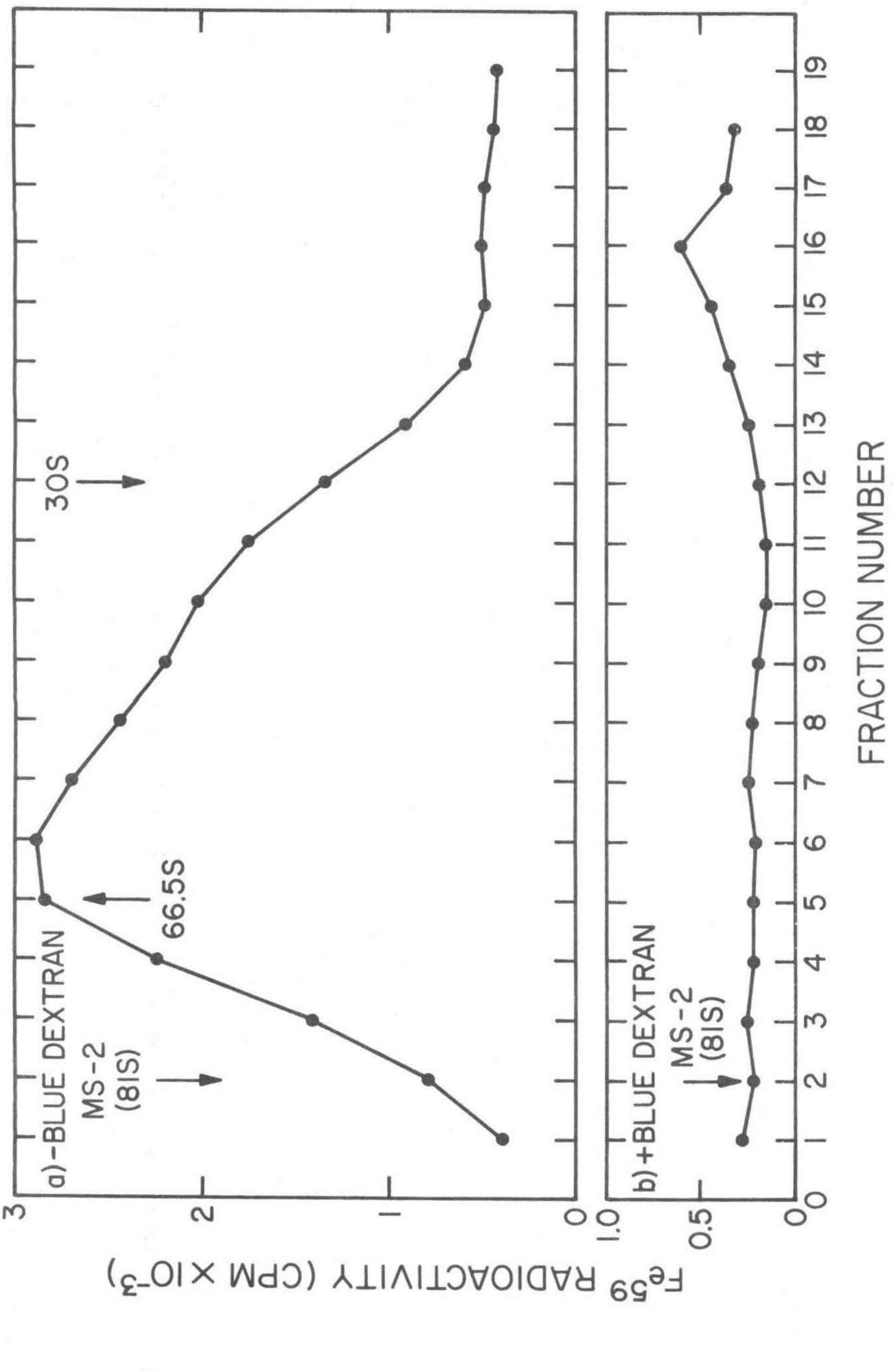
a) -BLUE DEXTRAN
MS-2
(81S)
66.5S
30S
b) +BLUE DEXTRAN
MS-2
(81S)
Fe59 RADIOACTIVITY (CPM x 10-3)
3
2
1
0
1.0
0.5
0
FRACTION NUMBER
0
1
2
3
4
5
6
7
8
9
10
11
12
13
14
15
16
17
18
19

approximately 65S.

This combination of properties is characteristic of the iron-containing protein ferritin (cf. (60)). Molecules of equine ferritin have a wide range of S values, from 65S for full ferritin down to 17.6S for apoferritin. The size of all the molecules is about 110 Å, and is independent of iron content.

(d) Electron Microscopy.

We have examined samples of Mopalia blood in the electron microscope to determine if ferritin is present. Figure 74a shows a field from an unstained preparation of whole blood. Several 55 to 60 Å electron-dense micelles, typical of ferritin, are visible. Negative-stained preparations also contain structures which are morphologically identical to ferritin. In Figure 74b, several ferritin molecules, 110 Å in diameter with a dense core of about 60 Å, are circled.

Purification of Blood Ferritin.

The stability of vertebrate ferritin at temperatures sufficient to cause denaturation of most other proteins has long been known (103). The ferritin present in the radula sac epithelium of chitons is also heat stable since it has been isolated by a procedure which includes a heat-denaturation step (40).

Since chiton blood is, at the start, a mixture of only a few protein components (89), we have devised a simple procedure to isolate and purify chiton blood ferritin for further study. The procedure consists

Figure 74. Electron micrograph of _Mopalia_ blood.

a. Unstained.

b. Negatively-stained with phosphotungstic acid.

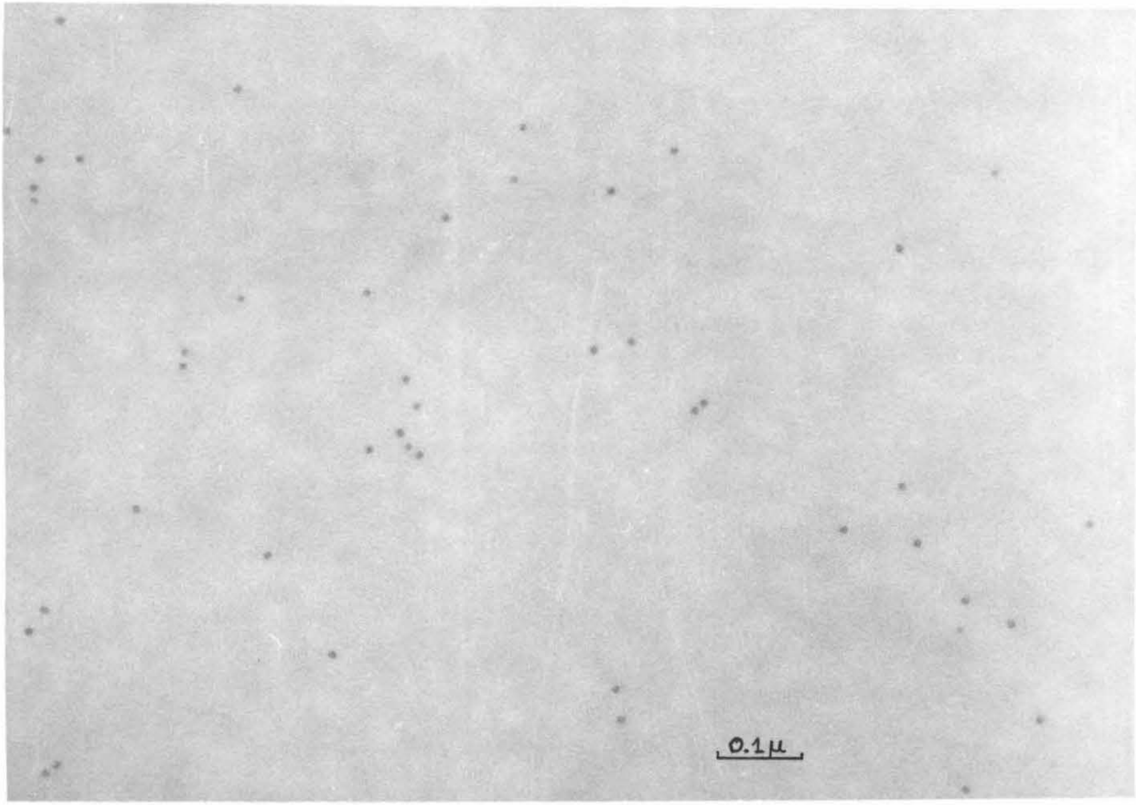
0.1 μ

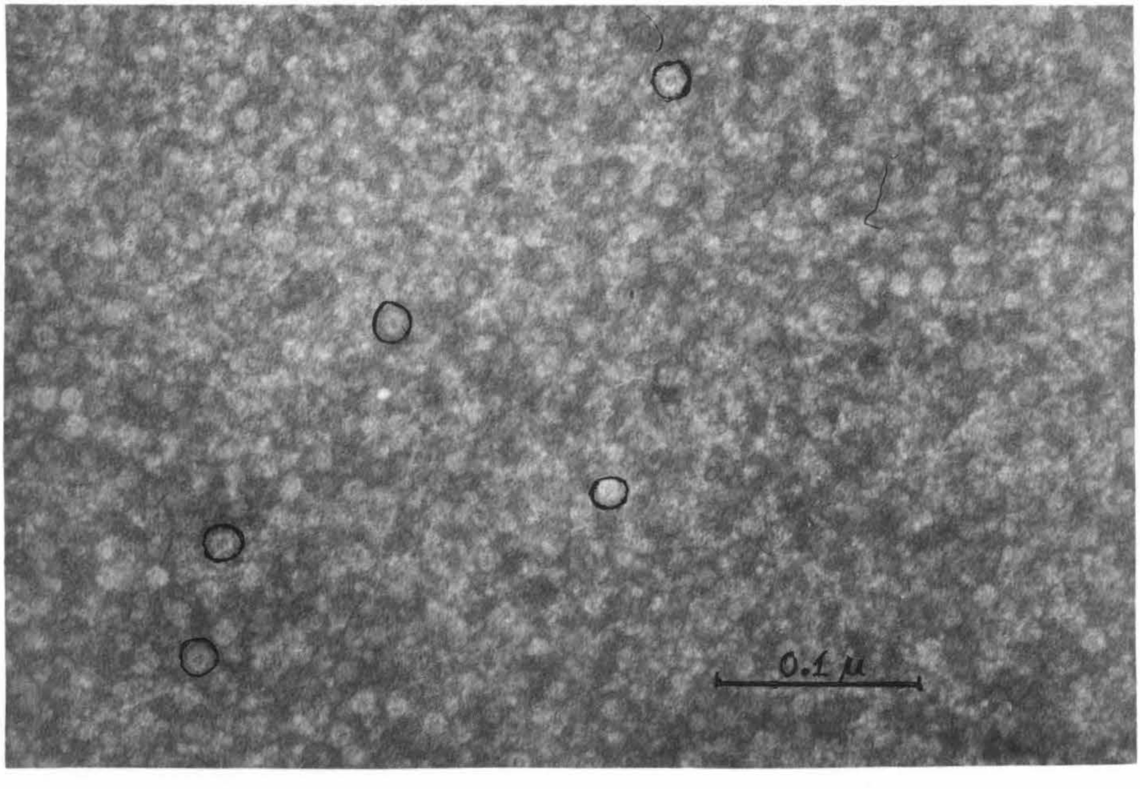
0.1 μ

of two main steps: first, the blood is heated to 75° C. to denature the bulk of the other proteins, and second, the ferritin is pelleted by high-speed centrifugation.

Table 3 presents the quantitative results of a typical purification. The starting material is 2 ml of Mopalia blood, obtained from an animal eight days after it was injected with 20 µc of Fe^{59}.

After the heating step, approximately 93% of the input iron and 97% of the radioactivity remain in the supernatant. In similar experiments with blood samples taken various times (up to 27 days) after labeling, the iron recovery after heating varies from 88 to 96%. The recovery of radioactivity varies from 91 to 102%, and shows no dependence on the labeling period.

The ferritin recovered from the reddish-brown pellet after the high-speed centrifugation step accounts for about 85% of both the input iron and the Fe^{59}. In five different samples, the amount of unpelleted iron varied from 12 to 21% of the input.

The calculated specific activities of the iron in all three stages in Table 3 do not differ by more than 5%, and may be considered equal within the limits of error of the method. However, a slight increase of specific activity after heating, as seen in Table 3, has also been observed in several other preparations. If this increase is real, it may indicate the presence in the blood of a small amount of one or more relatively unlabeled, heat-sensitive iron-containing components.

Figure 75 compares the agarose gel column elution patterns of the

Table 3. PURIFICATION OF BLOOD FERRITIN

Sample	Total Iron (μg Fe/ml)	Radioactivity (cpm/ml)	Specific Activity (cpm/μg Fe)
Whole Blood	47.6	686,000	14,400
After Heating	44.2	664,000	15,000
After Pelleting	37.6	561,000	14,940

Experimental details are given in the text.

radioactivity of the supernatant and pellet fractions after the high-speed centrifugation step of purification. The supernatant fraction (which contains about 15% of the input Fe^{59}) shows two peaks of radioactivity (Figure 75a). The first to emerge from the column elutes as a sharp peak at the expected position for ferritin. We suggest that this material consists of ferritin molecules with low iron content, which are not pelleted because of their low S value.

The second broad band elutes at a much greater volume, and therefore consists of small-sized molecules. Since no radioactive peak is detected in this position in the elution pattern of whole blood, we suggest that the material in this band arises from the breakdown of ferritin molecules during the heating step.

The elution pattern of the resuspended pellet ferritin (Figure 75b) is very similar to the whole blood pattern (cf. Figure 72). The radioactivity elutes as a single sharp peak which is slightly retarded by the agarose gel.

From these column results, we conclude that most, if not all, of the iron which is lost in the second step of purification is iron that was originally present as ferritin in the blood. The constant specific activity before and after the pelleting step gives additional support for this conclusion.

Consequently, the measurements of recovery of total iron and radioactivity after the heating step but before pelleting serve as an estimate of the total quantity of blood ferritin. Hence, we conclude that, of the 40 to 110 μg of iron per milliliter of blood, approximately 88 to 96% is present in the form of ferritin.

Figure 75. Bio-Gel A-1.5 m agarose column chromatography of a) supernatant and b) pellet of the high-speed centrifugation step of purification of Fe^{59}-labeled blood ferritin. Eight days after the injection of 20 μc of Fe^{59}, into a specimen of *M. muscosa*, a 2 ml blood sample is withdrawn. The ferritin purification procedure described in Materials and Methods is carried out.

In a): The high speed centrifugation pellet is resuspended in 2.0 ml of column buffer and an 0.03 ml sample is layered onto the column.

In b): 0.5 ml of the high-speed supernatant is layered directly onto the column.

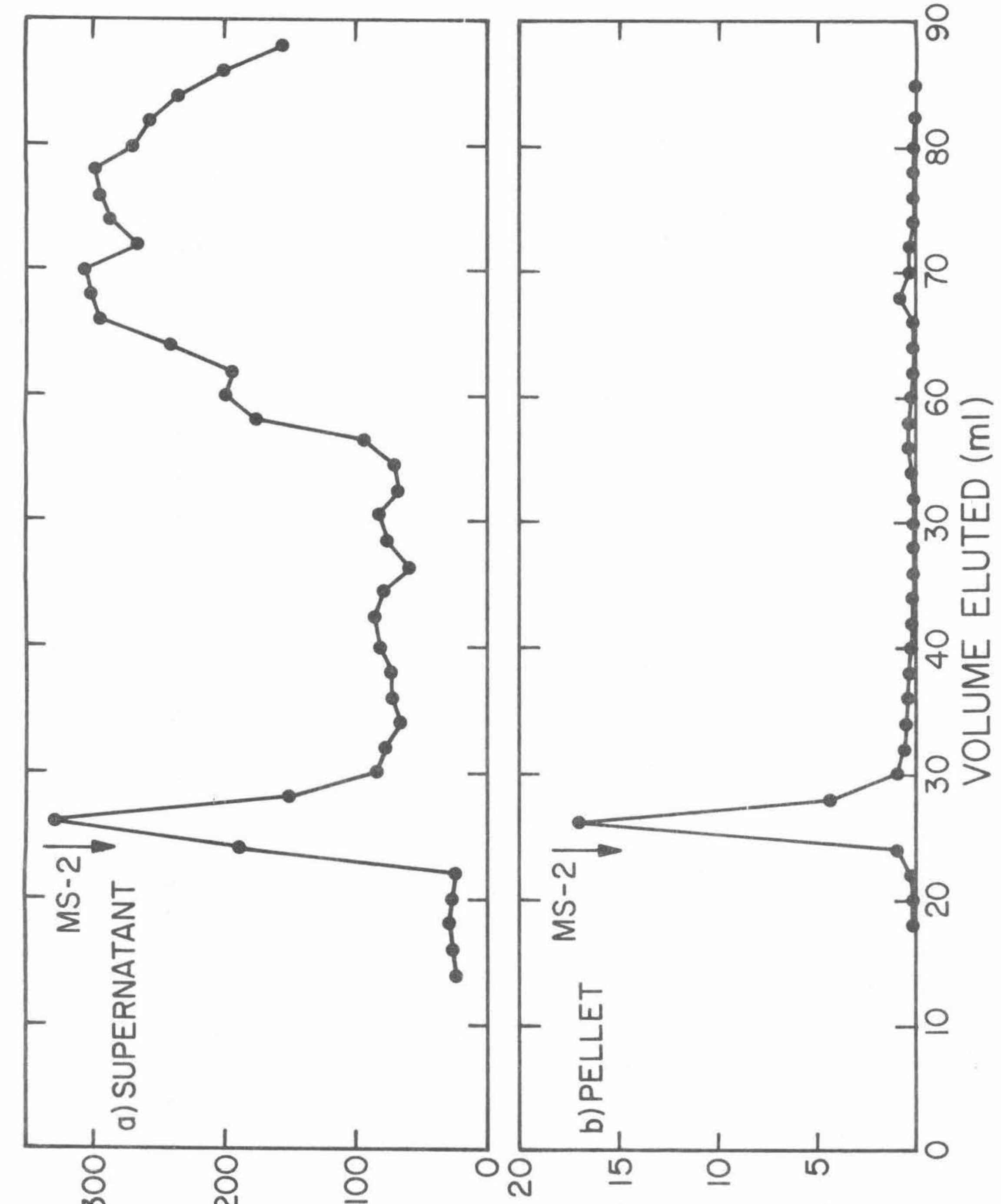
a) SUPERNATANT
MS-2
b) PELLET
MS-2
Fe^{59} RADIOACTIVITY (CPM)
0
100
200
300
Fe^{59} RADIOACTIVITY (CPM × 10^{-2})
0
5
10
15
20
VOLUME ELUTED (ml)
0
10
20
30
40
30
60
70
80
90

Studies of Purified Blood Ferritin.

(a) Absorption Spectra.

Figure 76 shows the absorption spectra of a sample of *Mopalia* blood ferritin, prepared as described in the preceding section, and a sample of purified horse ferritin. The two spectra are extremely similar: each sample has an absorption, caused by the contained iron (41), that increases gradually from beyond 450 mμ to below 270 mμ, and almost completely masks the protein absorption peak at 280 mμ.

(b) Electron Microscopy.

Preparations of purified chiton blood ferritin, both unstained and negative-stained, have been examined in the electron microscope (Figure 77).

From measurements of many molecules in several preparations, we estimate the size of the micelle (Figure 77a) to be 62±6 Å. The diameter of the protein shell, observable in negative-stained preparations, is 107±12 Å (Figure 77b).

The dimensions of chiton ferritin fall within the ranges previously reported for ferritins from many sources (51,52,53).

(c) Electron Diffraction.

Table 4 compares the d-spacings of the diffraction lines obtained from a sample of *Mopalia* blood ferritin and a sample of purified rabbit ferritin. The values for horse ferritin, which are also listed, have been taken from the report of Towe and Bradley (56). The spacings of

Figure 76. Comparison of the absorption spectra of ferritin isolated from the blood of Mopalia muscosa and cadmium-free horse ferritin.

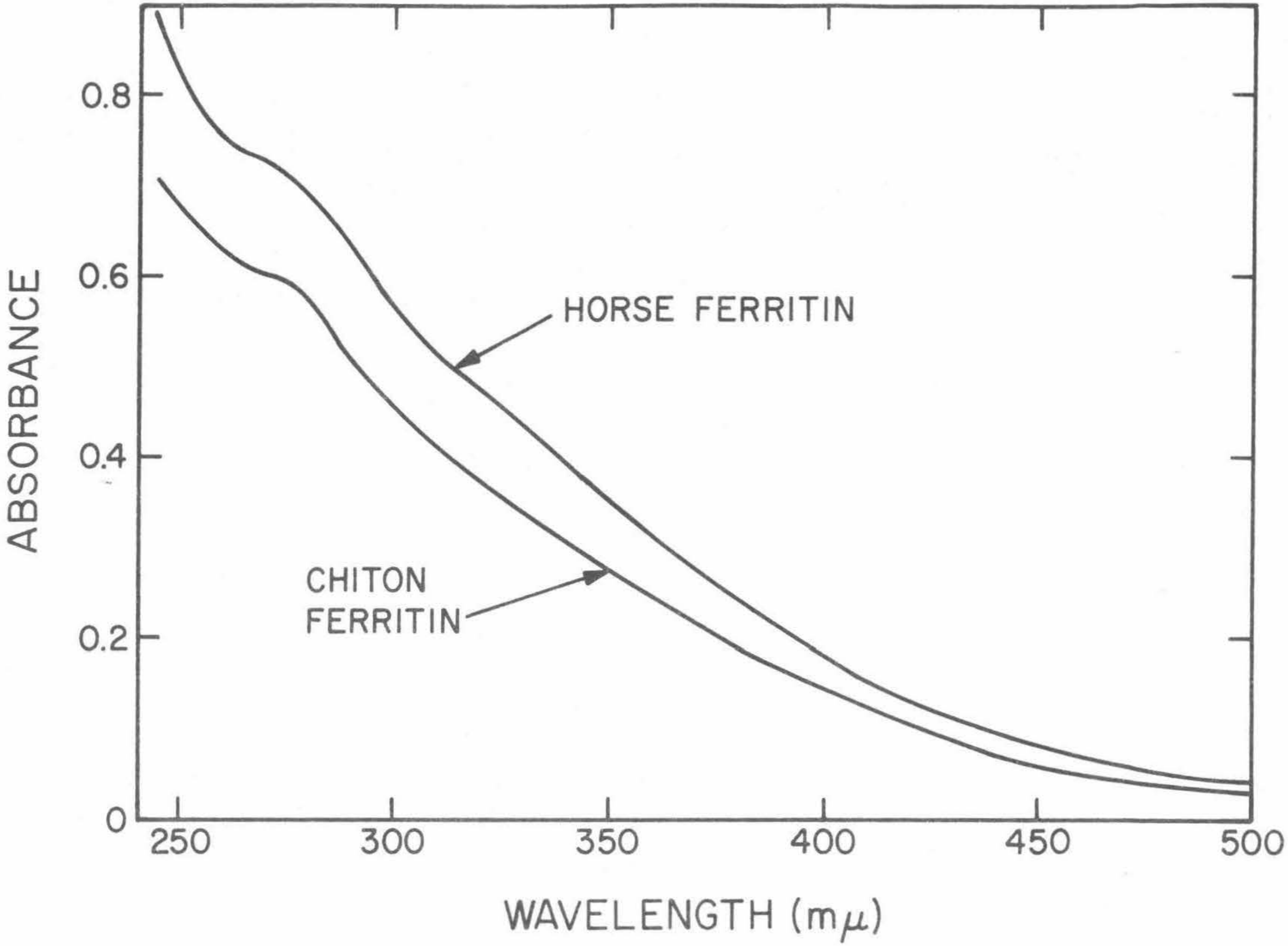
ABSORBANCE
0.8
0.6
0.4
0.2
0
250
300
350
400
450
500
WAVELENGTH (mμ)
HORSE FERRITIN
CHITON FERRITIN

Figure 77. Electron micrograph of purified _Mopalia_ blood ferritin.

a. Unstained.

X 340,000.

b. Negatively-stained with phosphotungstic acid.

X 340,000.

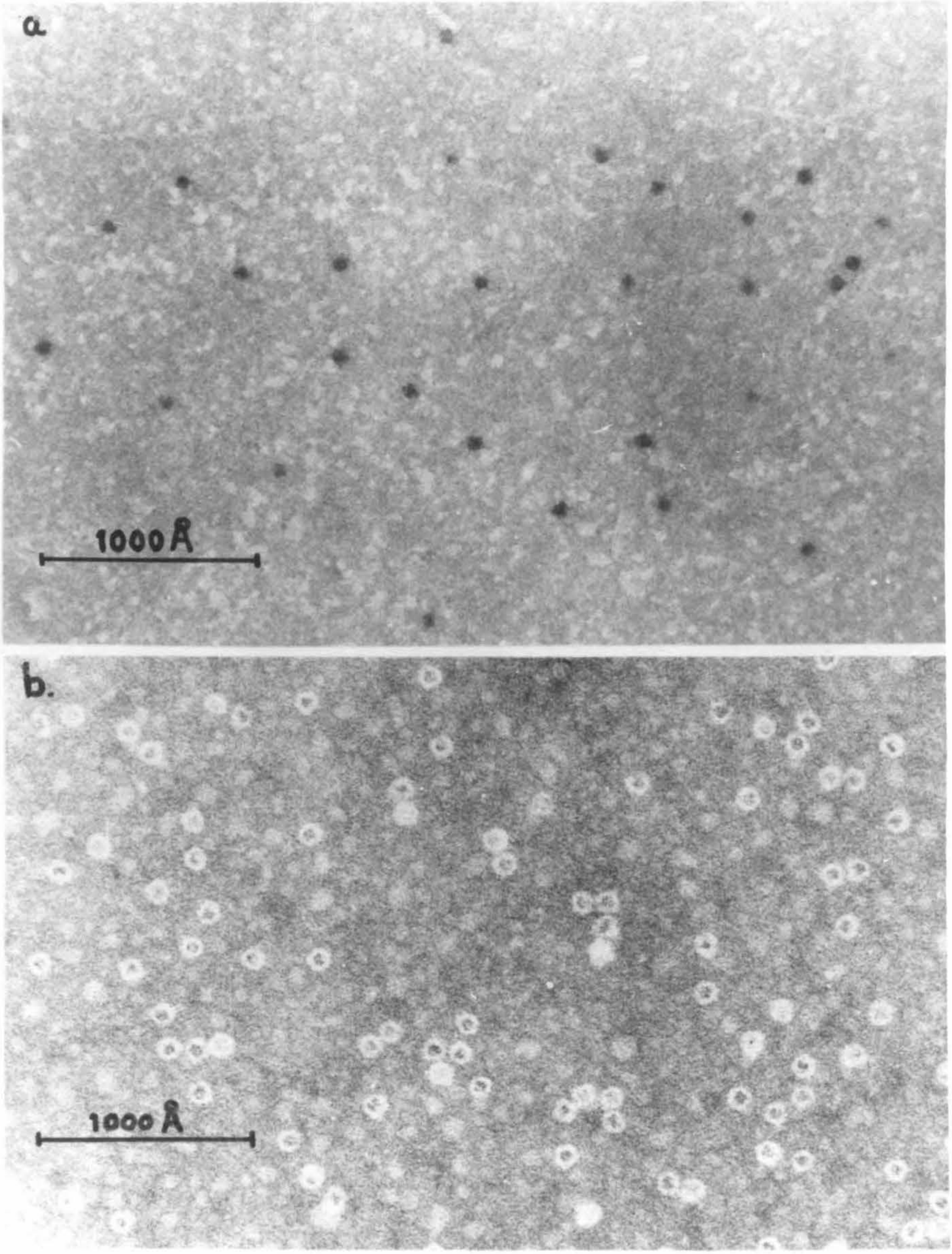
a
1000 Å
b.
1000 Å

Table 4. COMPARISON OF THE ELECTRON DIFFRACTION PATTERNS OF *MOPALIA*, RABBIT, AND HORSE FERRITIN.

Mopalia		Rabbit		Horse	
d (Å)	I	d (Å)	I	d (Å)	I
2.54	S	2.55	S	2.55	S
2.23	S	2.22	S	2.23	S
1.97	W	1.98	M	1.99	M
1.72	VW	1.71	M	1.72	W
--	--	1.51	VW	1.50	VW
1.46	M	1.46	S	1.47	S
--	--	--	--	1.33	VW
--	--	1.23	VW	1.23	W
1.16	VW	1.16	W	1.18	W
--	--	1.11	VW	1.11	VW
1.03	W	1.06	M	1.05	M

The d-spacings and their visually estimated intensities (I) of *Mopalia* and rabbit ferritin samples are from the present study. The values for horse ferritin are from Harrison *et al.* (57).

S - Strong; M - Medium; W - Weak; VW - Very Weak.

the major lines are in close agreement for all three samples, indicating that the micellar mineral of *Mopalia* ferritin is a hydrated ferric oxide (cf. (56)).

Comparison of Chiton Blood and Tissue Ferritin.

Fe^{59}-labeled ferritin is isolated from the epithelial tissue of the radula sac of *M. muscosa*, by the procedure described in Materials and Methods, Part II.

The sucrose gradient sedimentation pattern of an unheated tissue homogenate is shown in Figure 78. The material at the sharp front of the leading peak of radioactivity has a sedimentation coefficient of about 65S. This broad fast-moving band is quite similar to the pattern observed with blood ferritin (cf. Figure 73a). We have not attempted to characterize the radioactive material which is present near the top of the gradient.

The epithelial tissue ferritin is not detectably different from the blood ferritin on the basis of the following criteria: behavior on agarose gel columns, aggregation with Blue Dextran, absorption spectrum, appearance and size in the electron microscope.

Mopalia ferritin is not identical to vertebrate ferritins. Although our electron diffraction data suggest that the micellar portion of chiton ferritin is the same hydrated ferric oxide as found in horse ferritin (see above), several findings indicate that the protein shells differ. In control experiments, we have found that neither equine ferritin nor rabbit ferritin forms aggregates in the presence of Blue

Figure 78. Sucrose density-gradient analysis of a homogenate of Fe^{59}-labeled _M. muscosa_ radular epithelial tissue. The sample is prepared as described in Materials and Methods, Part II. Analytical details are given in Materials and Methods, Part II.

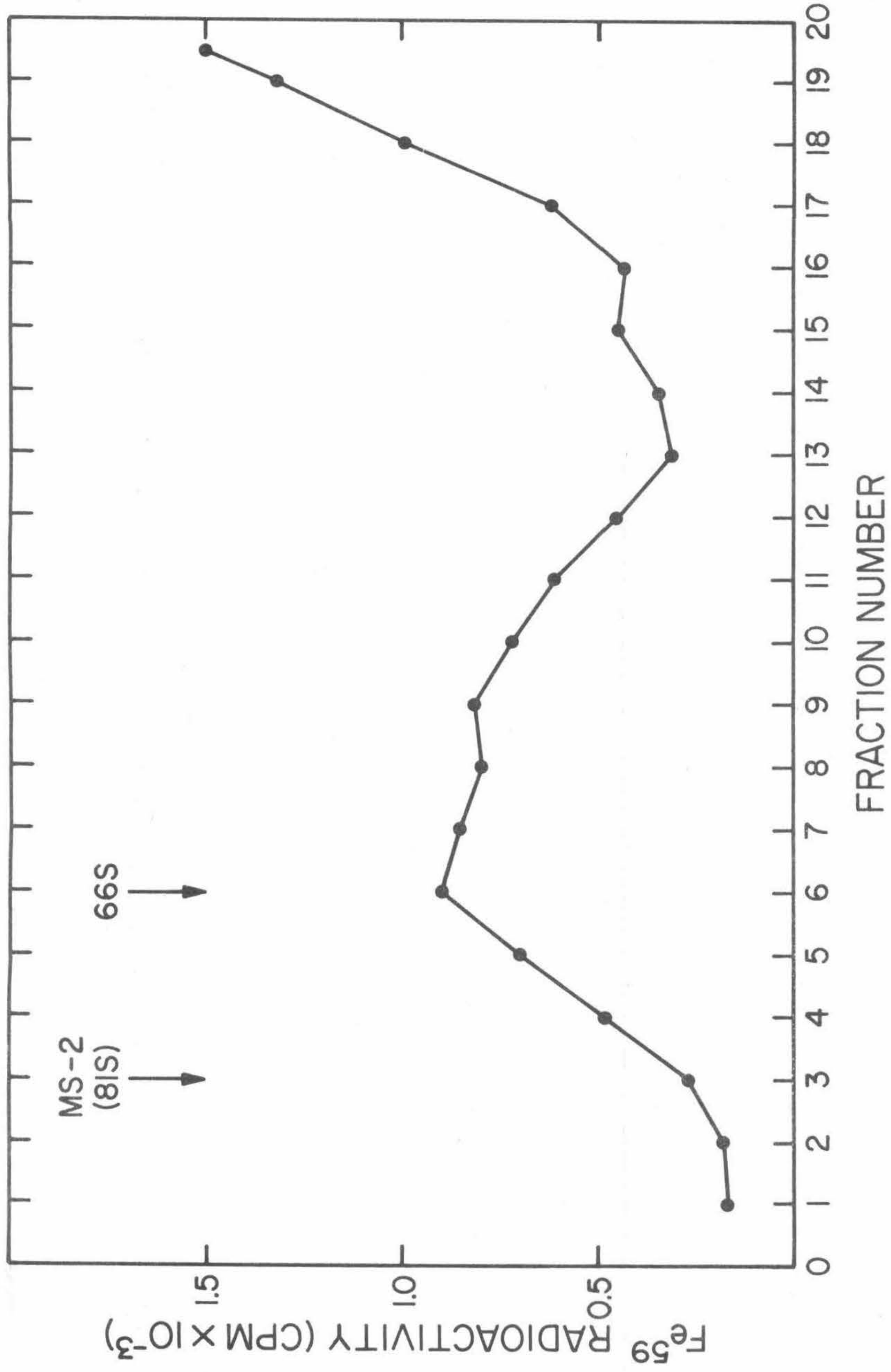
MS-2
(81S)
66S
Fe^{59} RADIOACTIVITY (CPM × 10^{-3})
1.5
1.0
0.5
FRACTION NUMBER
0
1
2
3
4
5
6
7
8
9
10
11
12
13
14
15
16
17
18
19
20

Dextran 2000. We have also observed, in several abortive attempts at acrylamide gel electrophoresis, that *Mopalia* ferritin does not move under conditions in which horse ferritin readily migrates.

DISCUSSION

At least 88% or the iron that is present in the blood of Mopalia muscosa occurs in the form of ferritin in solution in the haemolymph. If there are additional minor iron-containing components in the blood, they must be heat-coagulable molecules with a very low rate of iron turnover, as indicated by the specific activity data obtained in the ferritin purification procedure. Such components should be of little importance in iron transport. We suggest that contaminating amoeboid blood cells may be a likely source of these minor components.

Since the iron of the Mopalia ferritin micelle occurs as a ferric oxide hydrate, then a minimum of 88% of the iron of Mopalia blood is Fe^{3+}. This appears to be quite different from the situation in Cryptochiton, in which Carefoot has reported that 93% of the blood iron is in the ferrous state (15). Although we have not carried out experiments to resolve this apparent difference between the two species, we feel it is much more likely that the ferrous iron assay results are in error (perhaps due to degradation of the Cryptochiton blood sample) than that there are major differences in the blood chemistry of two species of Polyplacophora.

In the present study, we have not made any protein determinations, and hence we cannot give any direct quantitative estimates of the amount of ferritin protein in the blood. However, it has been reported that unfractionated preparations of ferritin from such widely divergent sources as vertebrates and plants typically contain approximately 15 to 20% iron by weight (50,99). If this holds true for chiton ferritin, then one milliliter of Mopalia blood would contain from 0.2 to 0.7 milligrams of ferritin, which is equivalent to the measured range of 40 to 110 μg of iron per milliliter.

The site of synthesis of ferritin and the site of its release into the blood have not yet been determined. Iron-containing granules have been observed in the digestive gland and the intestine of several species of chiton (4,39). Since both of these organs may be involved in the absorption and accumulation of iron from the algal food, either one is likely to be the site of ferritin synthesis.

It should be pointed out, in passing, that ferritin, by virtue of its occurrence over an extremely broad taxonomic range and because of the relative ease of its purification, ought to be a highly suitable candidate for the study of the evolution of proteins.

PART III

STUDIES ON THE REPLACEMENT RATE AND IRON CONTENT OF THE RADULA OF *MOPALIA MUSCOSA*

INTRODUCTION

An important parameter in the study of the process of radula tooth mineralization in the Polyplacophora is the rate of formation and replacement of the radula. Knowledge of this rate and of the iron content of the radula teeth can provide an estimate of the daily iron requirement of a chiton.

For only a few species of Gastropoda, out of the thousands of species of radula-bearing molluscs, is the rate of radula replacement known. Runham (34) and Runham and Isarankura (100) have directly measured values that range from 1.22 rows per day in *Pomatias elegans* to 5.02 rows per day in *Littorina littorea*. Analyses of the iron content of the major lateral teeth of the chitons, *Mopalia hindsii* and *Cryptochiton stelleri*, have been performed by Carefoot (15). Unfortunately he does not give values for the actual iron content of the teeth, since he reports his results in terms of the weight percentage of iron.

In this report, we present data on the iron content of the major lateral teeth of *Mopalia muscosa* and we report on the results of radioactive iron labeling experiments designed to provide a value for the rate of radula replacement in this species.

MATERIALS AND METHODS

Animals.

Specimens of Mopalia muscosa are collected and maintained as described in Materials and Methods, Part I.

Radioactive Iron Labeling.

Individuals of M. muscosa are injected with trace amounts (3 to 50 µc) of radioactive iron-59 (Fe^{59}) by the techniques described in Materials and Methods, Part II.

After an interval of from 5 to 37 days, animals are removed from the aquaria and are either immediately sacrificed for radula studies or are frozen and stored at -20° C. until they are to be analyzed.

Preparation of Radula Teeth.

The buccal region of an individual chiton is exposed by removing the first three valves. The radula and associated tissues are dissected free and placed in a shallow dish containing Clorox bleach (5.25% NaOCl, manufactured by The Clorox Company). While the specimen is in Clorox, the connective tissue radula sheath and other associated tissues are gently stripped from the radula. The strong oxidizing agent destroys the epithelial cells which surround the radula teeth without dissolving the teeth themselves. The Clorox also slowly weakens and can eventually dissolve the radula membrane. The radula is removed from the bleach and rinsed well with water after about 15 minutes, at which time the teeth are relatively free of attached cellular material and the radula membrane has been partially softened.

The radula is placed in a water-filled Petri dish and is pinned out flat onto a piece of modeling clay. The radula is examined and the number of tooth rows and the appearance of the cusps is recorded.

With the aid of a dissecting microscope, the individual major lateral teeth from one side of the radula are removed in order from the radula membrane. The teeth are placed in a small volume of Clorox for 15 minutes to remove all traces of epithelial tissue and are rinsed in water. In experiments in which the whole major lateral teeth are to be analyzed, the cleaned teeth are placed in individual test tubes. For other experiments, it is necessary first to separate the cusps and the styli before analysis. The cleaned teeth are stuck onto a strip of Scotch Brand Double-Stick Tape (Catalog #136) and are allowed to air-dry. The styli shrink upon drying, weakening the cusp-stylus junction, and generally the cusps can be cleanly broken off by applying gentle pressure with jeweler's forceps. The separated cusps and styli are then placed into tubes for analysis.

Iron Assay.

An appropriate volume (0.1 to 1.0 ml) of 6N HCl is added to each tube. Each sample is heated to 100° C. for 15 minutes to dissolve the iron. An 0.1 ml aliquot of each sample is assayed for total iron by the method described in Materials and Methods, Part II.

Determination of Radioactivity.

0.5 ml of each final iron assay mixture is added to 10 ml of Bray's solution and the radioactivity is measured with a Packard liquid scintillation counter. Specific activity of a sample is calculated from the measured radioactivity and the iron content. Since the half-life of Fe ^{59} is only 45 days, corrections are made in all determinations for the radioactive decay that occurs from the time of labeling to the time of assaying.

RESULTS

The radula of M. muscosa consists of approximately 50 transverse rows of teeth attached to a flexible radula membrane. Each transverse row contains a pair of major lateral teeth and fifteen minor teeth. Each major lateral tooth is composed of a long hollow stylus, attached to the radula membrane, and a tricuspid tooth cap which, in mature teeth, is impregnated with magnetite. Several workers have given a qualitative description of the changes in appearance of the major lateral tooth cusps from the posterior to the anterior of a chiton radula (5,13). Table 5 gives quantitative data on these changes obtained from examination of the radulas of eighteen specimens of M. muscosa. These data indicate, in summary, that a typical Mopalia radula bears 12 posterior rows of colorless major lateral cusps, 3 rows of brown cusps, and 35 rows of black cusps, of which the anterior seven rows show signs of mechanical wear.

The Iron Content of the Major Lateral Teeth.

Figure 79 shows the results obtained from series of iron assays carried out on the successive major lateral teeth from two M. muscosa radulas. The two radulas represented possess the highest and lowest mature tooth iron content that we found in a sample of eighteen radulas. In all of the radulas we have assayed, including the two shown, we find that the iron content of the major lateral teeth shows an almost linear increase over a segment of ten to fifteen rows. The tooth iron content starts from zero, one or two rows posterior to the first brown cusp

Table 5. MEASUREMENTS OF THE RADULA OF *MOPALIA MUSCOSA*.

	Average	Range
Total Number of Tooth Rows	51.2	47-56
Number of Rows of Colorless Cusps	12.5	10-16
Number of Rows of Brown Cusps	3.3	2-4
Number of Rows of Black Cusps	35.4	32-42
Number of Rows of Worn Black Cusps	7.06	5-9
Iron Content of a Mature Major Lateral Tooth (μg Fe)	39.4	30-48

The values given have been obtained from the radulas of 18 individuals.

Figure 79. The iron content of the major lateral teeth and of isolated styli.

The major lateral teeth or isolated styli from one side of an individual radula are assayed for total iron as described in Materials and Methods, Part III.

In this and all subsequent figures, we have normalized the tooth row numbers so that row 0 indicates the row bearing the first brown major lateral cusp. In this way, we can more easily compare radulas which have different numbers of unmineralized tooth cusps.

—○—○— Whole major lateral teeth, radula A.

—●—●— Whole major lateral teeth, radula B.

—△—△— Isolated styli, radula C.

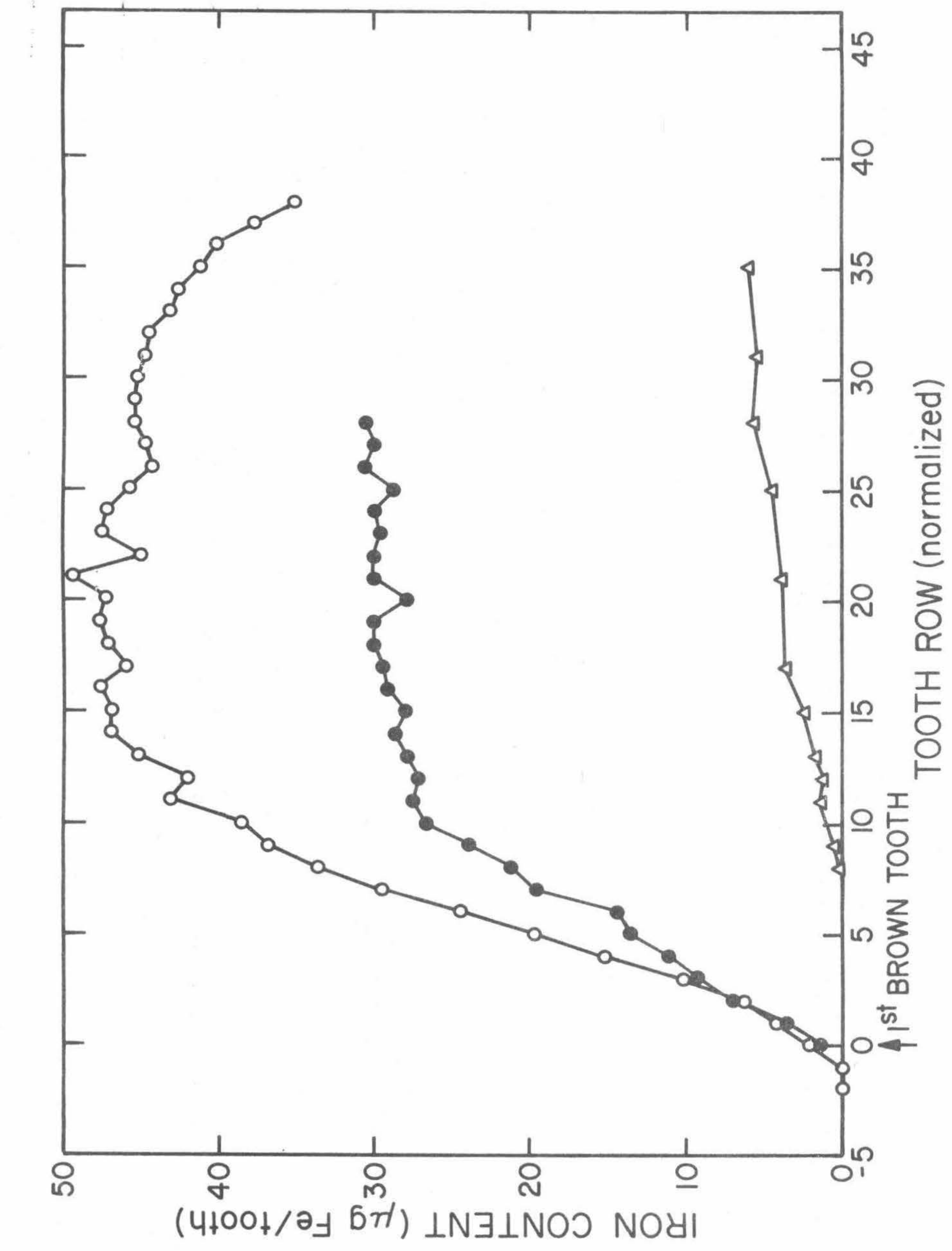
IRON CONTENT (μg Fe/tooth)
0
10
20
30
40
50
TOOTH ROW (normalized)
-5
0
5
10
15
20
25
30
35
40
45
1st BROWN TOOTH

(row 0 in Figure 79), and reaches a plateau value that is relatively constant within an individual radula. The plateau level, which ranges from a value of 30 to 48 μg of Fe per tooth in the different radulas, represents a measure of the iron content of the mature, fully-mineralized major lateral tooth. The average plateau value for the eighteen radulas assayed is 39.4 μg of Fe per tooth.

The top curve if Figure 79 shows that the iron content begins to decrease about seven rows from the anterior end of the radula. The row at which this decrease is first detectable coincides with the location of the first cusp that shows visible signs of mechanical wear. Clearly, the iron decrease is the result of the loss of magnetite produced by mechanical abrasion during the feeding process. No decrease is observed in the other radula shown in Figure 79, because the anterior most rows of teeth were not analyzed.

Figure 79 also shows the results of iron analyses of the isolated major lateral styli of a single radula. Iron is first detectable in the styli about eight or ten rows anterior to the first brown cusps. The stylus iron content increases gradually throughout the mature tooth region and eventually reaches a value of 5 to 6 μg Fe per stylus, which is equivalent to 10 to 15% of the total iron of a mature lateral tooth.

The Rate of Radula Replacement.

In preliminary experiments, it was determined that an easily detectable amount of Fe^{59} is secreted into the major lateral teeth, after the injection of microcurie amounts of radioactive iron-59 into the heart or abdominal cavity of M. muscosa. The three patterns of tooth iron specific activity shown in Figure 80 are typical of the reproducibility of the method. The labeling pattern of the teeth of animals A and B are similar: a steep drop in specific activity between rows 2 and 4 and a gentler decrease between rows 8 and 10. However, the labeling pattern of animal C differs markedly: it shows a single small peak of specific activity at row 10. We have observed three other instances of labeling patterns similar to C in radulas from animals sacrificed six, twelve, and twenty days after labeling. The more typical pattern of specific activity resembles those of animals A and B, in having high specific activities in the brown tooth region and regions of decreasing specific activity located farther posterior or anterior, depending upon whether the labeling period is respectively shorter or longer than fifteen days.

Since the iron assay data indicate that stylus iron impregnation starts at about row ten, it seemed reasonable to ask whether the anomalous labeling pattern of animal C might be due to a shutdown of the tooth mineralization process at the time of labeling, perhaps caused by damage produced by the injection process itself. It would follow that iron impregnation of the stylus occurred by a different path. To investigate further this possibility, we analyzed separately the cusps and styli of an animal sacrificed five days after the injection of 25 μc of Fe^{59}. The results, shown in Figure 81, support the above hypothesis. The

Figure 80. Comparison of labeling pattern of three specimens of _M. muscosa_, each injected with 4.5 μc of Fe^{59} and sacrificed after 15 days.

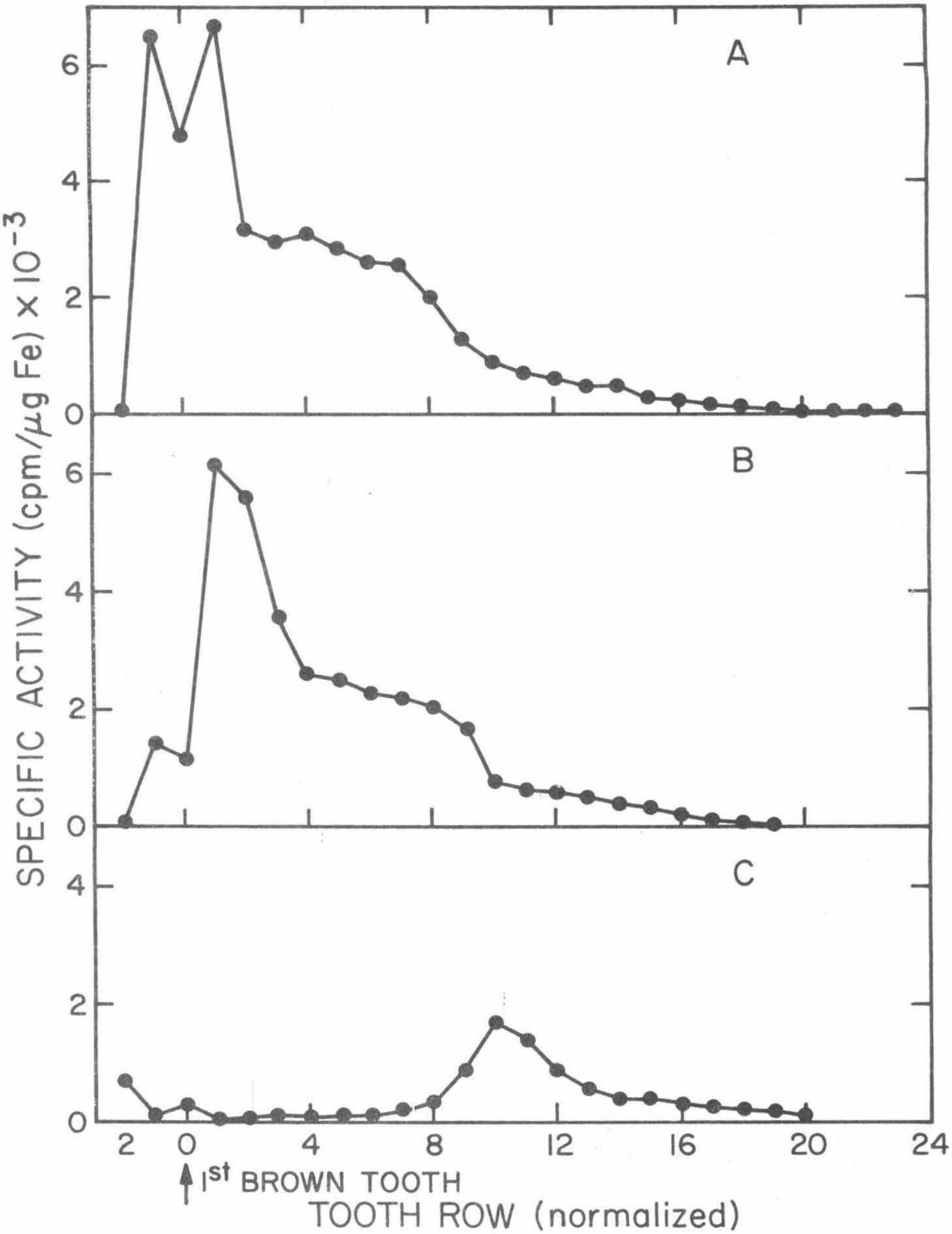
A
B
C
SPECIFIC ACTIVITY (cpm/μg Fe) × 10⁻³
0
2
4
6
2
0
4
8
12
16
20
24
1st BROWN TOOTH
TOOTH ROW (normalized)

Figure 81. A comparison of the labeling patterns of the cusps and the bases from a single radula. A specimen of M. *muscosa* is given 25 μc of Fe^{59}, 5 days before its radula is removed.

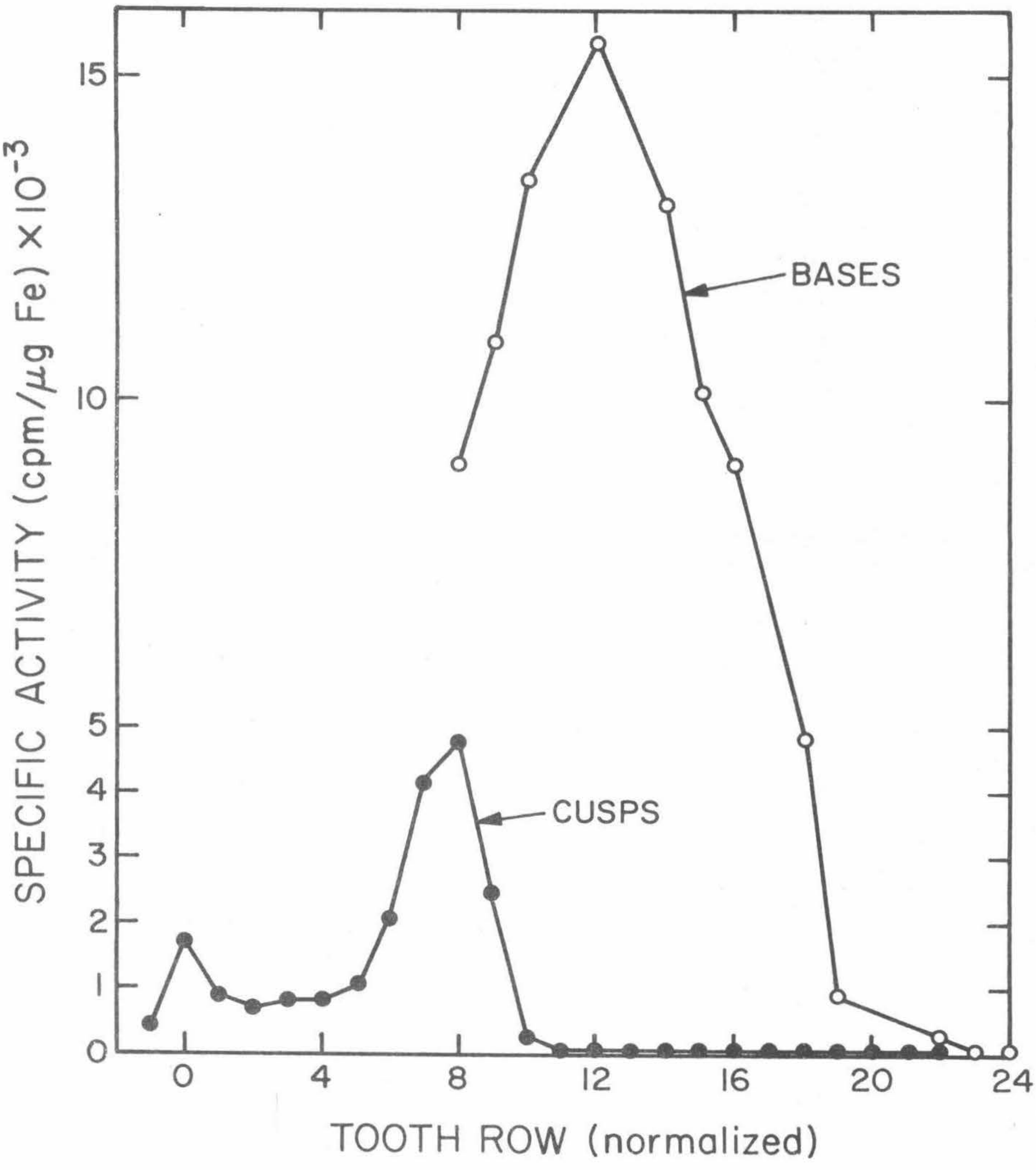
SPECIFIC ACTIVITY (cpm/μg Fe) × 10⁻³
15
10
5
4
3
2
1
0
0
4
8
12
16
20
24
TOOTH ROW (normalized)
BASES
CUSPS

specific activity of the iron in the styli is much higher than in the cusps. The stylus specific activity peaks at row 12. Hence, it appears that the process of iron deposition into the styli has different kinetics than the process of cusp mineralization. The rapid achievement of high specific activity by the styli may be the result of a much smaller iron pool for stylus iron deposition than for cusp mineralization.

Figure 82 compares the pattern of specific activity of the isolated major lateral cusps from radulas of animals labeled with 5 μc of Fe^{59} for 20, 26, 31, and 37 days before they were sacrificed. The curves of specific activity are of similar shape, but they are displaced along the length of the radula. Since all of the animals received the same amount of Fe^{59}, and since the anterior portions of all of the curves are within the plateau region of iron content, then the forward displacement of the specific activity curves as a function of labeling period must represent the anterior growth of the radula.

In Figure 83, we have plotted the row number at which each curve in Figure 82 has a specific activity of 1000 cpm/μg Fe _versus_ labeling period represented by that curve. The slope of the line drawn through the cusp points in Figure 83 gives a value for the rate of a radula replacement which is 0.59 rows per day.

The high specific activity of the styli interferes with attempts to determine the radular replacement rate by the analysis of whole teeth labeled for short periods. However, with longer labeling times, the specific activity curve determined for whole radula teeth is similar in slope but displaced two rows anterior to the specific activity curve

Figure 82. Specific activity pattern of isolated cusps from animals labeled with 5 μc of Fe^{59} and sacrificed 20 days (-●-●-), 26 days (-○-○-), 31 days (-▲-▲-), and 37 days (-△-△-) after labeling.

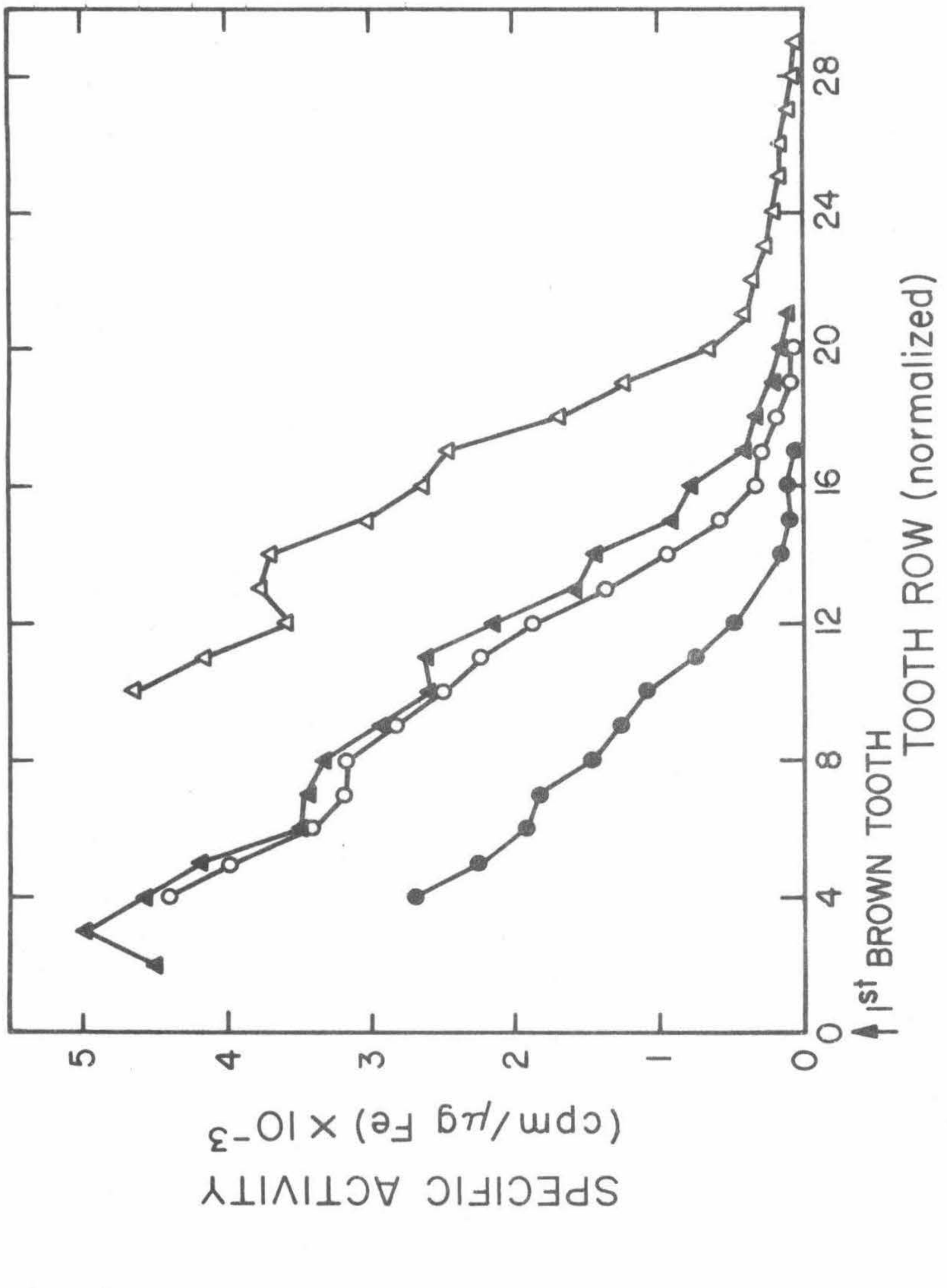
SPECIFIC ACTIVITY
(cpm/μg Fe) × 10⁻³
0
1
2
3
4
5
0
4
8
12
16
20
24
28
TOOTH ROW (normalized)
1st BROWN TOOTH

Figure 83. Anterior displacement of the tooth specific activity as a function of time after labeling.

From the cusp specific activity curves shown in Figure 82 and from similar curves obtained for whole major lateral teeth, we have determined the position along each radula (i.e., the row number) at which the value of the specific activity is 1000 cpm/μg Fe. These row numbers are then plotted as a function of the labeling period. All of the data points shown are obtained from animals which were given 5 μg of Fe^{59}.

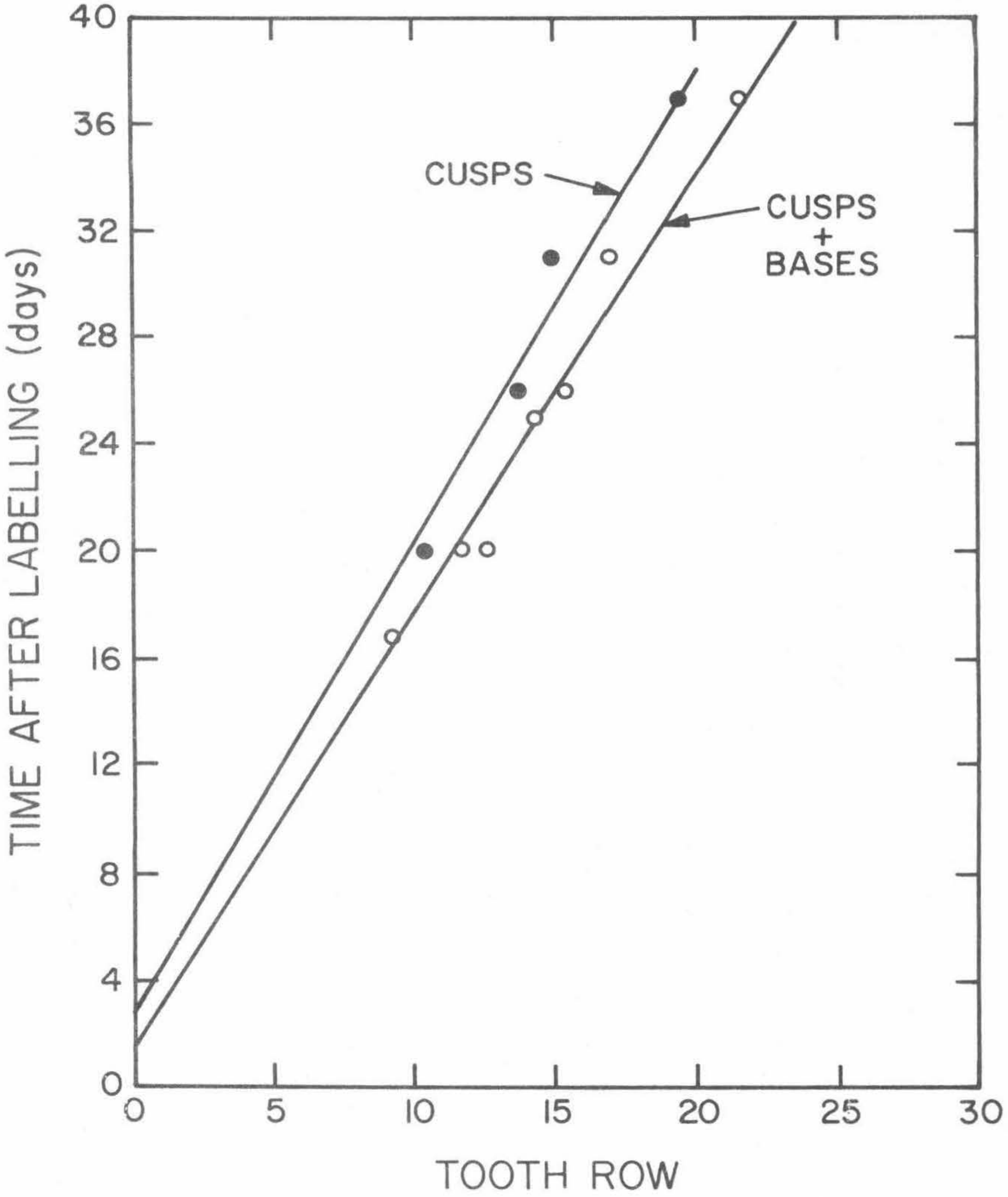
TIME AFTER LABELLING (days)
0
4
8
12
16
20
24
28
32
36
40
TOOTH ROW
0
5
10
15
20
25
30
CUSPS
CUSPS
+
BASES

determined for isolated cusps from the same radula. Hence, we have also made estimates of the radula replacement rate using the additional data from studies on whole teeth. In Figure 83, the line drawn through the base and cusp points has a slope of 0.61 tooth rows per day.

We have also made plots similar to those of Figure 83, for different selected values of specific activity (e.g., 500 and 2000 cpm/μg Fe). The rate of radula replacement determined from these graphs ranges from 0.55 to 0.7 tooth rows per day.

DISCUSSION

The results of the Fe^{59}-labeling experiments indicate that the rate of radula replacement in Mopalia muscosa is approximately 0.6 rows per day. The accuracy of this measurement relies upon the accuracy of the analytical techniques and upon the assumption that the rate is constant from individual to individual. The comparison of the labeling patterns of radulas from several animals labeled for the same period of time indicates that the replacement rate is nearly the same in animals maintained under laboratory conditions

Since the radula replacement is determined by comparing the labeling patterns of the radulas of several different individuals, it is important that each animal be given either the same amount of Fe^{59}, or, at least, amount that is accurately known. Unfortunately, we have not been entirely successful in attaining this goal. In some animals, we have observed that fluid escaped from the site of injection after removal of the needle. Although we attempted to prevent the loss of injected Fe^{59} by deeper insertion of the needle and by selecting various sites for injection, we were not able to determine whether these methods were fully reliable. Although this problem might be expected to cause merely an increase in scatter of the data points, given in Figure 83, and not a change in the slope, we feel that the actual rate of radula replacement may lie anywhere between 0.4 and 0.8 rows per day.

The results of determinations of the specific activity of isolated styli show that they are labeled much more heavily than the cusps, at early times after Fe^{59} injection. This finding suggests that the deposition of iron into the styli occurs by a path which differs from the cusp mineralization process. One possible interpretation of this difference is that there is a much smaller previously existing pool of unlabeled iron for stylus impregnation than for cusp mineralization. From the findings of Part I, it appears that the cusp cells do contain a large pool of iron, in the form of iron-containing granules, while the minor cells have but few iron granules. However, we have not examined the minor cells in the region, ten rows past the first brown tooth, where iron is being deposited in the styli. The process of stylus iron impregnation requires additional study before any conclusions can be drawn.

Assays of the iron content of the major lateral teeth of each individual radula show that the process of mineralization occurs over a segment of the radula that extends anteriorly for ten to fifteen rows, starting from the row preceding the first brown cusps. This finding can be correlated with the observation made by Gabe and Prenant (18,39) that the superior epithelial cusp cells that contain iron granules occur within the very same segment of the radula sac. Hence, the results of the iron analyses provide circumstantial support for the view that the cusp cells are responsible for cusp mineralization.

The average iron content of a mature lateral tooth is about 40 μg of iron. Hence, the pair of major lateral teeth in each transverse row contains a total of 80 μg of iron. In addition, we have recently determined (14) that the minor teeth at the anterior of the radula also contain some iron. We would estimate that each transverse row of the mature radula contains approximately 100 µg of iron. Since the radula replacement rate is between 0.4 and 0.8 rows per day, the tooth mineralization process of an individual *Mopalia muscosa* requires between 40 and 80 µg of iron per day.

GENERAL DISCUSSION

GENERAL DISCUSSION

The purpose of this general discussion is to consider some of the wider implications of our findings rather than to review all of the data that we have discussed in each part.

The findings of Part III indicate that an individual chiton of the species Mopalia muscosa requires 40 to 80 μg of iron per day for the mineralization of its radula teeth. Carefoot (15) has previously discussed the possible sources of iron that are available to the chitons. Sea water contains very little iron: less than 10^{-12} mg per cubic meter of dissolved ionic iron (108) and $10\text{-}60$ μg/l of iron-containing particulate matter (109). The substrate is unlikely to be a major iron source since chitons often grow on rocks that are deficient in iron (e.g., limestones). Hence, the iron requirement is most likely met from the algae which are the major dietary constituent of most chitons.

Carefoot (15) has measured the iron concentrations in various types of algae which are eaten by Mopalia hindsii. The values range from 0.2 to 0.9% dry weight. If we assume that the dry weight of algae is 20% of the wet weight (cf. (19)), then we can calculate that M. muscosa must injest 50 to 200 mg of algae per day in order to obtain the 80 μg of iron required each day for tooth mineralization. If additional studies reveal that the actual daily food intake of M. muscosa does not meet the iron requirement, then it would appear likely that the animals are able to reabsorb iron from the teeth that are shed at the anterior of the radula.

If 80 μg of iron are deposited each day into the radula of M. muscosa, then the same amount of iron must be transported daily to the cells which are responsible for iron deposition. Our observations on the dorsal sinus of the radula sac, described in Part I, and our studies on Mopalia blood, reported in Part II, strongly indicate that the transport of iron is effected by molecules of ferritin, dissolved in the haemal fluid of the chiton circulatory system. The site of synthesis of apoferritin and the means by which it is filled with the iron that is absorbed from the algal food are problems which have not been resolved in the present study. However, the rhopheocytotic uptake of ferritin from the dorsal sinus by the basal ends of the superior epithelial cusp cells is amply demonstrated by the electron microscope observations and is further supported by the finding that Fe^{59}-labeled ferritin accumulates within the radula sac epithelial tissue. Most direct proof of ferritin uptake by the radula sac tissues can be obtained by injecting known amounts of labeled chiton ferritin into the circulatory system, and measuring the kinetics of its disappearance from the haemal fluid and its appearance in the radula epithelia.

The total blood volume of Cryptochiton stelleri has been shown to comprise about 45% of the wet weight of the body with the shell removed (110). Assuming that this value holds for Mopalia, we have calculated that the total blood volume of M. muscosa is 7 to 10 milliliters. Thus, the superior epithelial cells must take up 7 to 28% of the total iron of the blood each day to meet the iron requriement of the tooth mineralization process.

We should point out that in all of the other organisms in which it has been studied, ferritin appears to function almost entirely as an intracellular storage depot for excess or reserve iron. Ferritin has been observed in the blood plasma of vertebrates, but only under conditions of severe shock or in certain pathological states (111,112). The role of ferritin as an iron transport protein in the blood is, at present, unique to *M. muscosa*.

Although the Polyplacophora are, at present, the only known organism that can make the ferric-ferrous oxide, magnetite, the deposition of other iron minerals is known to occur in the radula teeth of other Mollusca and in the true dental structures of higher animals. Lowenstam (112) has reported the occurrence of goethite ($\alpha Fe_2O_3 \cdot H_2O$) in the radula teeth of several species of Archaeogastropods which occupy ecological niches similar to those of the chitons. The dental enamel of the teeth of urodeles (114) and of the rat (115) is pigmented with orange-colored iron-containing materials, possibly hematite (Fe_2O_3) (114). The epithelial cells of the Archaeogastropod radula sac (14), the dental epithelial cells of urodeles (102), and the ameloblasts of the rat incisor (117) have all been observed to contain membrane-bound granules, similar to those in the chiton cusp cells. The dental tissue of the urodeles also contains granules that resemble the *Lepidochitona* ferruginous granules. It would appear that the protein-iron complex, ferritin, is involved in the secretion of iron into the teeth of all of these animals. Only by further study can we determine whether additional aspects of our findings on the Polyplacophoran iron mineralization process have wider applicability to the processes of iron secretion that occur in other animals.

BIBLIOGRAPHY

BIBLIOGRAPHY

1. Smith, A. G., in Treatise on Invertebrate Paleontology Part I (Mollusca I): R. C. Moore, Ed. (Geol. Soc. America and Univ. Kans. Press, 1960), p. 142.

2. Heath, H., Anat. Anz. 23, 92 (1903).

3. Arey, L. B. and W. J. Crozier, J. Exp. Zool. 29, 157 (1919).

4. Fretter, V., Trans. Roy. Soc. Edinburgh 59, 119 (1937).

5. Lowenstam, H. A., Geol. Soc. America Bull. 73, 435 (1962).

6. Barnawell, E. B., Veliger 2, 85 (1959).

7. Plate, L., Zool Jarb. 1, Suppl. 4, 1 (1898); ibid. 2, Suppl. 5, 5 (1899); ibid. 2, Suppl. 5, 28 (1901).

8. Giese, A. C., J. Comp. Cell. Physiol. 52, 341 (1958).

9. Manwell, C., Anat. Record 113, 609 (1952).

10. Theile, J., in Das Gebiss der Schnecken: F. Troschel, Ed. (Berlin, 1893), vol. II (Polyplacophora).

11. Runham, N. W., Ann. Histochim. 8, 433 (1963).

12. Theile, J., Zoologica, Stuttg. 22 (1909).

13. Towe, K., and Lowenstam, H. A., J. Ultrastruct. Res. 17, 1 (1967).

14. Nesson, M. H., unpublished observations.

15. Carefoot, T. H., Proc. Malac. Soc. Lond. 36, 203 (1965).

16. Lowenstam, H. A., personal communication.

17. Sollas, I. B. J., Quart. J. Micr. Sci. 51, 115 (1907).

18. Prenant, M., Arch. Anat. Microscop. Morphol. Exptl. 24, 1 (1928).

19. Jones, E. I., R. A. McCance, and L. R. B. Shackleton, J. Exp. Biol. 12, 59 (1935).

20. Tomlinson, J. T., Veliger 2, 36 (1959).

21. Ginsburg, R. N., Bull. Mar. Sci. Gulf Caribbean 3, 55 (1953).

22. Newell, N. D., Bull. Am. Museum Nat. Hist. *109*, 311 (1956).

23. Raven, C. P., *Morphogenesis: the Analysis of Molluscan Development, second edition* (Pergamon Press, Oxford, 1966).

24. Fretter, V. and A. Graham, *British Prosobranch Molluscs; their functional anatomy and ecology* (The Ray Society, London, 1962).

25. Hyman, L. H., *The Invertebrates*, vol. VI, Mollusca I (McGraw-Hill, New York, 1967).

26. Märkel, K., Z. wiss. Zool. *160*, 213 (1958).

27. Rottmann, G., Z. wiss. Zool. *70*, 236 (1901).

28. Schnabel, H., Z. wiss. Zool. *74*, 616 (1903).

29. Gabe, M., and M. Prenant, Ann. Histochim. *3*, 95 (1959).

30. Hubendick, B., Arkiv. Zool. *36*, 1 (1945).

31. Carriker, M. R., Nautilus *57*, 52 (1943).

32. Lowenstam, H. A., Science *156*, 1373 (1967).

33. Runham, N. W., Nature *194*, 992 (1962).

34. Runham, N. W., Quart. J. Micr. Sci. *104*, 271 (1963).

35. Hoffmann, H., Jen. Z. Naturwiss. *67*, 535 (1932).

36. Gabe, M. and M. Prenant, C. R. Acad. Sci. Paris *235*, 1050 (1952).

37. Spek, J., Z. wiss Zool. *118*, 313 (1921).

38. Runham, N. W., Quart. J. Micr. Sci. *102*, 371 (1961).

39. Gabe, M. and M. Prenant, Arch. Anal. microsc. *37*, 136 (1948).

40. Towe, K. M., H. A. Lowenstam, and M. H. Nesson, Science *142*, 63 (1963).

41. Granick, S., Chem. Rev. *38*, 379 (1946).

42. Michaelis, L., Adv. Prot. Chem. *3*, 53 (1943).

43. Tecce, G., Nature *170*, 75 (1952).

44. Roche, J., M. Bessis, and J. Breton-Gorius, C. R. Acad. Sci. Paris *252*, 3886 (1961).

45. Hyde, B. B., A. J. Hodge, and M. L. Birnstiel, Proc. 5th Intern. Conf. Electron Microscopy (Academic Press, New York, 1962), vol.2 p. T-1.

46. Hyde, B. B., A. J. Hodge, A. Kahn, and M. L. Birnstiel, J. Ultrastruct. Res. 9, 248 (1963).

47. David, C., personal communication.

48. Michaelis, L., C. D. Coryell, and S. Granick, J. Biol. Chem. 148, 463 (1943).

49. Granick, S. and P. F. Hahn, J. Biol. Chem. 155, 661 (1944).

50. Harrison,P. M., in Iron Metabolism, F. Gross, Ed. (Springer-Verlag, Berlin, 1964), p. 38.

51. Farrant, J. L., Biochim. biophys. Acta 13, 569 (1954).

52. Kuff, E. L., and A. J. Balton, J. Ultrastruct. Res. 1, 62 (1957).

53. Labaw, L. W., and R. W. G. Wyckoff, Biochim. biophys. Acta 25, 263 (1957).

54. Harrison, P. M., J. Mol. Biol. 6, 256 (1963).

55. Fischbach, F. A. and J. W. Anderegg, J. Mol. Biol. 14, 458 (1965).

56. Towe, K. M., and W. F. Bradley, J. Colloid and Interface Sci. 24, 384 (1967).

57. Harrison, P. M., F. A. Fischbach, T. G. Hoy, and G. H. Haggis, Nature 216, 1188 (1967).

58. Bielig, H. J., and E. Bayer, Naturwissenschaften 42, 466 (1955).

59. Mazur, A., S. Baez, and E. Schorr, J. Biol. Chem. 213, 147 (1955).

60. Pape, L., J. S. Multani, C. Stitt, and P. Saltman, Biochemistry (U.S.) 7, 613 (1968).

61. Mazur, A. and S. Green, in Sulfur in Proteins, R. Benesch et al., Eds. (Academic Press, New York, 1958) p. 189.

62. Towe, K. M., personal communication.

63. Luft, J. H., J. Biophys. Biochem. Cytol. 9, 409 (1961).

64. Venable, J. H., and R. Coggeshall, J. Cell Biol. 25, 407 (1965).

65. Brody, I., J. Ultrastruct. Res. 2, 482 (1959).

66. Pease, D. C., Histological Techniques for Electron Microscopy, second edition (Academic Press, New York, 1964) p. 52.

67. Richardson, K. C., L. Jarett, and E. H. Finke, Stain Technology 35, 313 (1960).

68. Bunting, H., Stain Technology 24, 109 (1949).

69. Gurr, E., Staining: Practical and Theoretical (Williams and Wilkins, Baltimore, 1962) p. 489.

70. Gurr, E., ibid., p. 555.

71. Humason, G. L., Animal Tissue Techniques (W. H. Freeman and Co., San Francisco, 1962) p. 152.

72. Greenstein, J. S., Stain Technology 36, 87 (1961).

73. Gomori, G., Amer. J. Pathology 12, 655 (1936).

74. Hukill, P. B., and F. A. Pott, J. Histochem. Cytochem. 10, 490 (1962).

75. Arvy, L., and M. Gabe, Bull. Soc. Zool. France 74, 173 (1949).

76. Policard, A., and M. Bessis, C. R. Acad. Sci. Paris 246, 3194 (1958).

77. Bessis, M., and J. Breton-Gorius, C. R. Acad. Sci. Paris 244, 2846 (1957).

78. Bessis, M., and J. Breton-Gorius, C. R. Acad. Sci. Paris 245, 1271, (1957).

79. Richter, G. W., J. Exp. Med. 112, 551 (1960).

80. Palade, G. E., Anat. Record 136, 254 (1960).

81. Jennings, M. A., and Lord Florey, Proc. Roy. Soc. London, Series B 167, 34 (1967).

82. Bruns, R. R., and G. E. Palade, J. Cell Biol. 37, 277 (1968).

83. Farquhar, M. G., and G. E. Palade, J. Biochem. Biophys. Cytol. 7, 297 (1960).

84. Ryser, H., J. B. Caulfield, and J. C. Aub, J. Cell Biol. 14, 255 (1962).

85. Shoden, A., and P. Sturgeon, Brit. J. Haematol. 9, 513 (1963).

86. Matioli, G. T., and R. F. Baker, J. Ultrastruct. Res. 8, 477 (1963).

87. Richter, G. W., Lab, Invest. 12, 1026 (1963).

88. Nicol, J. A. C., The Biology of Marine Animals (Interscience, New York, 1960) p. 86.

89. Stewart, D., W. Dandliker, and A. Martin, Fed. Proc. 11, 155 (1952).

90. Martin, A. W., F. M. Harrison, M. J. Huston, and D. M. Stewart, J. Exptl. Biol. 35, 260 (1958).

91. Redmond, J. R., Physiol. Zoöl. 35, 304 (1962).

92. Redfield, A. C., Biol. Rev. 9, 175 (1934).

93. Fischer, D. S., and D. C. Price, Clin. Chem. 10, 21 (1964).

94. Bray, G. A., Analyt. Biochem. 1, 279 (1960).

95. Strauss, J. H., and R. L. Sinsheimer, J. Mol. Biol. 7, 43 (1963).

96. David, J., and R. L. Sinsheimer, J. Mol. Biol. 6, 203 (1963).

97. Britten, R. J., and R. B. Roberts, Science 131, 32 (1960).

98. Martin, R. G., and B. N. Ames, J. Biol. Chem. 236, 1372 (1961).

99. Seckbach, J., personal communication.

100. Runham, N. W., and K. Isarankura, Malacologia 5, 73 (1966).

101. Nordquist, R. E., R. L. Olson, and M. A. Everett, Arch. Derm. 94 482 (1966).

102. Randall, M., Nature 210, 1325 (1966).

103. Laufberger, V., Bull. Soc. chim. biol. (Fr.) 19, 1575 (1937).

104. Bothwell, T. H., and C. A. Finch, Iron Metabolism (Little, Brown and Co., Boston, 1962).

105. Moore, C. V., and R. Dubach, in Mineral Metabolism, vol. 2, Part B, C. L. Comer and F. Bronner, Eds. (Academic Press, New York, 1962) p. 287.

106. Sognnaes, R. F., Ed., in Calcification in Biological Systems. (Am. Assoc. Advance. Sci., Washington, D. C., 1960).

107. Berry, L. G., and R. M. Thompson, Mem. Geol. Soc. Amer. 85, 1 (1962).

108. Cooper, L. H. N., Proc. Roy. Soc. London 118, 419 (1935).

109. Harvey, H. W., The Chemistry and Fertility of Sea Waters (Cambridge Univ. Press, 1960).

110. Martin, A. W., F. M. Harrison, M. J. Huston, and D. M. Stewart, J. Exp. Biol. 35, 260 (1958).

111. Reisman, K. R., and M. R. Dietrich, J. Clin. Invest. 35, 588 (1956).

112. Oki, V., Nature 184, 1944 (1959).

113. Lowenstam, H. A., Science 137, 279 (1962).

114. Schmidt, W. J., Z. Zellforsch. 49, 46 (1958).

115. Miles, A. E. W., Proc. Roy. Soc. Med. 96, 918 (1963).

116. Reith, E. J., J. Biophys. Biochem. Cytol. 9, 825 (1961).